UNIVERSITY OF CALIFORNIA
RIVERSIDE

Impacts of Controlling Reactivity and Temperature on Advanced Study of Secondary Organic Aerosol Formation

A Dissertation submitted in partial satisfaction
of the requirements for the degree of

Doctor of Philosophy

in

Chemical and Environmental Engineering

by

Mary Elizabeth Kacarab

June 2016

Dissertation Committee:
Dr. David R. Cocker III, Chairperson
Dr. Akua Asa-Awuku
Dr. Kelley Barsanti

The Dissertation of Mary Elizabeth Kacarab is approved:

_____

_____

_____

Committee Chairperson

University of California, Riverside

Acknowledgements

It is impossible to put into words how grateful I am to all of those who have supported, inspired, pushed, and guided me through these five years of graduate study. I have gone through many ups and downs on this journey and have come out of it a much wiser and stronger person. I could not have accomplished any of it without the support and guidance of numerous individuals. To all who have played any role, no matter how small, in my life throughout and leading up to this time, I must extend my heartfelt thanks for playing a part in who I am and what I have done.

Principally, I must acknowledge my parents, John and Barbara – thank you for your unending love and tireless support for me in all my endeavors. You have continually driven me to improve myself in all aspects of my life. With each passing year I see the fruits of the seeds you have planted and tended throughout my life and I realize that the benefits I reap are due to your diligence and foresight as parents. You laid the foundation for my faith, without which I would not have been able to overcome any of the numerous snares and trials that have arisen along this journey. I also must acknowledge my brother, Gabriel. As a young girl I idolized you. As an adult, I still idolize you. You have set a standard that I have always tried to live up to. Your example has driven me to continually work on improving myself and helping others around me to do the same.

To my advisor, Dr. David Cocker – I would not have even made it onto this path if it were not for your guidance and encouragement. I came into your office as a struggling, disillusioned undergraduate who couldn't seem to pick a major. Your

enthusiasm for your work and your ability to see students' strengths and embolden them is truly what brought me back onto a successful path in my undergraduate years. You gave me an opportunity to see what research was like and I never looked back. The amount of work and time you devote to your students is astounding. I could not have found a better advisor – you have set the bar for what to aspire to as a professor. Thank you for all of your advice, encouragement, and time.

I also must recognize Dr. Pamela S. Clute, who was an indispensable resource in my search for a career path. Dr. Clute has been and continues to be a shining example and source of inspiration. Thank you for seeing my potential and providing me with the tools and encouragement to reach it. Other indispensable advisors for both career path and research advice include Dr. Sharon Walker, Dr. Bill Carter, Dr. Akua Asa-Awuku, and Dr. Kelley Barsanti. Thank you for your guidance and the examples you have set.

To my colleagues – former and current – thank you. I must especially thank Dr. Shunsuke Nakao and Dr. Chris Clark for sharing so much of their knowledge with me as a young student. Also, thanks to Dr. Ping Tang and Dr. Xiaochen Tang for spending time training me and answering my many questions. To Dr. Chia-Li Chen – I count you among the kindest people I have ever met. Thank you for the time spent as a teacher to me about the lab, as a colleague in running the lab together and ensuring everything works, and as an example of hard work and understanding. To Dr. Derek Price – the things we were able to accomplish working together were astounding. I could not have asked for a better colleague to share the bulk of my graduate studies with. There was no problem too difficult or too big for us to solve. I am so grateful for your genuine

friendship and tireless support! To Dr. Diep Vu – though we rarely got the chance to work on the same project, we always found ways to help each other with tossing around ideas, supporting each other through difficulties, and finding delicious food to eat at lunch. Mmm. Thank you for your friendship and constant aid! To Dr. Lijie Li – you have been a constant source of inspiration and a good friend. I am so thankful to have you as a colleague throughout the entirety of our graduate studies and am looking forward to seeing the amazing things you are going to do! To Paul van Rooy, Patrick Roth, and Xinze Peng – it may have taken all three of you to fill Derek's shoes, but you did that and more. Thank you for your assistance in the lab and for being a source of humor and fun.

To Dr. Margaret Gover, all those in the Graduate Student Mentorship Program, and all of my mentees – thank you for the opportunity to know and work with you. The GSMP was a constant source of advice and encouragement. My graduate studies would not have been as successful or enjoyable without it. To all those involved in the Science and Technology Education Partenership – most notably John Fishell, Pamela Clute, and Gordon Bourns – thank you for the opportunity to make such a difference in the lives of students and for being excellent examples of leadership in service.

Lastly, but certainly not least, I would like to thank Kurt Bumiller. I can, without a doubt, say that I would be much less knowledgeable if it were not for your guidance. You taught me how to simplify and solve problems. Your wealth of knowledge and ability to quickly understand the principle of how things work is astounding and is a goal that I aspire to reach. Thank you for your time and effort through the years! I am a much smarter person because of you.

ABSTRACT OF THE DISSERTATION

Impacts of Controlling Reactivity and Temperature on Advanced Study of Secondary Organic Aerosol Formation

by

Mary Elizabeth Kacarab

Doctor of Philosophy, Graduate Program in Chemical and Environmental Engineering
University of California, Riverside, June 2016
Dr. David R. Cocker III, Chairperson

Secondary organic aerosol (SOA) is formed via the oxidation of volatile organic compounds emitted to the atmosphere from both biogenic and anthropogenic sources. Due to the complexity of atmospheric composition and range of ambient conditions, aerosol models, which are mostly based off observed yields from controlled laboratory chamber experiments, greatly underestimate global SOA formation. To increase the understanding of the formation and properties of ambient SOA, it is imperative to explore ways to improve the complexity of chamber studies while still maintaining a level of control not found outside of the laboratory.

A surrogate mixture of reactive organic gases (ROG) was developed to mimic atmospheric reactivity in an urban environment such as the Los Angeles basin. The ROG mixture controlled the reactivity of the chamber system such that all gas phase species were not heavily affected by the addition of an aerosol forming precursor. The ROG mixture was modified to represent an urban environment with a strong biogenic influence by the addition of isoprene. It was found that isoprene's behavior in the mixture yielded

high aerosol formation compared to previous NO_X photo-oxidation studies. Incremental aerosol formation was then defined in the different ROG systems from two aromatic compounds, a monoterpene, and a polyaromatic hydrocarbon. Slightly higher incremental yields were seen from each compound in the biogenic influenced ROG mixture than in the anthropogenic ROG mixture. Furthermore, it was found that the aerosol physical and chemical properties were dictated by the added precursor and were comparable to properties seen in single precursor experiments.

The effect of ambient temperature (5°C to 40°C) on aerosol formation was also explored for α-pinene ozonolysis, *m*-xylene/NO_X photo-oxidation, cyclohexene ozonolysis, and vehicle exhaust photo-oxidation with hydroxyl radical. In all systems except the complex vehicle exhaust mixture, severe hysteresis effects were seen in aerosol formation, with the cold temperature systems forming up to 5 times more aerosol mass. These findings do not support traditional gas/particle partitioning theory which assumes temperature effects are reversible. Physical and chemical properties of the aerosol tended to remain fairly consistent, despite changes in ambient temperature.

Table of Contents

List of Tables

List of Figures

Chapter 1: Introduction

Air pollution constitutes a major challenge facing global society today. Few current environmental issues can compare in both their abundance and complexity to the issues caused by atmospheric pollutants. Recently, the World Health Organization estimated that air pollution caused 1 in every 8 total premature global deaths in the year 2012 (WHO, 2014). A significant and heretofore not well-understood portion of air pollution is constituted by atmospheric particulate matter under 2.5 micrometers (PM2.5). Organic aerosol (OA) is estimated to account for 20-90% of PM2.5 (Jimenez, et al. 2009). Of this, 70% is projected to be secondary in nature (Hallquist, et al. 2009), thus making secondary organic aerosol (SOA) a major constituent of the global PM budget. Atmospheric PM has significant negative effects on human respiratory health (Pope and Dockery, 2006) and life expectancy (Pope, et al. 2009) and negatively affects atmospheric visibility (Eldering and Cass, 1996). Furthermore, it is estimated that suspended atmospheric aerosols play a complicated and significant role in the global climate, with both direct and indirect effects (IPCC, 2014).

Currently, the global understanding of SOA formation is still quite limited, but is considered to be governed by a complex series of reactions and a large number of organic species (Kroll and Seinfeld, 2008). Attempts to model SOA formation based on atmospheric chamber data regularly underestimate atmospheric aerosol levels (Volkamer, et al. 2006; de Gouw, et al. 2008; Matsui, et al. 2009; Ensberg, et al. 2014). Most aerosol yields are determined from the oxidation of a single precursor volatile organic compound (VOC) at a constant temperature. Yield (Y) is defined (Odum, et al. 1996, 1997) as the

mass of aerosol formed (M_o) over the amount of hydrocarbon consumed (ΔHC), as seen in Equation 1:

$$Y = \frac{M_o}{\Delta ROG} \qquad (1)$$

This yield can be further expressed in terms of aerosol partitioning theory, as follows:

$$Y = M_O \sum \left(\frac{\alpha_i K_{om,i}}{1 + K_{om,i} M_O}\right) \qquad (2)$$

where α_i is the stoichiometric mass coefficient of the aerosol forming species and K_{om} is the equilibrium partitioning coefficient for a given species, *i*. The equilibrium partitioning theory for secondary organic aerosol (Pankow, 1994a, 1994b), expressed thusly:

$$K_{om,i} = \frac{RT}{MW_{om,i} \gamma_i p^o_{L,i}} \qquad (3)$$

where *R* is the ideal gas constant, *T* is the temperature of the system, and MW_{om} is the molecular weight, γ_I is the activity, and $p^o_{L,i}$ is the saturation liquid vapor pressure of species *i*. These theories have defined the way that aerosol data from atmospheric chamber systems is approached and evaluated and have simplified the parameters necessary for modeling such complex atmospheric processes. Most yield data used for atmospheric models are derived from single precursor experiments held at constant temperature. This method makes several assumptions, including the concept that gas-to-particle phase equilibrium is reached on a very short time scale and that partitioning is the dominant driving factor for aerosol formation, as opposed to other drivers such as reaction kinetics. The vast majority of yield data used in models are taken from single

precursor chamber experiments. A traditional chamber experiment involves the injection of an aerosol forming precursor hydrocarbon and a gas-phase oxidant (typically NO_X or an OH radical source for daytime chemistry and O_3 or a NO_3 radical source for nighttime chemistry) into a Teflon® reactor filled with clean air. Existing data from chamber studies covers a range of different hydrocarbon precursors with varying levels of hydrocarbon-to-oxidant ratios and different relative humidities, light intensities, and temperatures.

Considering the atmosphere as a complex and uncontrolled system, it leads one to question how relevant single precursor derived yields are for a complex, real atmospheric system in which there will never exist a single precursor and oxidant without any other competing reactive atmospheric species. It is established that the hydrocarbon to nitric and nitrous oxides ratio (HC/NO_X) plays an important role in dictating aerosol formation for a given precursor, with the effects of varying NO_X levels being well studied (Song, et al. 2005). However, with a single precursor hydrocarbon experiment, that single precursor and its individual reactivity with NO_X are what set the levels of important radical species, such as $^{\cdot}OH$, $HO_2^{\cdot}$, and $RO_2^{\cdot}$ (Li, et al. 2015), which play a significant role in SOA formation chemistry. This work explores controlling the reactivity of the chamber system with a surrogate reactive organic gas mixture (ROG) mixture so as to define aerosol formation from an individual precursor without allowing that precursor to dictate the overall reactivity. Controlling chamber system reactivity with a surrogate ROG mixture has previously been explored for ozone (O_3) formation (Carter, et al. 2005)

and aided in the development of the maximum incremental reactivity (MIR) scales for O_3 formation potential.

Aside from the bulk reactivity of different ambient environments, another important aspect to consider in trying to continuously improve the complexity of atmospheric chamber experiments is the temperature at which aerosol is formed and exposed to as it ages. The majority of laboratory chamber experiments studying secondary organic aerosol have been performed at room temperature, meaning that the majority of available information on SOA yields and physical and chemical properties is quite limited. The vast majority of the work that has been done looking at SOA formation at a range of different temperatures has maintained a constant temperature throughout experiments (Takekawa et al. 2003; Pathak, et al. 2008; Saathoff, et al. 2009; Zhang, et al. 2015, Clark, et al. 2016). This forces aerosol models to make assumptions about how different SOA systems behave at different temperatures based on data from a single, stagnant temperature. To the author's knowledge, only two studies have been published to date on the effects of changing the temperature of the chamber system (Warren, et al. 2009 and Qi, et al. 2010). Both of these works challenged traditional partitioning theory in the reversibility of the aerosol system through different temperatures, with much higher yields being found at the initial cold temperatures than at the initial hot temperatures and the two systems not being reversible as the temperature was increased or decreased. It was hypothesized that the presence of thermally labile compounds could be playing a role in affecting the chemistry occurring at different temperatures. This work seeks to further explore the drastic aerosol yields seen at the different temperatures of

formation and how aerosol properties such as density, volatility, and bulk chemical composition are affected throughout different temperature cycles.

This thesis seeks to expand the current understanding of the drivers of secondary organic aerosol formation in the ambient atmosphere by increasing the complexity of the traditional chamber experiment (via use of a surrogate mixture or through changing the temperature of the aerosol formation and throughout aging). The groundwork was laid for establishing a method to evaluate and define incremental aerosol formation in different atmospheric systems by the development and testing of two surrogate mixtures representing different urban environment reactivity levels. The incremental aerosol formation was then tested and evaluated from *m*-xylene, a well-studied aromatic hydrocarbon (Izumi, et al. 1990; Odum, et al. 1997; Cocker, et al. 2001; Song, et al. 2005; Ng, et al. 2007; Li, et al. 2016), in both surrogate systems. The robustness of the surrogates in controlling the reactivity of the chamber system were further tested by the evaluation of incremental aerosol from a biogenic monoterpene (α-pinene), another well-known aromatic compound (1,2,4-trimethylbenzene), and a polyaromatic hydrocarbon (1-methylnaphthalene). This allowed for a wide range of data on trends in incremental aerosol formation and properties through the two different surrogate systems and probed the level of control each surrogate provided in controlling the gas phase chemistry.

Further, the effects of the formation temperature on secondary organic aerosol and effects of changing the temperature were tested and evaluated for four different aerosol forming systems: α-pinene ozonolysis, cyclohexene ozonolysis, *m*-xylene photo-oxidation in the presence of NO, and irradiation of dilute gasoline passenger vehicle

exhaust with hydroxyl radical. The bulk chemical composition and physical properties of each aerosol system were found to have small varying effects due to temperature between the systems, typically most notable in the fractions of organic matter at *m/z43* and *m/z44*. Both the α-pinene and *m*-xylene systems demonstrated extreme hysteresis in the aerosol mass yields between the temperatures, with the cold initial temperature system forming drastically more aerosol than the hot initial temperature system. As the temperatures were subsequently cycled, the mass at different initial temperatures was found to dictate the overall aerosol formation from that point, with a large disparity in values between the two systems. Previously, this has been hypothesized to be due to the presence of thermally labile compounds available for reaction into the aerosol phase at the cold initial temperature but not at the hot initial temperature (Warren, et al. 2009; Qi, et al. 2010). While that is still considered to have a role, recent work calling into question some of the bulk assumptions made for aerosol partitioning – mainly the timescales for gas-particle equilibrium to be reached – have been called into question and mounting evidence has been found for the formation of viscous, glassy aerosol (Zobrist, et al. 2008; Virtanen, et al. 2010; Koop, et al. 2011; Saukko, et al. 2012; Shiraiwa, et al, 2013; Bateman, et al. 2014; Zhang, et al. 2015). It is hypothesized here that due to the recent work highlighting the atmospheric relevance of glass phase transition temperatures, that the extreme disconnect between aerosol formation at different temperatures for some aerosol forming systems may be due to a shift in the aerosol phase state or changes in the reaction kinetics or stability of the products.

Chapter 2: Materials & Methods

All experiments were run in the University of California Riverside (UCR) College of Engineering Center for Environmental Research and Technology (CE-CERT) dual 90m^3 Teflon® chambers, described in Carter, et al (2005). The chambers are housed in an insulated, temperature-controlled enclosure, which is typically kept at 27^{O}C for most experiments, but can be set as low as 5^{O}C (278K) and as high as 40^{O}C (313K). The chamber enclosure is completely lined with reflective anodized aluminum for light uniformity and to maximize light intensity. The enclosure is continually flushed with clean, dry air. Enclosure and chamber air are generated by an Aadco-737 clean air system and are maintained at <0.01%RH for all experiments. A positive differential pressure of >0.015"H_2O is sustained in the chambers throughout experiments via a movable top frame that descends throughout an experiment once the slight positive differential pressure drops below the set value. This positive pressure differential ensures that if there are any leaks in the reactors that air from the enclosure does not enter the reactor and dilute the experiment. To further ensure this, an inert dilution tracer, perfluorohexane, is injected into all experiments and monitored throughout runs to ensure that no dilution effects are occurring.

All chemicals used in experiments were as follows: 1,2,4-Trimethylbenzene, ≥98%; 1-Methylnaphthalene, ≥95%; 1-Pentene, ≥98.5%; 2-Methylbutane, ≥99.5%; Acetaldehyde, ≥99.5%; α-Pinene, ≥98%; cyclohexene, ≥99%; Isoprene, ≥99%; Methylcyclopentane, ≥97%; Methyl ethyl ketone (MEK), ≥99%; *m*-Xylene, ≥99.5%; 50wt% H_2O_2 in H_2O (all liquid precursor chemicals from Sigma-Aldrich); nitrous oxide,

ultra-high purity, Matheson; carbon monoxide, Praxair; and n-Butane, Ethylene, Propylene, and trans-2-Butene, balance nitrogen, Scott-Marrin Specialty Gases.

Gas phase hydrocarbons were monitored by an Agilent 6890N GC-FID equipped with both PLOT and DB-5 columns. Before each experiment, the response factor on the GC is checked with a known concentration of *n*-hexane (Scott-Marrin Specialty Gases) to ensure proper operation of the instrument. The gas phase species were also tracked with a Syft Technologies Voice200 selected ion flow tube mass spectrometer, or SIFT-MS (Prince, et al. 2010). Hydroxyl radical concentrations were modeled with the SAPRC gas phase mechanism (Carter, 2010). A TECO 42C Trace Level NO_X analyzer, TECO 48C Trace Level CO analyzer, and Dasibi 1003-AH Ozone analyzer were used to measure the NO_X species, CO, and O_3, respectively, in each reactor, directly from the clean air system, and in the chamber enclosure. A LICOR LI-840A was used to monitor CO_2 and relative humidity when experiments required it.

Aerosol formation in the chambers was monitored by two in-house custom scanning mobility particle sizers (SMPS), as described by Cocker, et al (2001), equipped with TSI 3771 condensation particle counters (CPCs). Each SMPS monitored aerosol particles between 28 and 700nm. The system is regularly checked for proper calibration by injecting atomized polystyrene latex (PSL) spheres of known sizes.

A Kanomax aerosol particle mass (APM) analyzer followed in series by another house-built SMPS was used to track particle density (Malloy, et al. 2009). The aerosol is first selected based on mass of particles using the peak size seen from the independent SMPS

and an assumed density of 1.4g/cm^3. Two house-built tandem differential mobility analyzers were used to monitor both volatility (VTDMA) and hygroscopicity (HTDMA) (Rader and McMurry). A Dekati thermodenuder is used in the VTDMA and was set to 100°C for all experiments. The HTDMA was maintained between 85-95%RH for all runs. The APM-SMPS and both TDMAs are checked for proper calibration with aerosolized ammonium sulfate.

Aerosol bulk chemical composition was monitored in real time with an Aerodyne high resolution time-of-flight aerosol mass spectrometer (HR-ToF-AMS), introduced by deCarlo et al (2006). The high resolution (W) mode of the instrument was used to obtain the bulk chemical composition and elemental ratios of the aerosol. It is regularly checked for calibration with aerosolized ammonium nitrate. Data was processed and analyzed using the SQUIRREL ToF-AMS Toolkit (version 1.57) and PIKA Tof-AMS HR Analysis (version 1.16).

All incremental aerosol formation experiments utilizing either of the developed surrogate reactive organic gas (ROG) mixtures were run such that the surrogate mixture and oxidant(s) were injected into both reactors and subsequently well mixed. After mixing, the reactors were isolated from each other and the compound of interest for incremental aerosol formation was added to one reactor. The dual nature of these chambers allows for baseline aerosol formation ($M_{o,B}$) from the surrogate-only reactor for every experiment. All surrogate experiments were run at a constant temperature of 300K.

Experiments exploring the effect of temperature on aerosol formation and evolution were run in temperature cycles – either a "cold-hot-cold" cycle starting at 278K, and once aerosol volume stabilized increasing to 313K, and then decreasing back down to 278K again, or a "hot-cold-hot" cycle which started at 313K, and cycled the temperature to 278K after aerosol formation stabilized and then back up to 313K, when possible. On occasion, the aerosol formation took so long to level off at 313K (seen in the *m*-xylene/NO system) that the third temperature setting was not able to be reached within the runtime of the experiment. For photo-oxidation experiments, varying numbers of blacklights were used to maintain a constant NO_2 photolysis rate throughout the experiment. The testing and evaluation of the NO_2 photolysis rate at different temperatures in the UCR/CE-CERT chambers was evaluated by Qi, et al (2010).

Tables & Figures

Table 2.1: All gas and particle phase instruments used

Instrument	Make/Model	Measurement
Gas Phase		
Gas chromatography flame ionization detector (GC-FID)	Agilent 6890N	Hydrocarbon concentration
Selected ion flow tube mass spectrometer (SIFT-MS)	Syft Technologies Voice 200	Gas phas species and mass spectra
Trace level NO_X analyzer	TECO 42C	NO, NO_2, and NO_X concentrations
Trace level CO analyzer	TECO 48C	CO concentration
Ozone analyzer	Dasibi 1003-AH	O_3 concentration
CO_2/H_2O gas analyzer	LICOR LI-840A	CO_2 concentration and relative humidity
Particle Phase		
Scanning mobility particle sizer (SMPS)	House-built	Aerosol size distribution and concentration
Aerosol particle mass analyzer (APM-SMPS)	Kanomax 3600	Aerosol density
Volatility tandem differential mobility analyzer (V-TDMA)	House-built with a Dekati thermodenuder	Aerosol volatility
High reolution time-of-flight aerosol mass spectrometer (HR-ToF-AMS)	Aerodyne	Bulk aerosol chemical composition

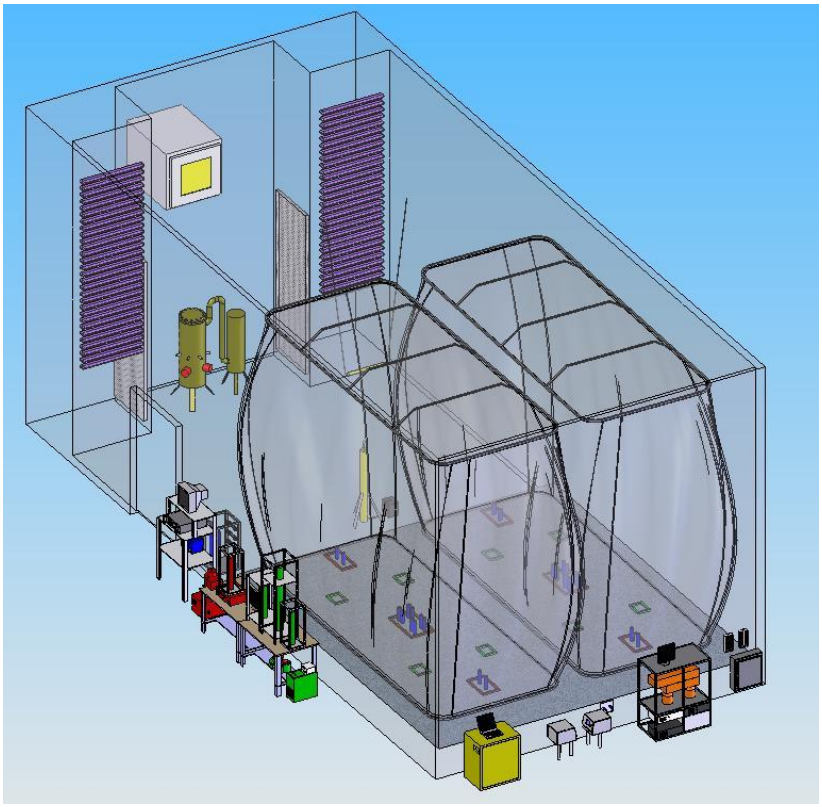

Figure 2.1: The UCR/CE-CERT dual 90m^3 chambers

Chapter 3: Development of an Anthropogenic Surrogate Mixture for Studying SOA Formation & Resulting Incremental Yields from m-Xylene

Introduction

Aerosol yields are determined by measuring the aerosol formed from the oxidation of a single precursor volatile organic compound (VOC), where the gas phase chemistry is dictated by the single VOC present. Yield (Y) is defined (Odum et al, 1996) as the mass of aerosol formed (M_o) over the amount of VOC consumed, as seen in Equation 1:

$$Y = \frac{M_o}{\Delta VOC} \qquad (1)$$

This work explores options to control the reactivity of the chamber system with a surrogate ROG mixture so as to define aerosol formation from an individual precursor without allowing that precursor to dictate the overall system reactivity.

The concept of controlling chamber system reactivity with a surrogate ROG mixture has previously been explored for ozone (O_3) formation (Carter, et al. 1995) and aided in the development of the maximum incremental reactivity (MIR) scales for O_3 formation potential. The MIR scales are still used as a benchmark for O_3 regulation in California. Behind the development of the ROG surrogate was the idea of "incremental reactivity" (Carter and Atkinson, 1987; Carter, 1994), which is essentially defined as the amount of additional O_3 formed from the addition of a compound to a system divided by

the amount of compound added. The concept of incremental aerosol reactivity was first suggested by Griffin, et al (1999). Here, it is sought to test and define the incremental aerosol formation in a controlled reactivity chamber system along the same lines of the development of the ozone reactivity scales.

Reasoning & Development

A surrogate ROG mixture was developed to represent an anthropogenic urban atmospheric system such as that of the Los Angeles Basin. The surrogate was developed based off of average overall concentrations of Los Angeles ambient VOCs (Sullivan, et al. 2011). This speciation data was then lumped into categories according to the SAPRC model (e.g. ALK1, ALK2, ARO1, ARO2, etc.) and each category was weighted by both the abundance and atmospheric reactivity potential (via MIR value) of the different VOCs within it to determine the most representative categories for the Los Angeles basin. One or two representative compounds from each category were then chosen based on their MIR and abundance to constitute the bulk percentage of that category. The final surrogate Los Angeles basin atmospheric mixture for aerosol formation can be found in Table 3.1. Final species selected for the surrogate mixture were both representative of the typical Los Angeles atmosphere and sufficiently reactive to minimize perturbations to the overall gas phase reactivity when target molecules for SOA formation were added. Compounds were weighted by MIR so that the system had a strong propensity for O_3 formation, with only a small baseline of aerosol formation. In comparison to the surrogate VOC mixture used for determining ozone formation potential, the SOA surrogate presented here has similar light hydrocarbon composition (same percentages of

ethylene, propylene, n-butane, and trans-2-butene), however, it has a higher concentrations of aromatic hydrocarbons toluene and *m*-xylene and replaces *n*-octane with 1,2,4-trimethylbenzene.

All experiments were conducted in the UCR/CE-CERT dual chambers, described in detail in Chapter 2. These chambers are ideal for this work as the base case surrogate ROG mixture and radical sources can be injected and subsequently well-mixed between the two reactors to ensure that each reactor has the same starting ROG and radical source composition. Then, the reactors can be isolated from one another and the hydrocarbon of interest can be added to one reactor only, allowing for comparison of the aerosol formation with and without the added SOA precursor over the course of an experiment. From this, an incremental aerosol yield, *Y**, is defined as follows:

$$Y^* = \frac{M_{o,A} - M_{o,B}}{\Delta HC} \qquad (2)$$

Where $M_{o,A}$ is the aerosol formed from the surrogate with additional aerosol-forming precursor, $M_{o,B}$ is the aerosol formed from the surrogate alone, and ΔHC is the change in the gas-phase concentration of the additional aerosol precursor.

The surrogate is first tested and incremental aerosol yields are defined from *m*-xylene, a widely studied aromatic hydrocarbon. A wealth of *m*-xylene data has been collected using the UCR/CE-CERT chamber and there is also considerable amount of published data on SOA from *m*-xylene as well, thus making it a suitable compound to first test and explore the concept of incremental aerosol formation with. Experiments were run with 1.1ppmC anthropogenic surrogate, 25ppb NO_X, and 25ppb *m*-xylene and

2.2ppmC anthropogenic surrogate, 25ppb NO_X, and 50ppb *m*-xylene. Initial conditions are summarized in Table 3.2.

Results & Discussion

Overall, it was seen that the addition of *m*-xylene to the anthropogenic surrogate mixture had little to no effect on measured gas phase species. The initial NO and NO_X concentrations, final O_3 formation, and integrated OH (predicted by SAPRC11 mechanism) are summarized in Table 3.2. NO decay and NO_2 formation (Figure 3.1) were extremely similar for all systems whether or not *m*-xylene was added. This is a good indication that the reactivity levels are being well controlled by the ROG mixture, as the major drivers for gas-phase reactions are the initial hydrocarbons and the overall NO_X. Having NO_X trends remain unaffected by the addition of *m*-xylene suggests that the strong reactivity of the ROG mixture is buffering the effect on radical species from *m*-xylene. This can be further seen in the decay trends of hydrocarbons present in the surrogate (Figure 3.2). For all species measured, the hydrocarbon decay in each experiment matches almost exactly between the two reactors with and without the added *m*-xylene.

The O_3 formation was about 10-20ppb lower for the reactor with added *m*-xylene than for the associated surrogate only reactor (Figure 3.4). For the 1.1ppmC surrogate with 25ppb *m*-xylene, the rate of O_3 formation was slightly faster than in the surrogate only system. It is hypothesized that overall O_3 formation is lower because the added *m*-xylene slightly lowers the average MIR for the system. The integrated OH from the

SAPRC11 model is also slightly lower in the surrogate system with *m*-xylene than without. SAPRC uses *m*-xylene decay to adjust modeled OH concentrations, so it is likely that the additional *m*-xylene increases the OH decay rate, thus decreasing the integrated OH value.

The aerosol formation from the surrogate mixture with and without *m*-xylene can be found in Figure 3.5. Significantly more aerosol is formed in the reactor with the added *m*-xylene in both the 1.1ppmC and 2.2ppmC surrogate environments, which contrasts heavily with the small differences seen in the gas phase species trends. This achieves the goal of this work, which was to isolate the overall gas phase reactivity from being affected by the aerosol precursor of interest. What is particularly unique about this system is that the large overall HC/NO_X ratio allows us to define yields from small amounts of *m*-xylene, which was previously very difficult to control because it was hard to get a low NO_X system in comparison with such a low concentration of hydrocarbon precursor. For example, to maintain a high HC/NO_X ratio (e.g. a ratio of ~6) in a single precursor experiment with only 25ppb of *m*-xylene, one would need to only have added only 4ppb of NO_X. While the large size of the UCR/CE-CERT chambers allows for precise and controllable low concentration injections, the aerosol yields from such small amounts are often not repeatable. Here, the data indicates a nicely controlled system for studying incremental yields from small amounts of aerosol forming precursors.

In comparison to previous literature yields of *m*-xylene in the presence of NO_X (Izumi, et al. 1990; Odum, et al. 1997; Cocker, et al. 2001; Song, et al. 2005; Ng, et al. 2007; Li, et al. 2015), the data from this work falls along what would be considered the

high-yield (low NO_X regime) curve (Figure 3.6). However, looking at the data from this perspective is difficult due to not only the extreme differences in overall HC/NO_X in the single precursor studies compared with the surrogate work, but also the low concentration of starting precursor (25ppb). This difference can be more starkly illustrated in Figure 3.7, which plots the change in M_O due to *m*-xylene versus the *m*-xylene consumed. It can be seen that not only are repeatable yield values obtained at this low precursor concentration but that the trend in yields is similar to the data found in previous works and could potentially be providing slightly higher yields, thus putting the incremental yields from *m*-xylene in this surrogate mixture on a higher trajectory yield curve than has been estimated with data from single precursor studies. Additional compounds acetaldehyde, 2-methylbutane, methylcyclopentane, 1-pentene, methyl ethyl ketone, and isoprene were added to complete the surrogate.

In comparison to previous single precursor *m*-xylene/NO_X studies in the UCR/CE-CERT chambers (Li et al), we find that the physical and chemical properties of the incremental aerosol (Table 3.3) in the surrogate mixture are quite similar to aerosol from *m*-xylene/NO_X alone. The average density of the *m*-xylene incremental aerosol is 1.43±0.08 g/cm^3, which is in the typical range of SOA densities. The average final volume fraction remaining (VFR) at 100C is 0.3, matching well with the final VFR seen in Li et al. for single *m*-xylene/NO_X aerosol. The bulk H:C and O:C ratios for the *m*-xylene and surrogate system also line up fairly closely with previous HR-ToF-AMS data from Li et al.'s single precursor *m*-xylene aerosol characterization. This result is quite

encouraging as it could be indicating that the chemistry in the aerosol phase is remaining the same whether or not the aerosol precursor is in a controlled reactivity system.

Conclusion

This work documents the development of reactive organic gas mixture to control the reactivity of the chamber system in an attempt to mimic an urban environment such as Los Angeles. *m*-Xylene was added to the surrogate mixture to explore what effects it would have on perturbing the reactivity of the system. It was found that the gas phase species trends had little to no change when *m*-xylene was added to the system. The aerosol formation was greatly affected by the additional VOC, allowing for the definition of an incremental aerosol yield, Y*. Further, it was found that the incremental aerosol from *m*-xylene displayed comparable properties to single precursor *m*-xylene/NO_X aerosol. This method can be future employed in attempts to define relevant, accurate aerosol yields for urban areas and may provide an important stepping stone in reconciling modeled aerosol yields with atmospheric observations. Next steps should include defining yields at a range of different *m*-xylene concentrations and evaluating at what point is the amount of additional *m*-xylene high enough to perturb the overall reactivity of the system. The concept of using a surrogate mixture for studying incremental effects on aerosol formation has been defined and initially tested here, but the limits of this method still need to be explored and defined.

Tables & Figures

Table 3.1: Composition of Anthropogenic Surrogate ROG Mixture

ppb/ppmC	Compound
46	Acetaldehyde
5	*m*-Xylene
5	1,2,4-Trimethylbenzene
90	n-Butane
14	trans-2-Butene
14	Toluene
22	2-Methylbutane
13	Methylcyclopentane
16	Ethylene
14	Propylene
3	1-Pentene
17	Methyl Ethyl Ketone
2	Isoprene

Table 3.2: Experimental conditions and aerosol formation from anthropogenic surrogate mixture with (side A) and without (side B) *m*-Xylene

Run	Δ*m*-Xylene (ppb)	NO_{init} (ppb)	$NO_{X,init}$ (ppb)	O_3 (ppb)	$^{\cdot}OH^{\dagger}$ (ppt)	M_O (μg/m^3)	Y* (%)
1.1ppmC Anthropogenic Surrogate – with added *m*-Xylene on side A only							
1961A[a]	22	20.0	30.4	169	37	3.1	3.0
1961B[a]	-	20.2	30.5	184	-	0.3	-
1968A[a]	26	16.6	31.8	189	49	2.6	1.7
1968B[a]	-	16.6	31.7	205	75	0.1	-
2132A	25	13.6	22.2	185	37	4.4	5.9
2132B	-	13.4	22.1	199	53	0.5	-
2150A	33	14.7	22.8	164	52	3.7	2.2
2150B	-	14.7	22.9	174	41	0.3	-
2.2ppmC Anthropogenic Surrogate – with added *m*-Xylene on side A only							
1973A	42	23.0	32.2	158	15	11.8	4.6
1973B	-	23.2	34.8	186	18	3.5	-
2032A	40	20.0	29.7	148	13	5.7	3.1
2032B	-	20.0	30.0	175	26	0.4	-

† Integrated OH concentrations as modeled by SAPRC11
a Experiment was run with 1ppmC surrogate

Table 3.3: Physical and chemical properties of incremental aerosol from *m*-Xylene in the anthropogenic surrogate mixture

Run	Density (g/cm^3)	VFR‡	H:C	O:C
Anthropogenic Surrogate + *m*-xylene				
1961A	1.40±0.06	0.33±0.01	1.5±0.04	0.4±0.05
1968A	1.40±0.08	0.30±0.05	1.6±0.14	0.4±0.07
1973A	1.47±0.04	0.29±0.02	1.4±0.02	0.4±0.02
2032A	1.43±0.02	-	1.4±0.04	0.5±0.04
2132A	1.45±0.06	0.29±0.01	1.4±0.14	0.5±0.07
2150A	1.42±0.08	0.25±0.03	1.4±0.14	0.5±0.10

‡ Volume fraction remaining at 100°C at end of experiment

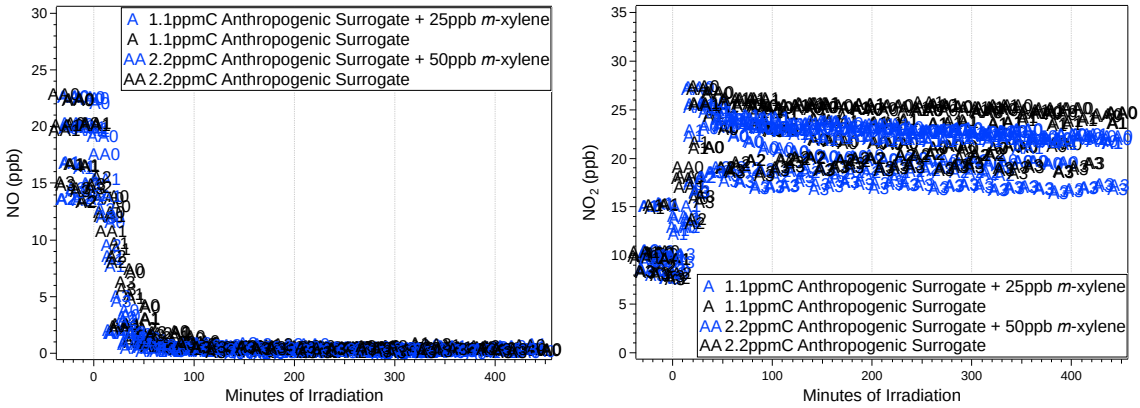

Figure 3.1: NO and NO_X trends for the surrogate mixture with and without added *m*-xylene

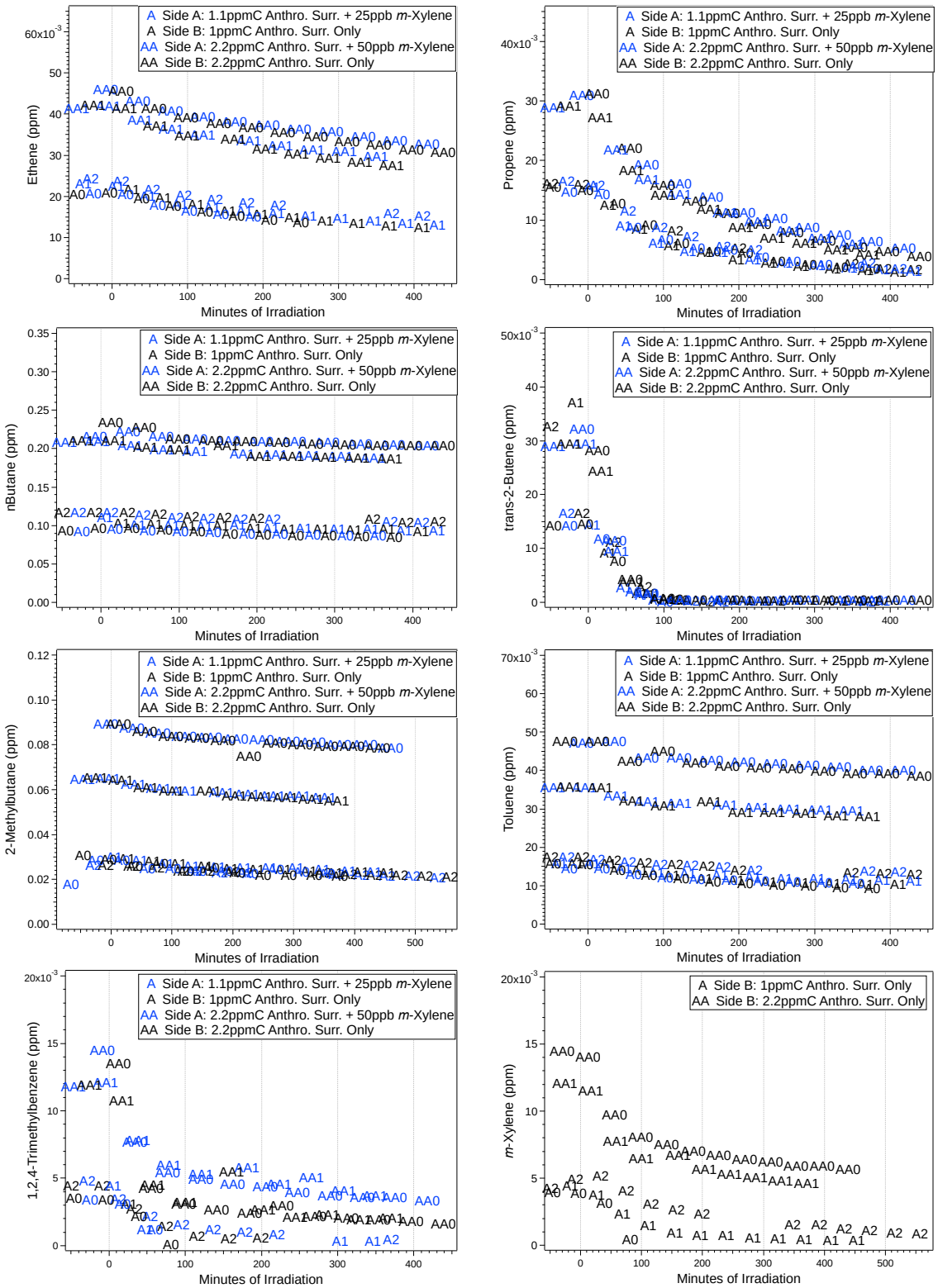

Figure 3.2: Traces of surrogate mixture hydrocarbon species throughout experiments

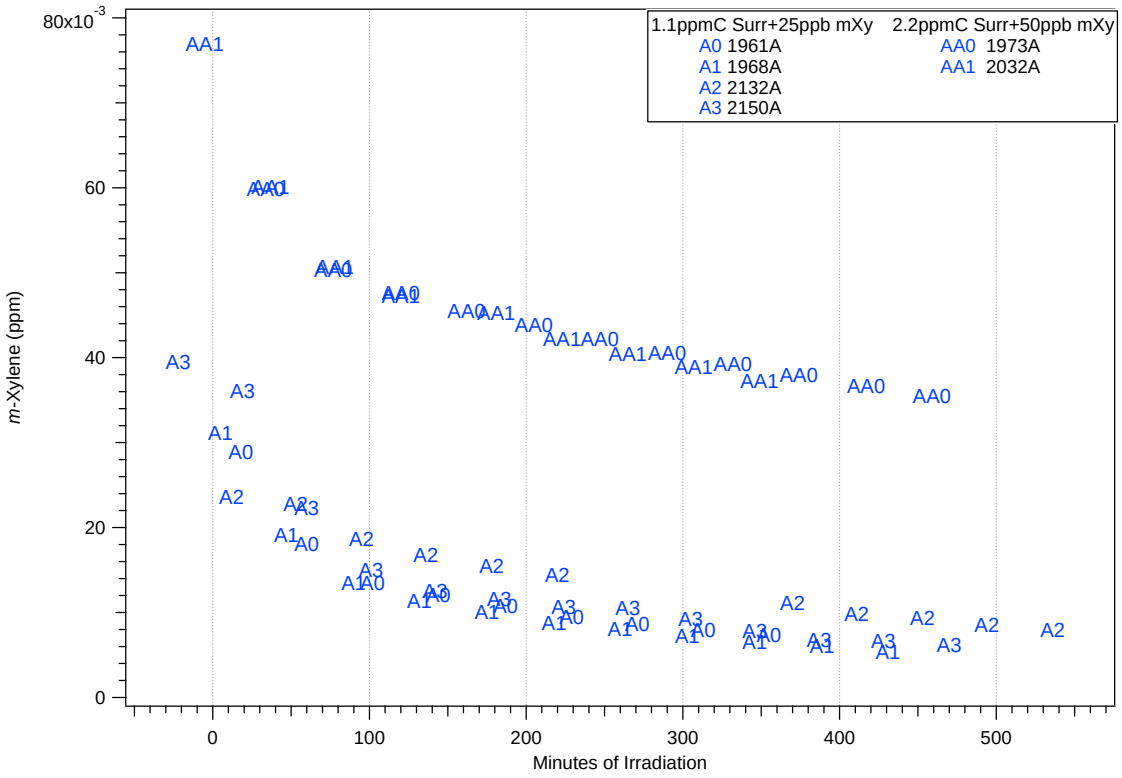

Figure 3.3: Decay of additional *m*-xylene for incremental aerosol experiments

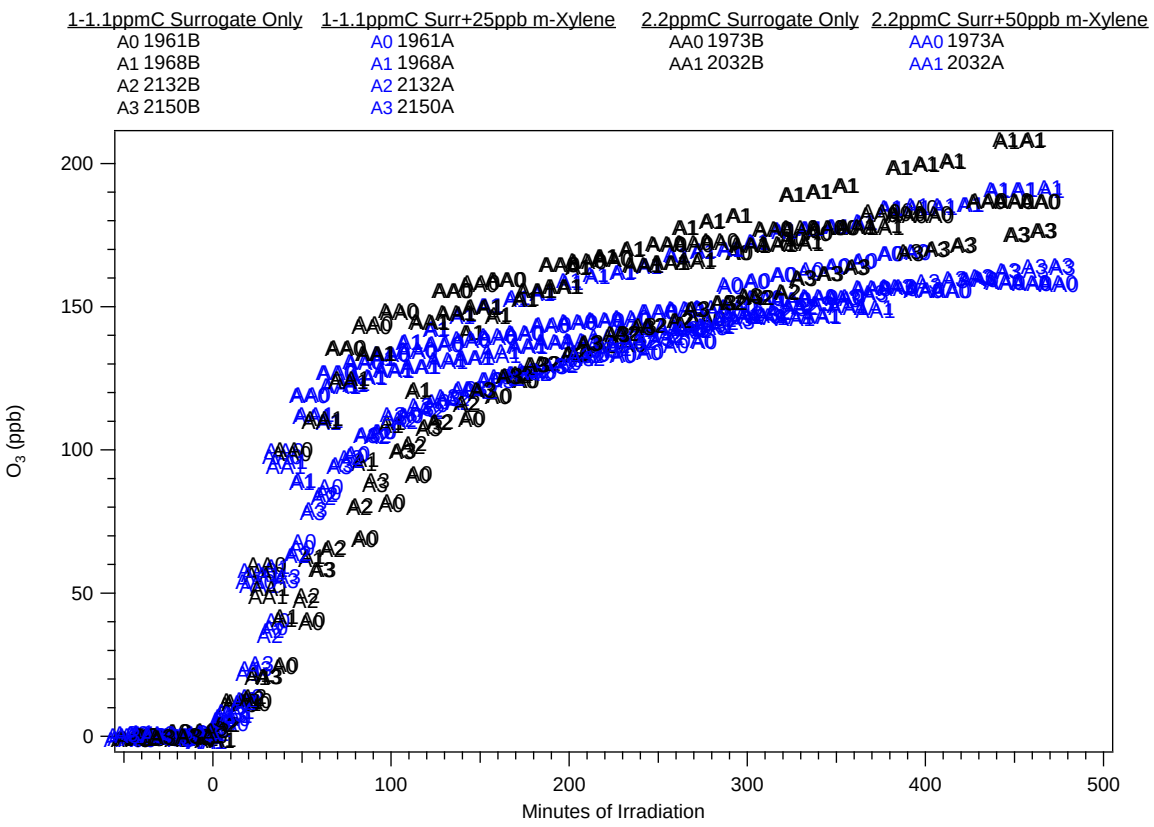

Figure 3.4: O_3 formation for anthropogenic surrogate mixture with and without added *m*-xylene

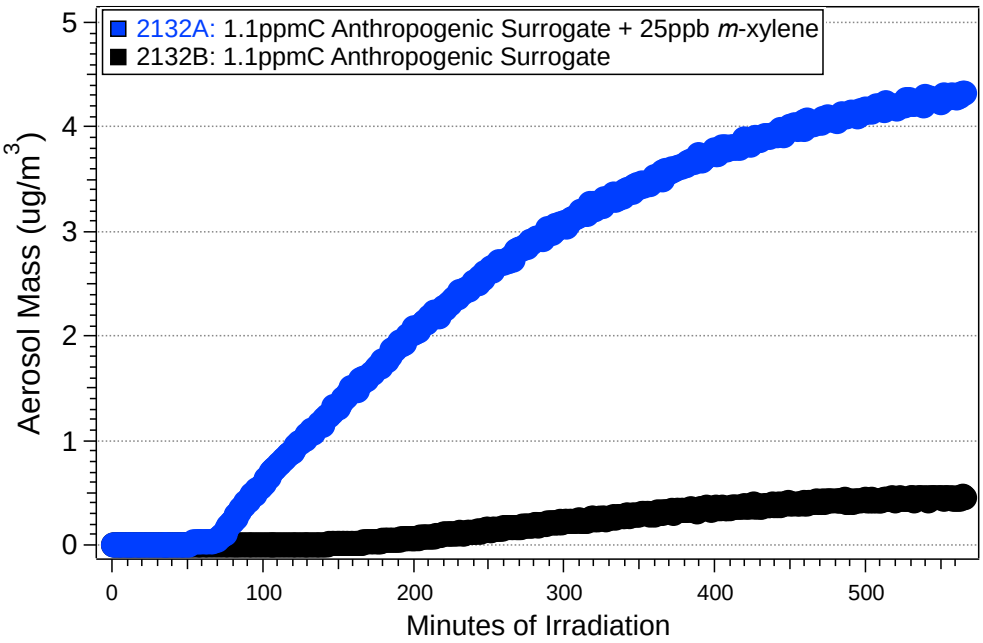

Figure 3.5: Aerosol formation from the surrogate mixture and with added *m*-xylene

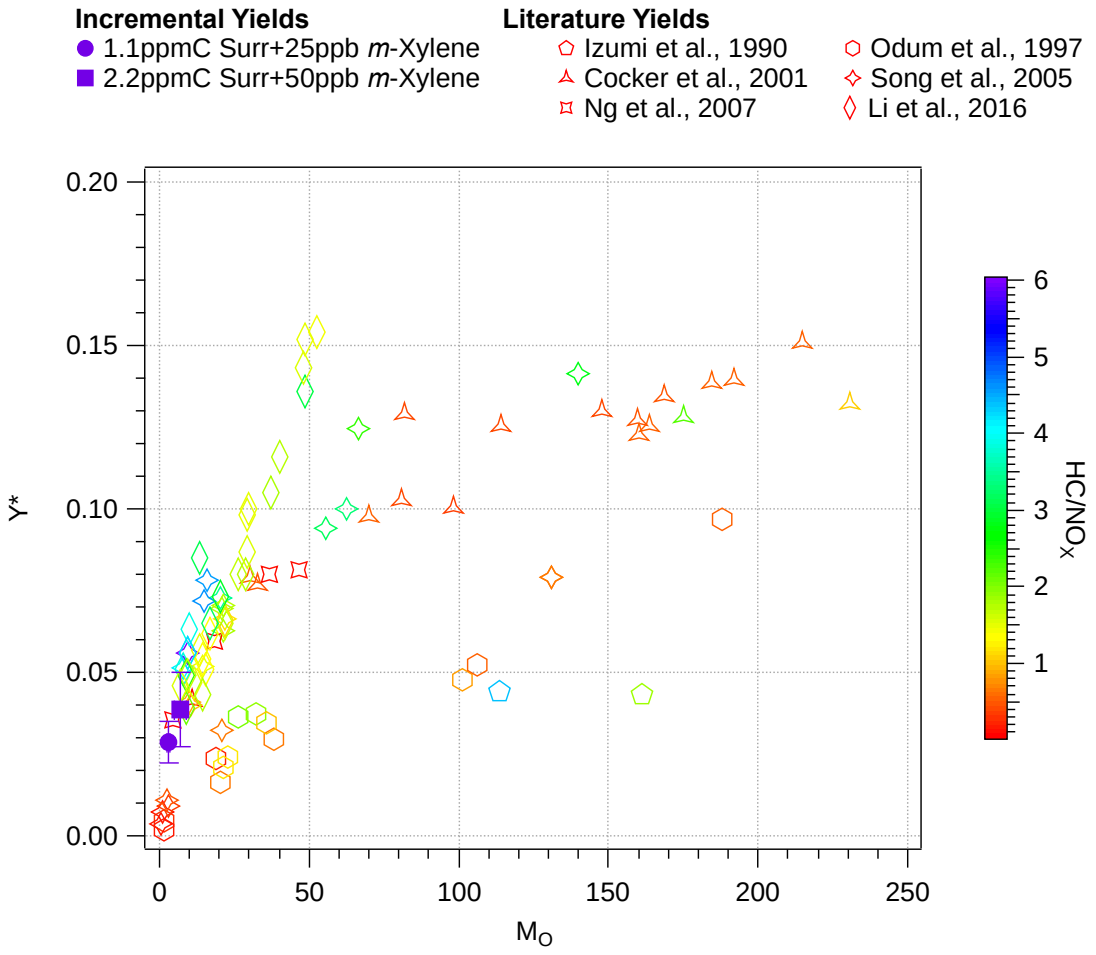

Figure 3.6: Yield curves from literature values for *m*-xylene/NOX chamber experiments and incremental aerosol yields for 25ppb and 50ppb *m*-xylene.

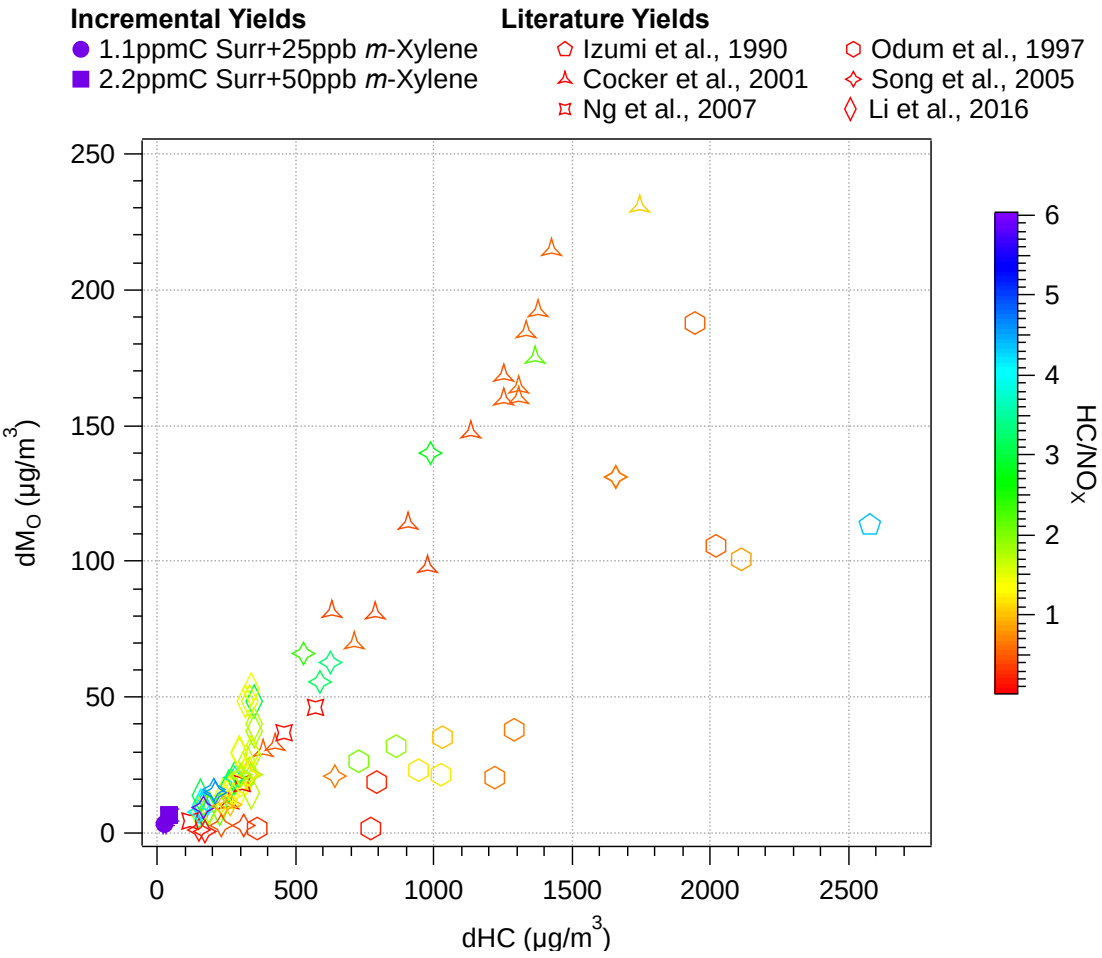

Figure 3.7: Aerosol formation (dMo) vs *m*-xylene decay (dHC) for incremental aerosol formation and literature values

Chapter 4: Development & Testing of Biogenic Influenced Surrogate Mixture

Introduction/Reasoning & Development

In the previous chapter, a surrogate mixture was developed and explored that sought to define chamber reactivity levels to be a simplified version of an urban environment such as Los Angeles. Here, we seek to modify that surrogate so that it can represent an urban atmosphere that also has a strong biogenic influence, such as Atlanta. A significant fraction of SOA is formed from biogenic hydrocarbon precursors (Kanakidou, et al. 2005), especially in remote areas, but in urban areas anthropogenic emissions are also major SOA formers, thus making the inclusion of biogenic emissions to the anthropogenic surrogate ROG system of high importance to accurately represent different reactive environments. To modify the anthropogenic surrogate mixture defined in Chapter 3, it was decided to use equal parts by ppmC of the anthropogenic ROG mixture and isoprene. Isoprene's selection to represent all biogenic emissions is twofold. First, it is globally the most abundant non-methane hydrocarbon with up to 600Tg/year emitted into the atmosphere (Guenther, et al. 2006), making it undoubtedly relevant for inclusion in any surrogate ambient mixture. Second, it has relatively low aerosol yields, especially in comparison to other aerosol forming biogenic terpenes, which if they had been included would have dominated the aerosol formation of the system too heavily to discern any incremental aerosol from the addition of other compounds. Until recently, isoprene had been considered too small of a hydrocarbon to participate in the formation

of SOA. It is now considered to be of clear relevance to global SOA formation as even though its aerosol yields are small, so much is emitted per year that despite its low aerosol formation it still contributes significantly to the global SOA budget. SOA from isoprene has been widely studied in recent years and is still of significant interest (Kroll, et al. 2006; Dommen, et al. 2006; Carlton, et al. 2009; Sato, et al. 2011; Clark, Kacarab, et al. 2016). This chapter explores the characterization of the proposed "biogenic" surrogate ROG mixture and explores the properties of the resulting isoprene aerosol.

Results & Discussion

To first explore isoprene formation, only 25ppb was added to 1ppmC of the existing anthropogenic surrogate established in Chapter 3. Similar to the addition of *m*-xylene to the surrogate mixture, the addition of isoprene had little to no effect on the gas phase species trends of NO and NO_2 (Figure 4.1) and hydrocarbon decays (Figure 4.2). The added isoprene caused the rate of O_3 formation to be slightly faster, but overall the same amount of O_3 was formed with or without the added isoprene (Figure 4.3). Incremental aerosol formation from 25ppb of isoprene in the anthropogenic surrogate can be seen in Figure 4.4. Initial concentrations and resulting O_3 and aerosol levels and yields for this run and all biogenic surrogate runs can be found in Table 4.1.

For the testing of the biogenic surrogate, the surrogate only runs are compared at both 2.2ppmC and 1.1ppmC total surrogate levels with 25ppb NO_X with and without 1ppm H_2O_2. The NO and NO_2 trends and gas phase hydrocarbon decays were very similar in all runs, with those having added H_2O_2 having slightly faster NO decay. O_3

formation and modeled OH levels were comparable across all surrogate mixtures with similar conditions. The gas phase decays of anthropogenic surrogate species were comparable in all runs and their decays were much slower in comparison with the anthropogenic surrogate alone, which is to be expected due to the strong reactivity of isoprene dominating the gas phase.

The baseline aerosol formation from the biogenic surrogate is much higher than the baseline aerosol formation from the anthropogenic surrogate. The large addition of only isoprene (50% ppmC) to form the biogenic surrogate mixture provides an interesting opportunity to further look at aerosol formation from isoprene. The SOA yields from isoprene in this study as part of the surrogate mixture along with literature yields for isoprene/NO_X systems is found in Figure 4.7. It was found that the yields of isoprene as part of the biogenic surrogate mixture were comparable if not quite higher than previous isoprene/NO_X works (Kroll, et al. 2006; Dommen, et al. 2006; Sato, et al. 2011; Clark, Kacarab, et al. 2016). With yields in this study ranging from 1.4-11.9%, a huge sensitivity of isoprene to SOA formation is seen. Furthermore, it is concluded that something in the set reactivity of the biogenic surrogate is allowing isoprene to achieve higher yields than most previous studies with NO_X at room temperature, especially considering that the high yields seen for other isoprene/NO_X systems are in low HC/NO_X regimes as opposed to this work with a very high overall HC/NO_X.

The isoprene yields are fairly consistent with each other under most similar starting conditions, however, they prove to be quite sensitive if the initial NO or anthropogenic surrogate injections differ slightly. However, the changes seen in the yield

are not always consistent. For instance, the second 2.2ppmC biogenic surrogate run (2118B) has a higher isoprene yield compared to the previous run (2045B) with the same target initial concentrations (8.1% vs 2.4%). Unfortunately, an error in the injection of the gas phase portion of the surrogate on 2118B lead to a ~25% higher concentration of those species (ethene, propene, n-butane, and trans-2-butene). This is the only identifiable difference between the two runs that can be isolated as a potential reason for the yield differences. When comparing the 2.2ppmC biogenic surrogate runs with added hydroxyl, we also see a large difference in the yields, with run 2119B having a much higher yield than run 2149B. There was again, unfortunately, an error in the gas phase surrogate injection, however, this time the gas phase was ~25% lower than the standard surrogate concentration. So we see two runs that both have higher overall isoprene yields potentially due to injection errors, however these two errors would have been expected to have opposite effects from each other rather than similar effects. It is also hypothesized that the lower yields seen in runs 2045B and 2047B compared to their later counterparts 2118B and 2119B could be due to suppressed aerosol formation that is sometimes seen towards the end of the chamber lifetime. Shortly after the 2045 and 2047 runs the bags were determined to be suppressing aerosol yields and new bags were constructed and used for all subsequent experiments.

Another notable point can be seen when looking at the yield from 25ppb (0.125ppmC) and comparing it to yields for much higher isoprene ppmC composition. Similar to adding only 25ppb of *m*-xylene to the anthropogenic surrogate, when adding only 25ppb isoprene we are able to observe aerosol yields from very small amounts of

initial precursor hydrocarbon with use of the surrogate to control the overall hydrocarbon/NO_X, which otherwise would be hard to maintain with low precursor concentrations. Interestingly, a yield of 2.4% is seen from only 25ppb isoprene in the anthropogenic surrogate, which is comparable to the some of the yields seen from 0.55ppmC isoprene (110ppb) in the biogenic surrogate. Typically one would expect to see lower yields for lower concentrations, so seeing this consistent yield across a range of concentrations brings up another interesting point – if the reactivity of the system is being controlled with different set mixtures (in this case a small amount of isoprene in the anthropogenic surrogate versus a large amount of isoprene in the biogenic surrogate) then isoprene is behaving differently in these two different reactive environments.

The physical and chemical properties of the resulting isoprene aerosol in the anthropogenic and biogenic surrogate mixtures can be found in Table 4.2. Overall, the density, volatility, and bulk hydrogen to carbon and oxygen to carbon ratios are fairly similar. In Figure 4.8 we can see the time trends for aerosol density for the 1:0.125 and 1:1 ppmC anthropogenic surrogate to isoprene ratio experiments. While the final density is quite similar for both systems (and within the normal range seen for SOA, ~1.4g/cm3), the 25ppb isoprene system has an initial density for about 1 hour that is quite low (~1g/cm3). This could be indicating that initial aerosol formation in this system is comprised of very small solid phase particles that are forming small fractal conglomerates and as the aerosol evolves are transitioning to a more traditional SOA phase and density. This trend is most prominent in the anthropogenic surrogate mixture with 25ppb isoprene added and is also seen with *m*-xylene added to the anthropogenic

surrogate. Neither of these precursors sees such a strong trend of this initial low density in single precursor chamber studies, which could be indicating that something in the controlled reactivity of the surrogate system is affecting the chemistry of the aerosol formation and thus possibly changing the composition or phase of the initial aerosol formed.

Conclusion

The reactive organic gas mixture defined in Chapter 3 was modified to include a significant biogenic emission represented by isoprene. The aerosol formed from low and equal isoprene to surrogate ratios was characterized. The yields measured from isoprene with the surrogate mixture were found to be on the higher side of what has been previously reported in the literature. This is especially relevant considering the higher aerosol yields for the previous isoprene chamber studies were all found under low HC/NO_X conditions, when in this work the overall HC/NO_X was very high due to the presence of the surrogate mixture. There was a small spread of isoprene yields without any clear indication as to what perturbed the aerosol formation to be different in varying runs. This brings up the importance of studying isoprene aerosol, not only due to its abundance in the atmosphere, but because its aerosol formation seems to be quite affected by small differences in the chamber system as a whole. This work introduced the idea of developing this "biogenic" urban surrogate and showed that at least the gas phase species seem to be held fairly consistent by the overall surrogate reactivity levels. The concept of this surrogate should be further explored by looking at number of different surrogate to isoprene ratios. It is believed that systematically exploring the aerosol formation from a

wide and in-depth range of isoprene to surrogate ratios will highlight what factors are affecting isoprene chemistry in the ambient environment. Furthermore, considering that isoprene is known to produce larger yields in high NO_X environments, it follows that this work of defining an isoprene-based biogenic urban surrogate should also be explored in a range of NO_X conditions as opposed to the single NO_X concentration used here.

Tables & Figures

Table 4.1: Biogenic surrogate mixture

ppb/ppmC	Compound
46	Acetaldehyde
5	*m*-Xylene
5	1,2,4-Trimethylbenzene
90	n-Butane
14	trans-2-Butene
14	Toluene
22	2-Methylbutane
13	Methylcyclopentane
16	Ethylene
14	Propylene
3	1-Pentene
17	Methyl Ethyl Ketone
100	Isoprene

Table 4.2: Initial conditions, isoprene consumption, modeled OH, final O3 and aerosol formation and resulting isoprene yields for the anthropogenic surrogate with isoprene and all biogenic surrogate runs.

Run	ΔIsoprene (ppb)	NO_{init} (ppb)	$NO_{X,init}$ (ppb)	O_3 (ppb)	$^{\cdot}OH$	M_O (µg/m^3)	Y (%)
1ppmC Anthropogenic Surrogate + 0.125ppmC Isoprene							
1962A	17	18.6	31.2	190	81	1.3	2.4
1.1ppmC Anthropogenic Surrogate + 1.1ppmC Isoprene							
2045B	203	18.6	27.7	121		13.4	2.4
2118B[a]	218	19.6	33.1	157		50.1	8.1
1.1ppmC Anthropogenic Surrogate + 1.1ppmC Isoprene + 1ppm H_2O_2							
2047B	236	19.1	30.1	124	19	37.0	5.7
2119B[b]	216	22.7	35.4	176	28	71.1	11.9
0.55ppmC Anthropogenic Surrogate + 0.55ppmC Isoprene							
2120B	99	15.2	22.9	157		17.4	6.3
2131A	111	10.9	22.1	155		10.4	3.4
2131B	110	10.2	21.0	153		10.1	3.3
2134B	110	14.1	23.3	155	30	7.0	2.3
2136B	107	16.5	24.4	162		8.0	2.7
2138B	105	19.6	27.6	150	30	6.5	2.2
2139B	113	20.1	28.0	150	28	6.2	2.0
2158B	110	14.1	22.8	146	27	4.4	1.4
2159B	106	15.1	23.5	141		5.2	1.8
2160B	105	14.2	21.3	148	23	2.8	1.7
0.55ppmC Anthropogenic Surrogate + 0.55ppmC Isoprene + 1ppm H_2O_2							
2121B	102	16.8	24.6	177	61	25.1	8.9
2155B		18.4	26.4	165	-	19.9	
2168B	91	12.1	20.0	135	-	20.8	8.2
2169B	95	12.7	19.9	138	48	19.3	7.4
2170B	*	11.7	18.9	144	-	21.5	7.6*

Table 4.3: Physical and chemical properties of resulting aerosol from 1:0.125 and 1:1 ppmC ratios of anthropogenic surrogate to isoprene

Run	Density	VFR	H:C	O:C
1ppmC Anthropogenic Surrogate + 0.125ppmC Isoprene				
1962A	1.40±0.06	0.38±0.10	1.75±0.10	0.38±0.08
0.55ppmC Anthropogenic Surrogate + 0.55ppmC Isoprene				
2131A	1.45±0.05	0.32±0.09	1.47±0.10	0.43±0.05

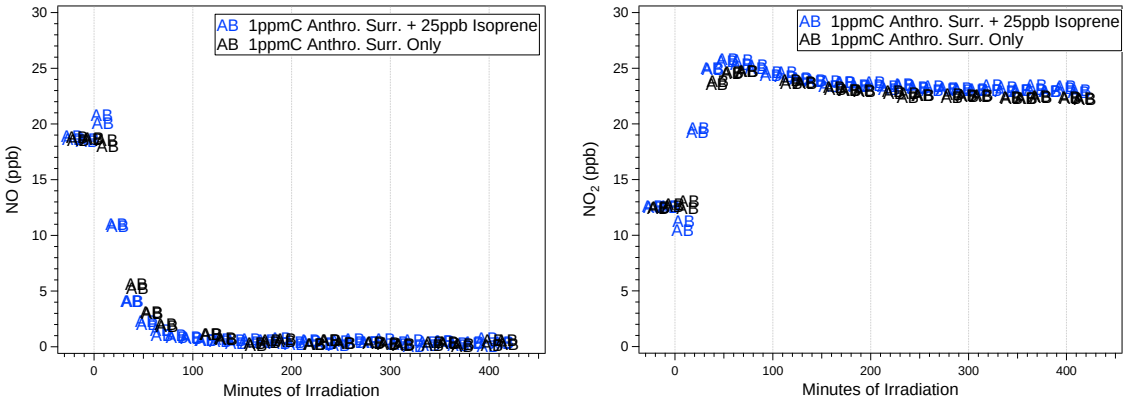

Figure 4.1: NO and NO_X trends for the anthropogenic surrogate with 25ppb isoprene

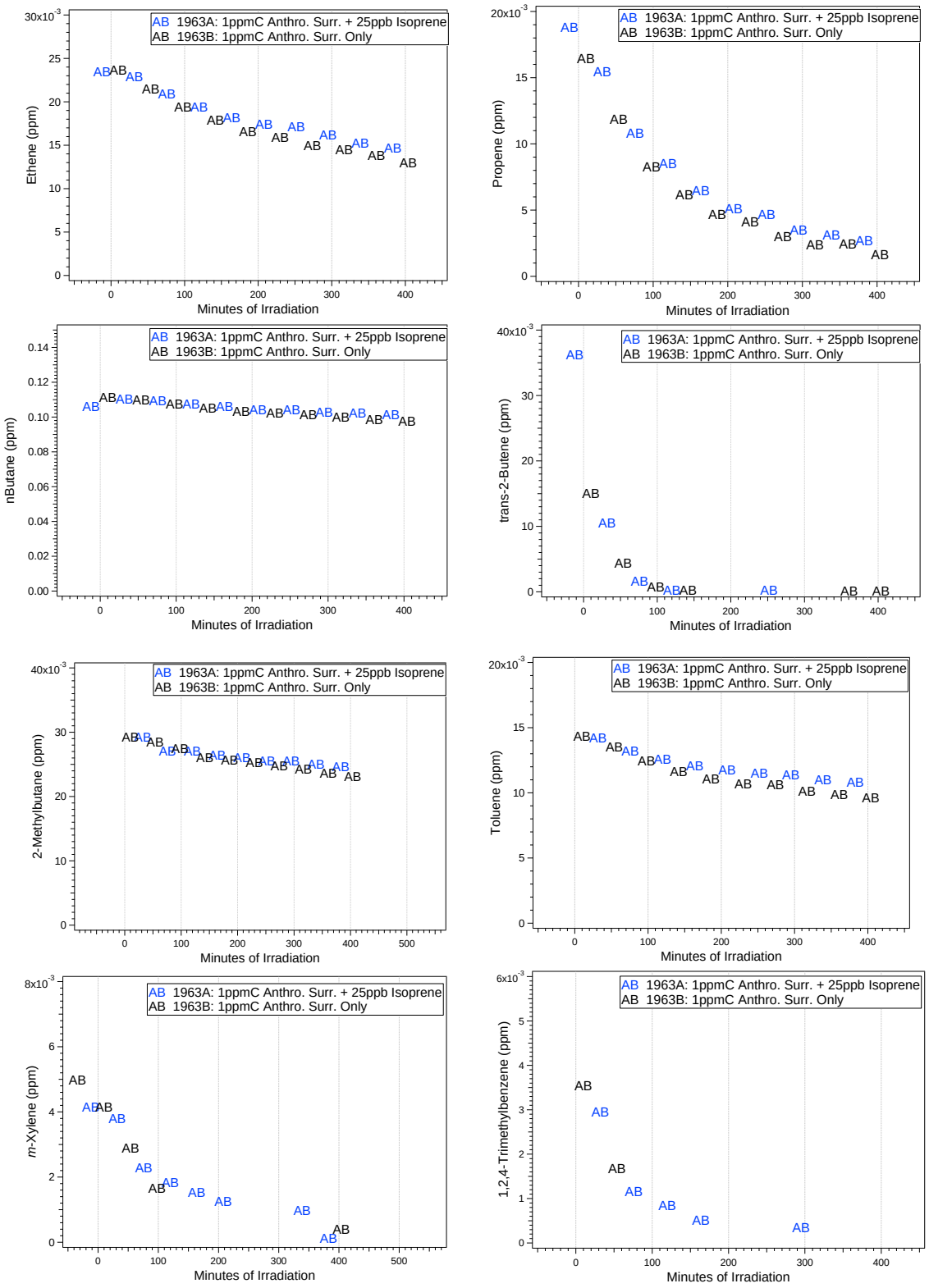

Figure 4.2: Gas phase decay for the anthropogenic surrogate with 25ppb isoprene

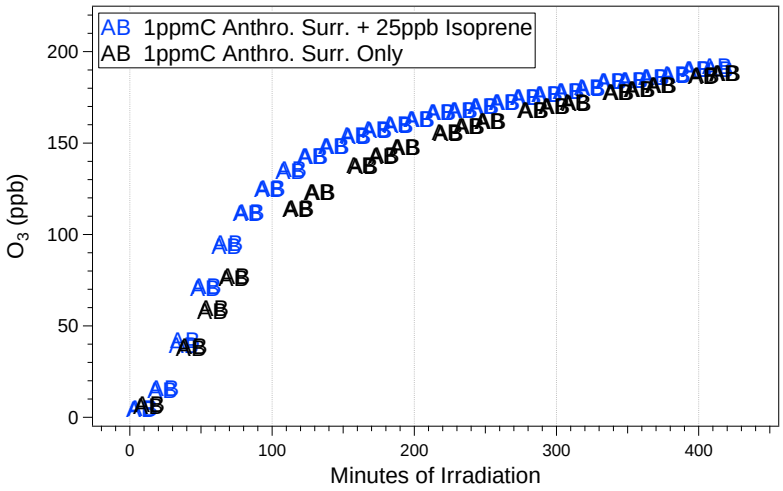

Figure 4.3: O_3 formation for the anthropogenic surrogate with 25ppb isoprene

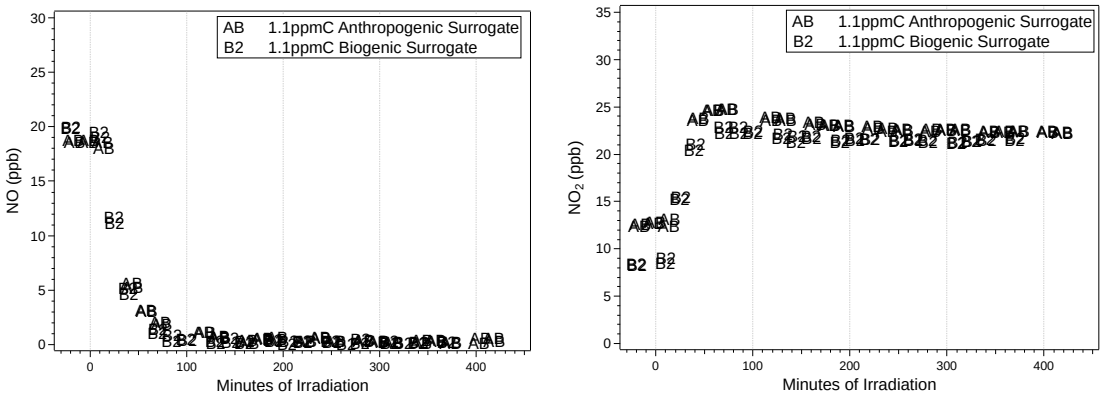

Figure 4.4: NO and NO_X trends for the biogenic surrogate compared to the anthropogenic surrogate

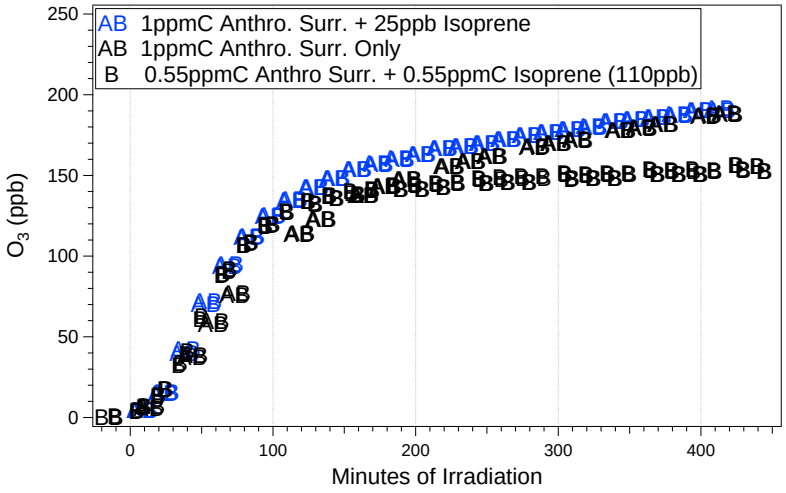

Figure 4.5: O_3 formation in the anthropogenic surrogate with and without 25ppb isoprene and in the biogenic surrogate

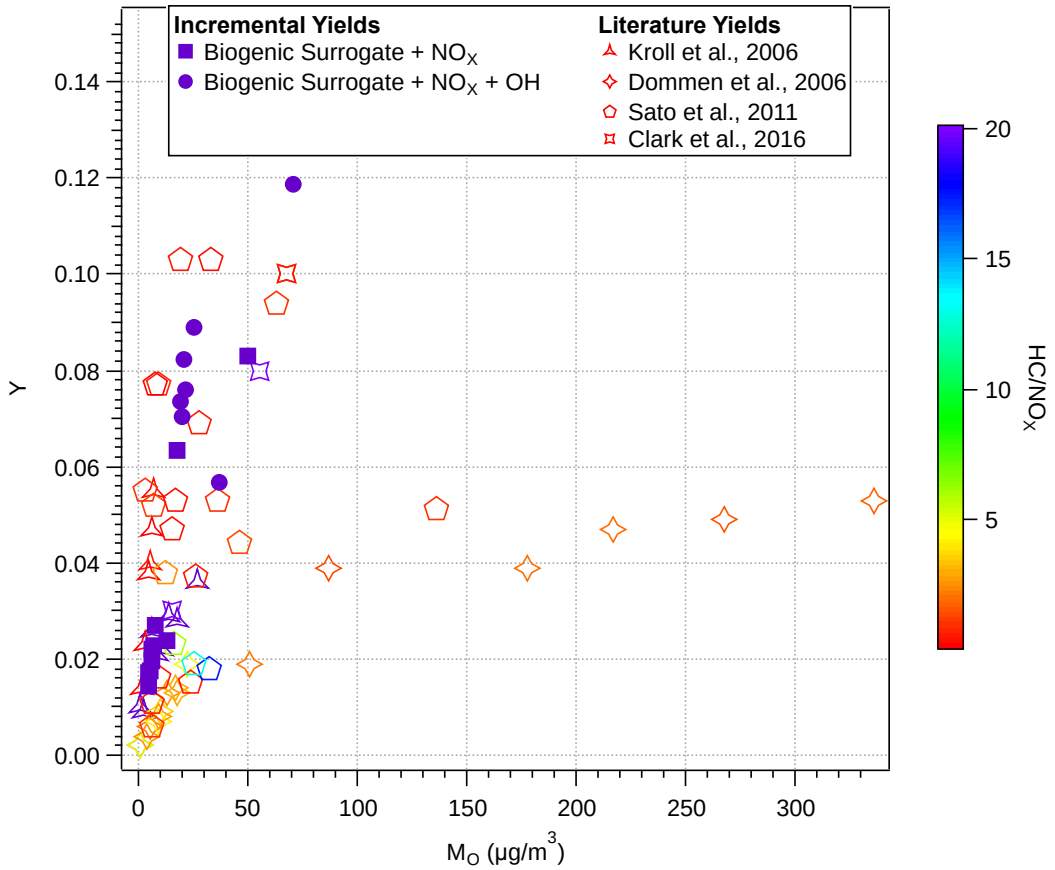

Figure 4.6: Aerosol yields from isoprene in the biogenic surrogate contrasted with literature values

Chapter 5: Incremental Aerosol Formation from *m*-Xylene in Biogenic Influenced Anthropogenic Surrogate Mixture

Introduction

As introduced in the previous chapters, the importance of controlling the reactivity of the chamber system is an important topic that needs to be explored as a way to create reactive conditions in the chamber that are comparable when comparing yields from different aerosol formers. Typically data is collected from single precursor experiments, but this work has introduced two different reactive gas mixtures to provide a base mixture to study aerosol formation across different species without variation in reactive conditions. This can enable a more accurate representation of aerosol formation from individual compounds in different environments, as the compound is no longer defining the overall reactivity of the chamber system. In Chapter 3, an anthropogenic surrogate reactive organic gas mixture was defined and the incremental aerosol formation from *m*-xylene was explored in that system. In Chapter 4, a biogenic influenced surrogate was defined by combining equal parts by ppmC of the anthropogenic surrogate and isoprene. Here, the incremental aerosol formation from *m*-xylene in this biogenic surrogate mixture will be explored and compared with incremental aerosol formation from the anthropogenic mixture. *m*-Xylene was selected due to its importance for aerosol formation as an aromatic hydrocarbon and due to the large amount of *m*-xylene/NO_X SOA data from the UCR/CE-CERT chambers to compare with. In all of these

experiments, the biogenic surrogate, NO_X, and hydrogen peroxide solution (when used), were injected into both of the dual reactors and well mixed between the two, then the reactors were isolated from each other and *m*-xylene was added to one reactor only, so as to have a comparable surrogate baseline for each experiment.

Results & Discussion

As was seen in the anthropogenic surrogate, the NO_X trends (Figures 5.1 and 5.2) are extremely similar in the biogenic surrogate mixtures whether or not *m*-xylene was added. For some experiments, 1ppm 50wt% H_2O_2 was added to ensure sufficient hydroxyl radical was available to maintain a comparable *m*-xylene decay to that seen in the anthropogenic surrogate runs. In these experiements, the NO decay is slightly sharper in both surrogate-only and surrogate with *m*-xylene experiments. Slightly more NO_2 decay was seen in the runs with added *m*-xylene. The hydrocarbon decay for all species (Figure 5.3) was extremely similar between the two sides in every experiment, regardless of the addition of *m*-xylene. The *m*-xylene decay for the side with added *m*-xylene and the surrogate only side can be seen in Figure 5.4. Despite the differences in initial *m*-xylene concentration, the overall decay rates are comparable in each side-by-side experiment. Ozone formation (Figures 5.5 and 5.6) was relatively similar (within ~20ppb) for all side-by-side experiments with and without added *m*-xylene, though it was fairly variable (ranging as low as 113ppb for 2045A and 176ppb for 2119B) between different experiments in the 2.2ppmC experiments. Similar to the anthropogenic surrogate runs, the side with added *m*-xylene formed slightly less O_3 in almost all cases. The trend in modeled OH was also fairly comparable to the trends seen in the

anthropogenic surrogate runs, with the added *m*-xylene having slightly lower overall integrated OH. Notable exceptions are the 2.2ppmC biogenic surrogate runs (with added OH), which the model estimated to have the exact same integrated OH levels. Overall, the gas phase species of the biogenic surrogate all seem to be very well controlled, having little change when 25ppb of *m*-xylene is added to the system. This indicates that the reactivity levels in the chamber are not being affected by the additional VOC.

In contrast to the well-controlled and repeatable gas phase data and to the isoprene yields from the biogenic surrogate alone (seen in Chapter 4), the incremental aerosol formation was highly variable across the repeat runs of the *m*-xylene/biogenic surrogate system. In a few scenarios (three of the runs without added hydroxyl), the added *m*-xylene actually suppressed aerosol formation in comparison with the surrogate only side, which is what led to the addition of H_2O_2 as a hydroxyl radical source so as to overcome the OH consumption by the *m*-xylene. The average positive yield values are plotted along with incremental *m*-xylene yields and literature values from single precursor *m*-xylene/NO_X experiments in Figure 5.6. The high variability in the *m*-xylene incremental yields in the biogenic surrogate poses a very interesting problem about how the reactivity of isoprene is dominating the chamber system in this mixture. Particularly perplexing are the repeatable and well-controlled gas-phase species trends seen in contrast with the widely varying incremental (in some cases negative) aerosol formation. This highlights the importance of isoprene chemistry not simply on its own but in mixtures with other aerosol forming precursors, as this data points to it having a very complicated and volatile relationship with other species present.

The density, volatility, and bulk chemical composition properties of the resulting incremental aerosol from *m*-xylene in the biogenic surrogate mixture can be found in Table 5.2. In contrast to the variance seen in the incremental aerosol yield, the bulk physical and chemical properties of the aerosol are fairly consistent over all runs. The density falls within the typical range of SOA, averaging around 1.45g/cm3. The volatility is fairly high, with only ~0.26 volume fraction remaining at 100C. Both of these physical properties compare well with the incremental *m*-xylene aerosol in the anthropogenic surrogate and with the isoprene surrogate only aerosol. Which is quite surprising, considering that the isoprene seems to have such a dominant role in overall aerosol formation. *Discuss AMS data & compare with literature

Conclusion

The use of the newly defined biogenic reactive organic gas surrogate mixture was explored for incremental aerosol formation from *m*-xylene. The gas phase species (NO_X trends, hydrocarbon decay, and ozone formation) between the surrogate only and surrogate with *m*-xylene experiments compared very well in the parallel runs and overall with each other. The measured yields of incremental aerosol from *m*-xylene in this isoprene-dominated surrogate, however, were extremely fickle despite well-controlled and repeatable gas phase conditions. It is proposed that isoprene plays a very complicated role in overall aerosol formation, with a significant sensitivity to the presence of other aerosol forming species. This highlights the need for more in depth study of isoprene aerosol and its role in the overall aerosol formation in the atmosphere, as it seems to be significantly impacted by the presence of other molecules. Future work should explore

incremental aerosol from a wide range of ratios of anthropogenic surrogate to isoprene. It is also thought that the impacts of different radical chemistry conditions should be explored by varying hydroxyl radical concentrations and overall HC/NO_X ratios of the surrogate and *m*-xylene system. It will be important to compare these same parameters on incremental aerosol from the anthropogenic surrogate alone so as to explore how isoprene is changing the aerosol formation and evolution in the controlled reactivity system.

Tables & Figures

Table 5.1: Initial conditions and aerosol yields for all experiments

Run	Δ*m*-Xylene (ppb)	NO_{init} (ppb)	$NO_{X,init}$ (ppb)	O_3 (ppb)	$^{\cdot}OH$	M_O (µg/m^3)	Y* (%)
1.1ppmC Anthropogenic Surrogate + 1.1ppmC Isoprene							
2045A	8	18.9	27.8	113	-	13.3	-0.3
2045B	-	18.6	27.7	121	-	13.4	-
2118A	14	19.5	32.9	151	-	31.5	-30.9
2118B	-	19.6	33.1	157	-	50.1	-
1.1ppmC Anthropogenic Surrogate + 1.1ppmC Isoprene + 1ppm H_2O_2							
2047A	18	18.8	29.7	115	19	39.1	2.6
2047B	-	19.1	30.1	124	19	37.0	-
2119A	15	22.7	35.3	164	26	76.4	8.2
2119B	-	22.7	35.4	176	28	71.1	-
0.55ppmC Anthropogenic Surrogate + 0.55ppmC Isoprene							
2120A	12	15.3	23.0	144	-	8.1	-3.7
2120B	-	15.2	22.9	157	-	17.4	-
2139A	11	19.7	27.2	146	22	13.6	15.0
2139B	-	20.1	28.0	150	28	6.2	-
2158A	15	13.9	22.5	135	17	5.9	2.3
2158B	-	14.1	22.8	146	27	4.4	-
2160A	12	14.4	21.1	141	18	8.1	6.1
2160B	-	14.2	21.3	148	23	2.8	-
0.55ppmC Anthropogenic Surrogate + 0.55ppmC Isoprene + 1ppm H_2O_2							
2121A	22	16.9	24.6	155	45	30.4	5.6
2121B	-	16.8	24.6	177	61	25.1	-
2155A	31	17.8	25.7	147	-	40.9	15.5
2155B	-	18.4	26.4	165	-	19.9	-
2170A	*	11.7	19.0	122	-	22.2	0.8*
2170B	-	11.7	18.9	144	-	21.5	-

Table 5.2: Incremental aerosol physical and bulk chemical properties

Run	Density (g/cm^3)	VFR‡	H:C	O:C
1.1ppmC Anthropogenic Surrogate + 1.1ppmC Isoprene				
2045A	1.44±0.03	-	1.46±0.02	0.52±0.04
2118A	1.45±0.04	0.26±0.05	1.42±0.01	0.46±0.01
1.1ppmC Anthropogenic Surrogate + 1.1ppmC Isoprene + 1ppm H_2O_2				
2047A	1.45±0.03	-	1.52±0.02	0.50±0.02
2119A	1.48±0.04	0.25±0.06	1.45±0.02	0.47±0.02
0.55ppmC Anthropogenic Surrogate + 0.55ppmC Isoprene				
2120A	1.46±0.04	0.23±0.05	1.41±0.03	0.46±0.02
2139A	1.46±0.04	0.24±0.04	1.46±0.09	0.49±0.04
2158A	1.41±0.06	0.26±0.02	1.40±0.18	0.65±0.13
2160A	1.43±0.05	0.28±0.03	1.47±0.21	0.57±0.10
0.55ppmC Anthropogenic Surrogate + 0.55ppmC Isoprene + 1ppm H_2O_2				
2121A	1.48±0.05	0.30±0.05	1.44±0.03	0.49±0.05
2155A	-	0.25±0.02	-	-
2170A	1.42±0.04	0.21±0.02	1.5±0.04	0.6±0.04

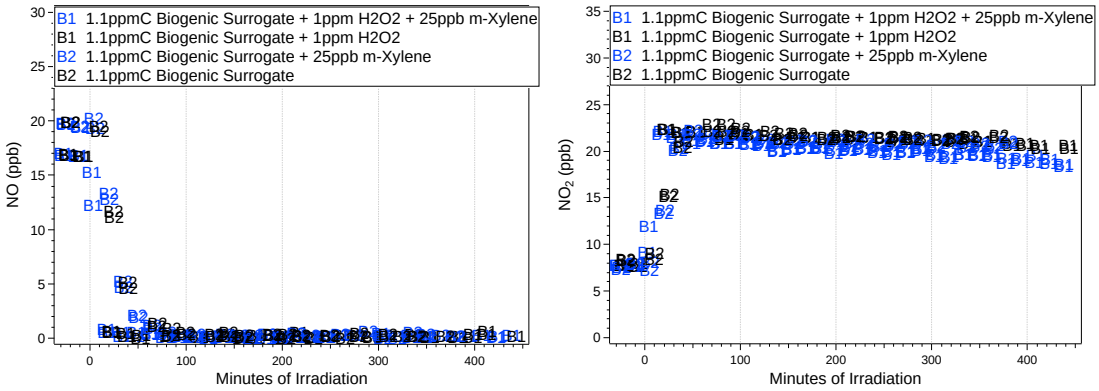

Figure 5.1: NO and NO_X trends in 1.1ppmC biogenic surrogate with and without *m*-xylene

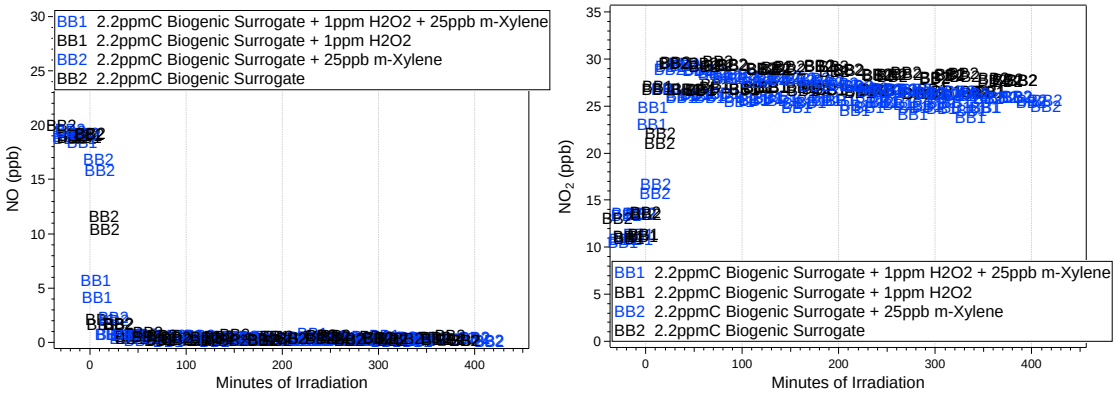

Figure 5.2: NO and NOX trends in 2.2ppmC biogenic surrogate with and wihout *m*-xylene

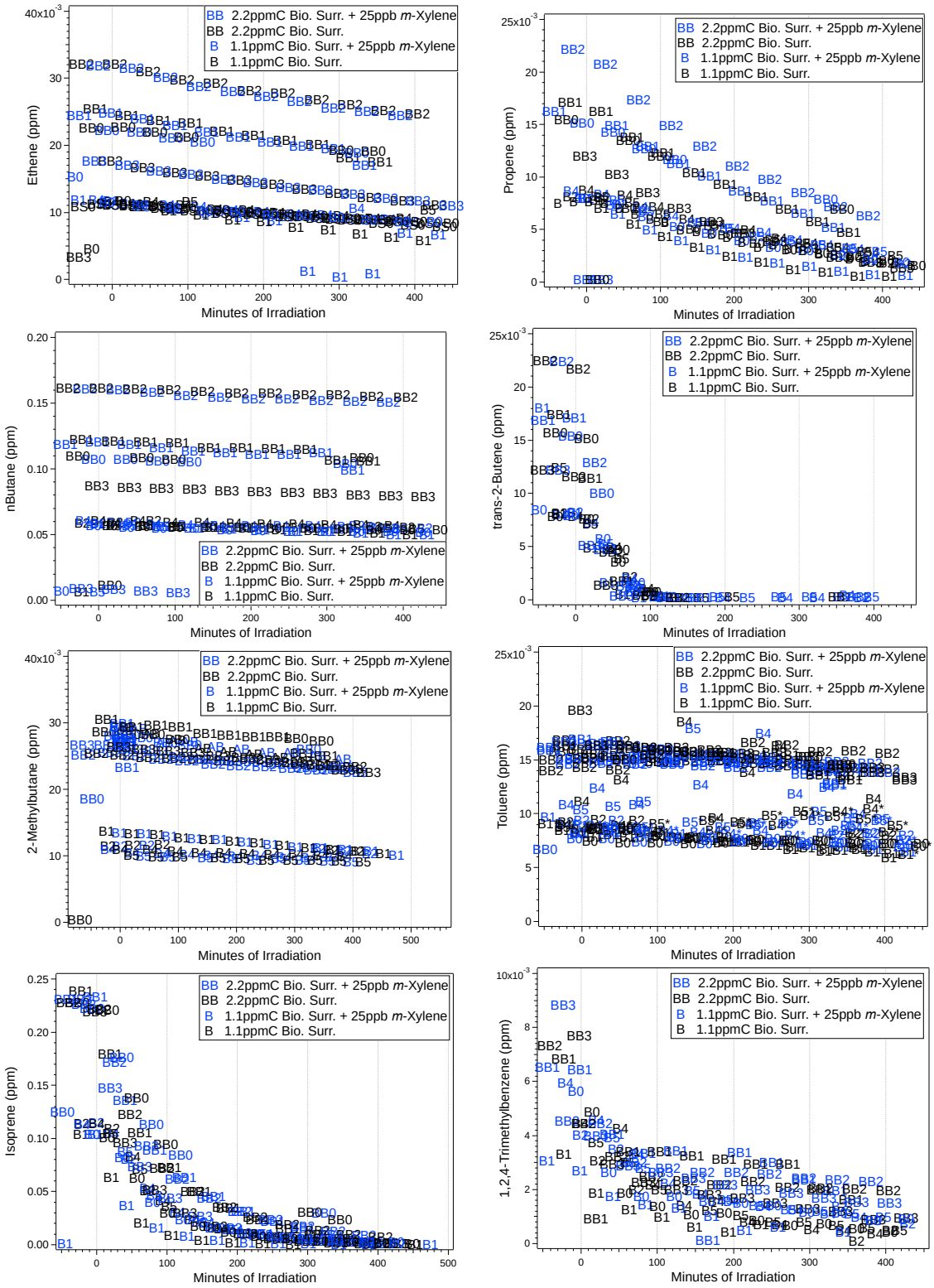

Figure 5.3: Gas phase decay trends of surrogate compounds

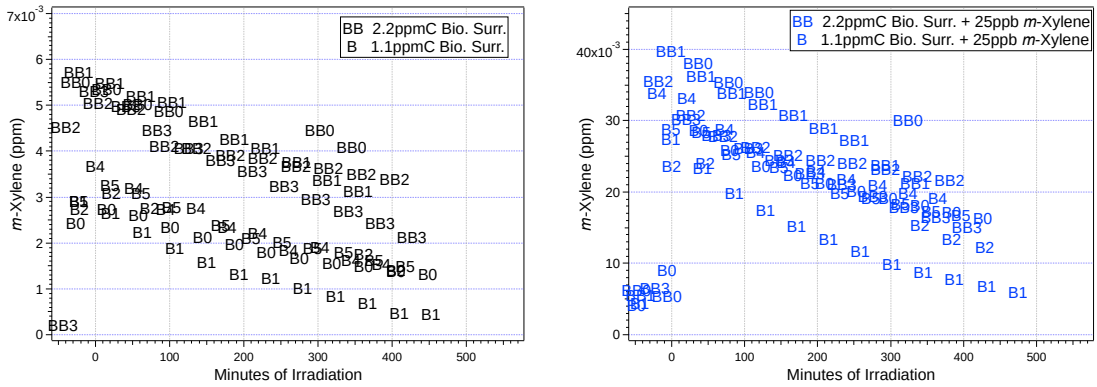

Figure 5.4: *m*-Xylene decay trends in the surrogate alone and with added *m*-xylene

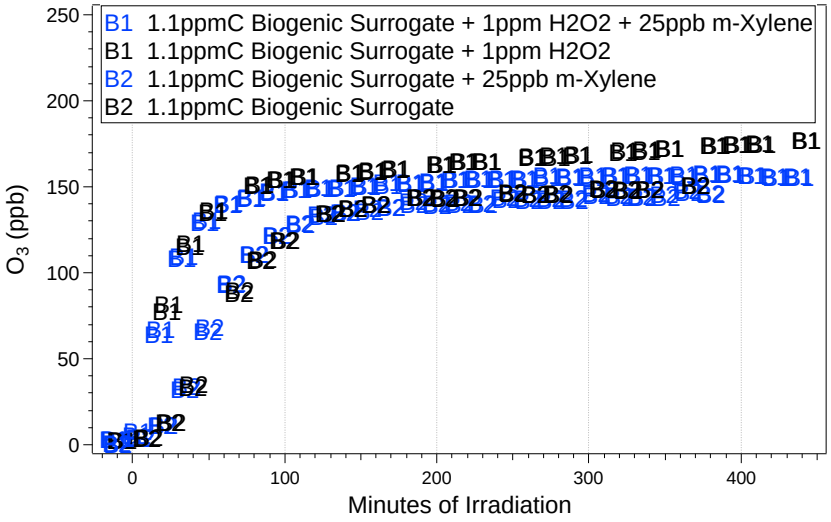

Figure 5.5: O_3 formation in 1.1ppmC biogenic surrogate with and without added *m*-xylene

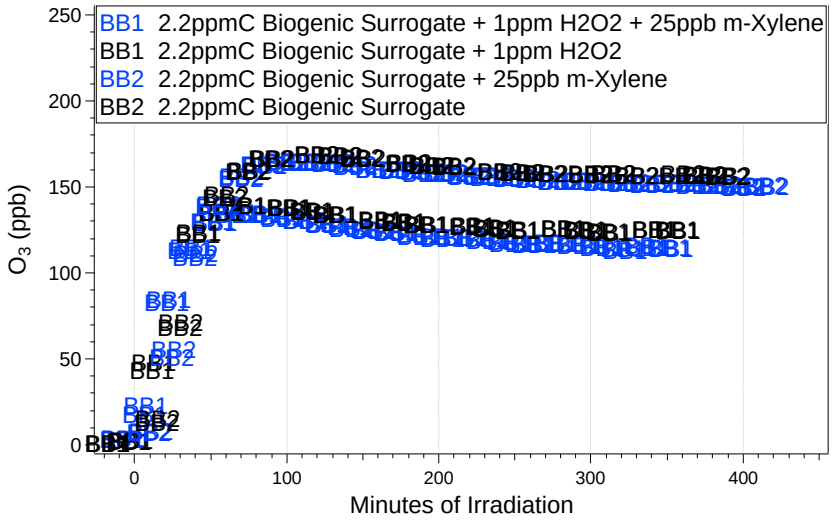

Figure 5.6: O_3 formation in 2.2ppmC biogenic surrogate with and without added *m*-xylene

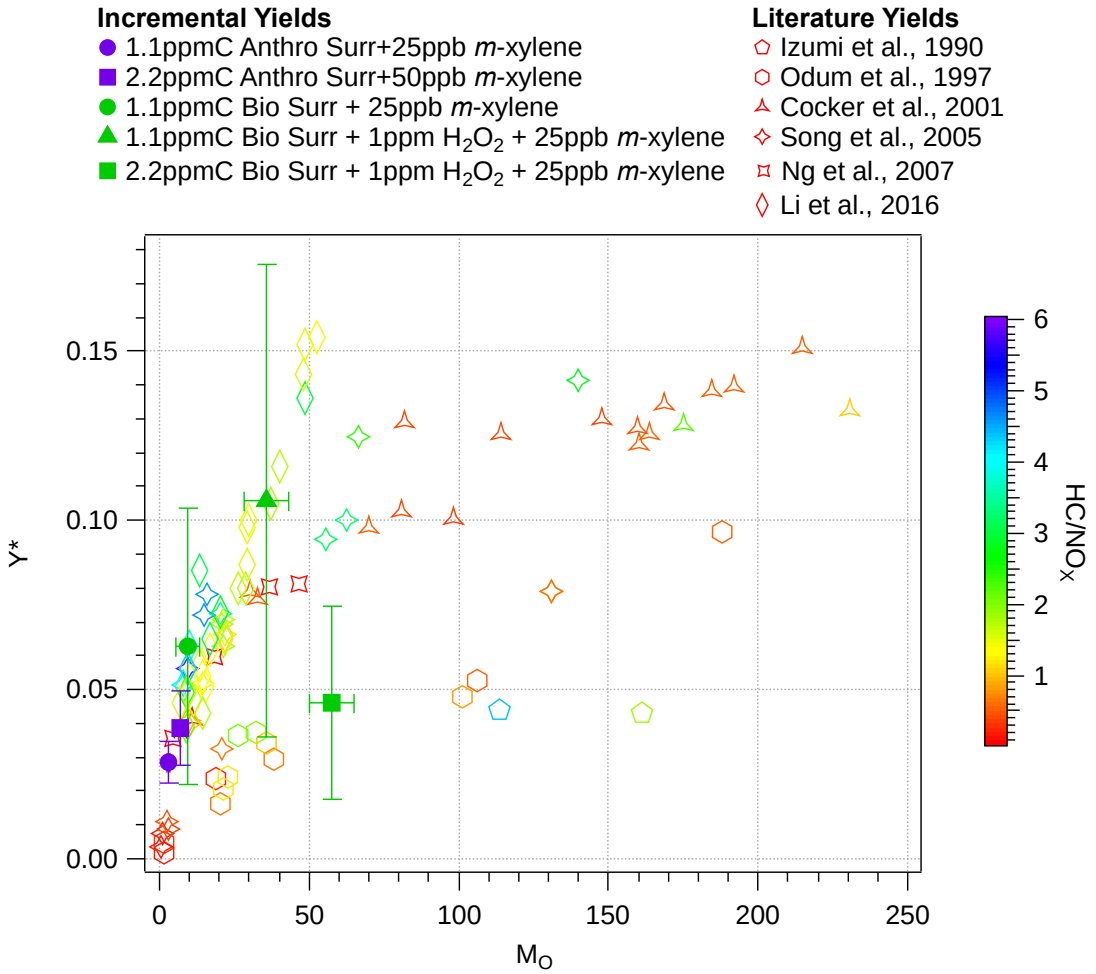

Figure 5.7: Incremental *m*-xylene yields in the biogenic and anthropogenic surrogates and contrasted with literature values

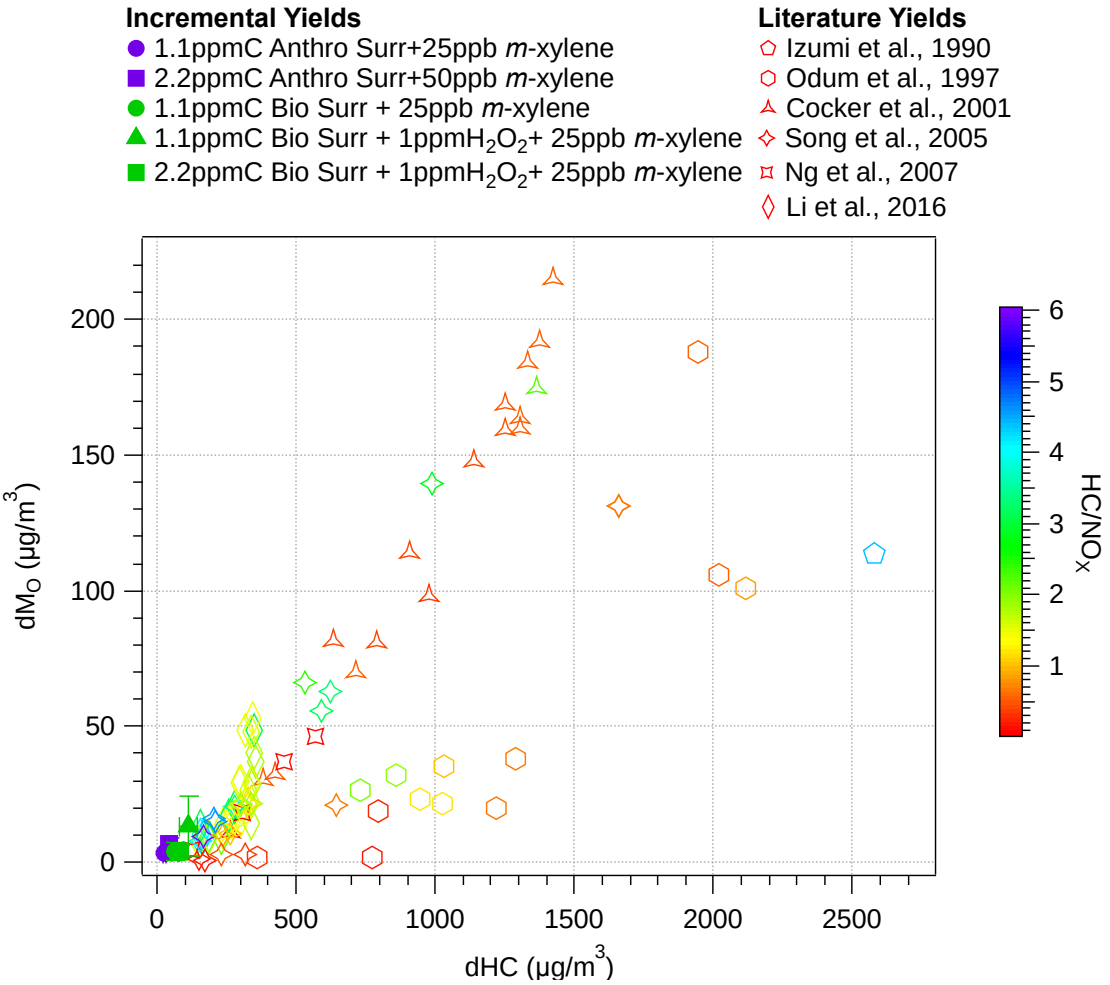

Figure 5.8: Aerosol formation (dMo) vs *m*-xylene decay (dHC) for incremental aerosol formation and literature values

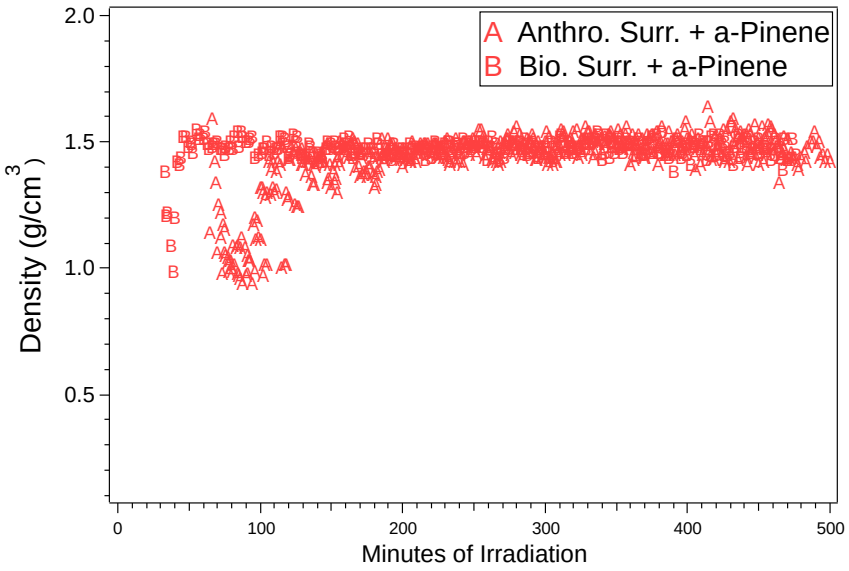

Figure 5.8: Density of aerosol from *m*-xylene in the anthropogenic and biogenic surrogate mixtures

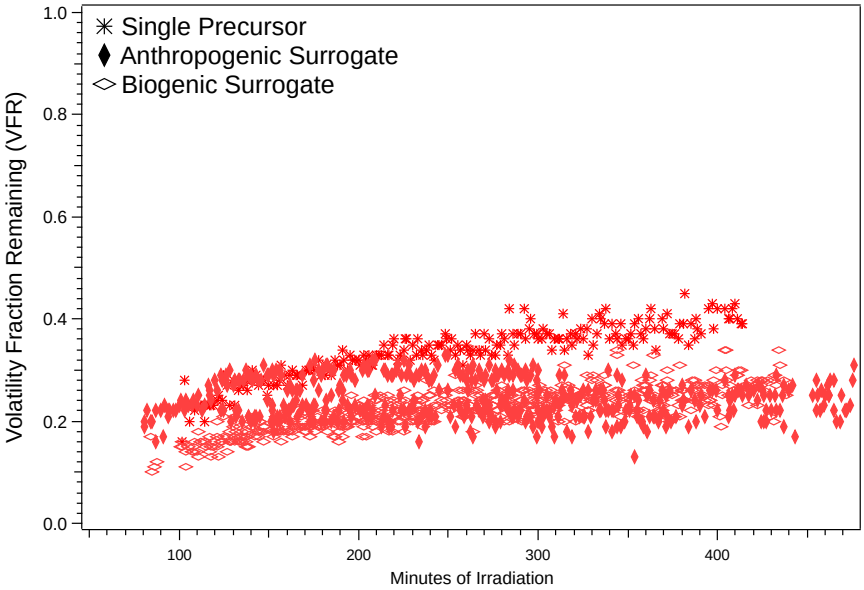

Figure 5.9: Volume fraction remaining (VFR) at 100C for incremental *m*-xylene aerosol in the biogenic and anthropogenic surrogates and in a single precursor NO_X system (Li et al)

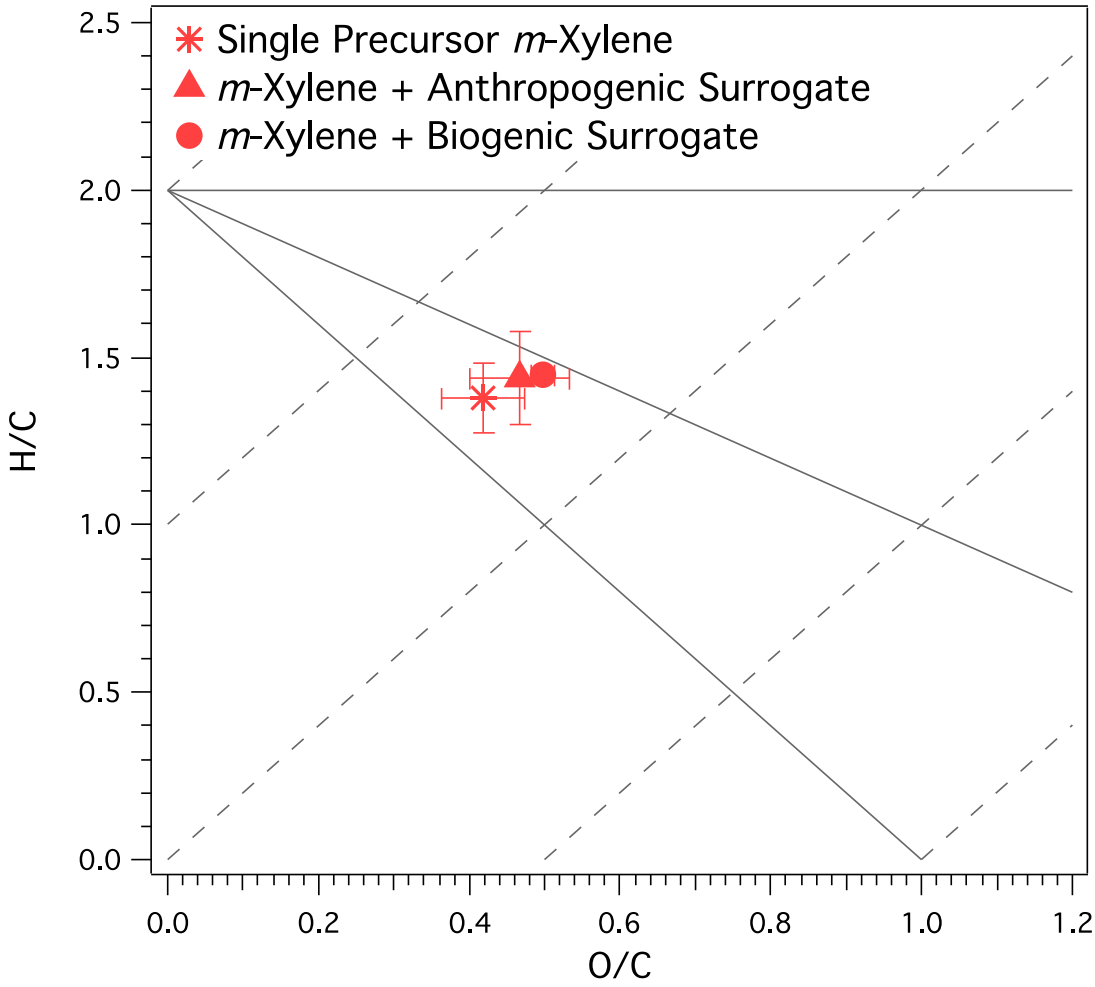

Figure 5.10: Van Krevelen diagram showing the bulk chemical composition of aerosol from *m*-xylene in the biogenic and anthropogenic surrogates and in a single precursor with NO_X system (Li et al)

Chapter 6: Incremental Aerosol Formation from Additional Compounds in Both Surrogate Mixtures

Introduction

In the previous chapters two different reactive organic gas surrogates (anthropogenic and biogenic influenced) were introduced and their control on the overall reactivity of the chamber system and impact on incremental aerosol formation from *m*-xylene was evaluated. To further test the robustness of the surrogates in controlling the gas phase and dictating overall aerosol formation, three additional aerosol-forming hydrocarbons were explored with both surrogates. The additional compounds evaluated are α-pinene (a widely studied biogenic monoterpene), 1,2,4-trimethylbenzene (a well-known aromatic hydrocarbon), and 1-methylnaphthalene (a polyaromatic hydrocarbon). These three compounds were selected as being representative of a range of different emission sources and types of functional aerosol forming species. Again, the experiments were run in the UCR/CE-CERT dual atmospheric chambers, which allow for each incremental species studied (added to reactor A) to have its own surrogate baseline (reactor B) at well controlled initial surrogate and NO_X concentrations.

Results & Discussion

The initial experimental conditions, amount of hydrocarbon reacted, and O_3 and aerosol formation for all runs can be found in Table 6.1. The NO and NO_2 traces for all runs can be found in Figure 6.1. The NO decay matches very well between surrogate-

only and surrogate with added hydrocarbon sides for all three compounds. The NO_2 trends are very close in the 1,2,4-trimethylbenzene with surrogate experiments, while NO_2 seems to decay slightly more towards the end of the experiments in both the α-pinene and 1-methylnaphthalene runs. 1,2,4-Trimethylbenzene has a k_{OH} of $3.15x10^{-11}$ $cm^3mol^{-1}sec^{-1}$ (Atkinson, 1986) while α-pinene and 1-methylnaphthalene have higher k_{OH} values of $5.32x10^{-11}$ and $5.3x10^{-11}$ $cm^3mol^{-1}sec^{-1}$, respectively (Atkinson, 1986; Atkinson and Aschmann, 1987). For comparison, *m*-xylene has a lower k_{OH} than all three compounds looked at here at $2.22x10^{-11}$ $cm^3mol^{-1}sec^{-1}$(Atkinson, 1985).

Despite the slight difference in NO_2 trends, the overall gas phase trends for both the anthropogenic (Figure 6.2) and biogenic (Figure 6.3) surrogates match well between surrogate-only and surrogate with added compound runs. When 1-methylnaphthalene is added to the surrogate, it slightly slows the decay of both *m*-xylene and 1,2,4-trimethylbenzene in the anthropogenic surrogate. It doesn't have as strong of an effect on any compounds in the biogenic surrogate, which is attributed to those compounds being at such lower concentrations in the biogenic mixture. Even though α-pinene has a comparable k_{OH} value to 1-methylnaphthalene, it does not seem to slow any of the surrogate species decay rates down, most likely due to how quickly it reacts out of the system. The decay rate of α-pinene is the same whether it is added to the anthropogenic or the biogenic surrogate, however, the decay rates of both 1,2,4-trimethylbenzene and 1-methylnaphthalene are slightly slower in the biogenic surrogate than in the anthropogenic surrogate (Figure 6.4). In an attempt to resolve this, 1ppm of H_2O_2 was added to the 1,2,4-trimethylbenzene and 1-methylnaphthalene biogenic surrogate systems to ensure

that sufficient radical species were available for everything to react uninhibited. However, even with the added hydroxyl radical, the decays of 1,2,4-trimethylbenzene and 1-methylnaphthalene were slower in the biogenic surrogate mixture than in the anthropogenic surrogate mixture.

The O_3 formation trends for both surrogate mixtures with α-pinene, 1,2,4-trimethylbenzene, and 1-methylnaphthalene added can be found in Figure 6.5. O_3 levels were slightly lower in both the anthropogenic and biogenic surrogate systems when α-pinene was added, though the formation rate was fairly similar in all cases. The addition of 1,2,4-trimethylbenzene to either surrogate did not have any effect on O_3 formation, except when H_2O_2 was added to the system, in which case a slight depression of O_3 was seen. 1-Methylnaphthalene actually causes interference in the O_3 analyzer due to its having the same UV absorption as O_3, which is why a positive O_3 value is seen before the lights are turned on in the 1-methylnaphthalene runs and also why there appears to be a decaying O_3 value throughout the experiments with 1-methylnaphthalene added. Considering that 1-methylnaphthalene is actually causing a positive bias on the O_3 readings, then we actually observe a strong decrease in overall O_3 formation in both the anthropogenic and biogenic surrogates when it is added to the system, particularly when additional hydroxyl radical is added.

The aerosol yields from α-pinene in the anthropogenic and biogenic surrogate mixtures and in single precursor experiments with NO_X can be found in Figure 6.6. It was found that α-pinene exhibited a higher incremental yield in the biogenic surrogate than in the anthropogenic surrogate (0.5 vs 0.3). Further, these incremental α-pinene yields are

much higher than previous yields seen in literature for α-pinene/NOX systems and only compare with a few higher NO_X runs in the UCR/CE-CERT chambers. Aerosol yields from 1,2,4-trimethylbenzene in the anthropogenic and biogenic surrogate systems can be found in Figure 6.7 along with single precursor yields from UCR/CE-CERT data. In a similar trend as was seen with the α-pinene incremental aerosol, the incremental 1,2,4-trimethylbenzene aerosol formation is slightly higher in the biogenic surrogate than in the anthropogenic surrogate (0.10 vs 0.07). However, when H_2O_2 is added to the biogenic system in an attempt to increase the decay rate of trimethylbenzene, a significant increase is seen in aerosol formation from the biogenic surrogate and the incremental effect of 1,2,4-trimethylbenzene is significantly outweighed, leading to a much smaller incremental yield of 0.02. The incremental aerosol formation from 1-methylnaphthalene in the biogenic and anthropogenic surrogates juxtaposed with single precursors 1-methylnaphthalene chamber yields is seen in Figure 6.8. Again it was found that the incremental aerosol formation in the biogenic surrogate was greater than in the anthropogenic surrogate (0.74 vs 0.61). The hydroxyl radical concentration was also increased in the 1-methylnaphthalene/biogenic surrogate system in an attempt to reconcile the decay rate with that seen in the anthropogenic surrogate. As was expected, the biogenic surrogate itself formed much more baseline aerosol with the added H_2O_2. However, contrary to results seen in the *m*-xylene and 1,2,4-trimethylbenzene systems, the reactor with the added 1-methylnaphthalene formed even more additional aerosol, resulting in a yield of 1.4. Previous yields of over 100% have been seen from 1-methylnaphthalene in the work done by Chen et al (2016) and were seen in irradiation

with NO. The results here are extremely surprising given that the 1-methylnaphthalene decay was actually slower in the biogenic surrogate yet exhibited higher additional aerosol formation. All physical and chemical properties of resulting aerosol in this work can be found in Table 6.2.

The resulting aerosol density was around 1.4g/cm^3 for all compounds added to either the anthropogenic or biogenic surrogate mixtures. Similar to the results from the *m*-xylene incremental aerosol, the 1,2,4-trimethylbenzene incremental aerosol exhibits a low initial density in both surrogate mixtures, possibly indicating the formation of small solid particles upon initial nucleation. The incremental α-pinene and 1-methylnaphthalene aerosols did not exhibit any low initial density values, despite the fact that the formation of small fractal particles has been observed and verified for chamber studies of 1-methylnaphthalene with NO_X by Chen et al (2016). The α-pinene incremental aerosol density in both systems did show a decreasing trend throughout aging, which is not typical of chamber generated SOA.

Figure 6.12 displays the volume fraction remaining (VFR) at 100°C for incremental aerosol in the anthropogenic and biogenic surrogate systems for α-pinene, 1,2,4-trimethylbenzene, and 1-methylnaphthalene along with VFR data from single precursor with NO_X experiments for all compounds. It is found that the volatility trends for each compound compare very well with each other for each separate precursor. This is also exhibited when looking at the *m*-xylene volatility comparison (Figure 5.9). This result is quite encouraging because it could be indicating that while the surrogate mixture

is influencing the total aerosol formed, the bulk aerosol properties are still being heavily steered by the added aerosol-forming precursor.

This concept of the incremental SOA precursor dictating the properties of the resulting aerosol despite the surrogate itself directing the total aerosol formed is further supported by the bulk chemical composition results from the HR-ToF-AMS. A Van Krevelen diagram juxtaposing the H:C and O:C ratios of each resulting aerosol in the different surrogate mixtures and their single precursor counterparts can be found in Figure 6.13. It can be seen that, by and large, the aerosols from the different precursors (including *m*-xylene) seem to cluster together at different points on the chart. This adds further weight to the trend indicated by the volatility that the overall properties of the aerosol may still be controlled by the added incremental aerosol former. This sets an interesting juxtaposition for what factors are influencing aerosol formation and composition in the ambient atmosphere where many different species are in play.

Conclusion

The two different surrogate mixtures representing urban atmospheres with and without a heavy biogenic influence (e.g. anthropogenic surrogate and biogenic surrogate) were further tested by the addition of α-pinene, 1,2,4-trimethylbenzene, and 1-methylnaphthalene. The robustness of the surrogate's control over the gas phase chemistry was challenged by the high k_{OH} of 1-methylnaphthalene, though overall the trends were still remarkably similar. Compared to literature values for single precursor chamber studies with NO_X, the incremental yields from all three additional compounds

tended to be quite high, with the exception of incremental aerosol from 1,2,4-trimethylbenzene in the biogenic surrogate with added hydroxyl radical. The additional aerosol formation from the biogenic surrogate with the added hydroxyl diluted the strong incremental aerosol formation seen in the system without added hydroxyl. Despite the strong control of the surrogate over the incremental aerosol yields from these different compounds, the bulk aerosol properties remained remarkably similar for each compound between single precursor/NO_X and biogenic and anthropogenic surrogate experiments. This result is very encouraging as it portends a potential disconnect between the factors driving overall aerosol formation and the factors dictating aerosol composition.

This work sets the stage for additional studies on controlling the chamber environment with different surrogate mixtures. Further exploration is recommended in evaluating these two mixtures with different aerosol forming compounds at an array of surrogate to added precursor ratios. Further, it will be important to look at varying radical source concentrations in the system so as to test both the robustness of the mixtures and the limits of this type of incremental aerosol evaluation.

Tables & Figures

Table 6.1: Initial conditions, ozone and aerosol formation for α-pinene, 1,2,4-trimethylbenzene, and 1-methylnaphthalene in the anthropogenic and biogenic surrogates

Run	HC	ΔHC (ppb)	NO_{init} (ppb)	$NO_{x,init}$ (ppb)	O_3 (ppb)	$^{\cdot}OH$	M_O ($\mu g/m^3$)	Y* (%)
1.1ppmC Anthropogenic Surrogate + 25ppb Additional Hydrocarbon								
2133A	α-Pinene	22	13.5	22.6	145	31	41.7	33.9
2133B	-	-	13.3	22.6	166	50	0.1	-
2137A	124-TMB	18	15.5	25.2	172	38	7.6	6.5
2137B	-	-	15.4	25.0	173	55	1.7	-
2163A	1-MN	36	14.7	23.4	121	-	125.8	60.8
2163B	-	-	14.4	23.4	143	-	<0.1	-
1.1ppmC Biogenic Surrogate + 25ppb Additional Hydrocarbon								
2134A	α-Pinene	23	13.8	22.8	139	24	71.2	49.9
2134B	-	-	14.1	23.3	155	30	7.0	-
2138A	124-TMB	13	19.3	27.0	147	22	13.0	10.2
2138B	-	-	19.6	27.6	150	30	6.5	-
2169A*	124-TMB	14	12.7	19.9	126	34	20.3	1.5
2169B*	-	-	12.7	19.9	138	48	19.3	-
2159A	1-MN	21	15.2	23.3	127	-	95.0	73.7
2159B	-	-	15.1	23.5	141	-	5.2	-
2168A*	1-MN	26	12.3	19.8	103	-	230.6	139.3
2168B*	-	-	12.1	20.0	135	-	20.8	-

Table 6.2: Physical and chemical properties of aerosol formed from surrogate + additional hydrocarbon mixtures

Run	HC	Density (g/cm^3)	VFR	H:C	O:C
1.1ppmC Anthropogenic Surrogate + 25ppb Additional Hydrocarbon					
2133A	α-Pinene	1.42±0.07	0.27±0.14	1.43±0.01	0.42±0.01
2137A	124-TMB	1.48±0.02	0.39±0.09	1.33±0.19	0.51±0.10
2163A	1-MN	1.42±0.03	0.70±0.03	0.97±0.07	0.52±0.08
1.1ppmC Biogenic Surrogate + 25ppb Additional Hydrocarbon					
2134A	α-Pinene	1.37±0.08	0.21±0.08	1.44±0.05	0.42±0.02
2138A	124-TMB	1.47±0.04	0.27±0.07	1.48±0.13	0.47±0.06
2169A	124-TMB	1.42±0.05	0.25±0.02	1.52±0.06	0.53±0.05
2159A	1-MN	1.43±0.02	0.63±0.06	1.15±0.14	0.56±0.06
2168A	1-MN	1.39±0.05	0.60±0.01	1.11±0.04	0.48±0.05

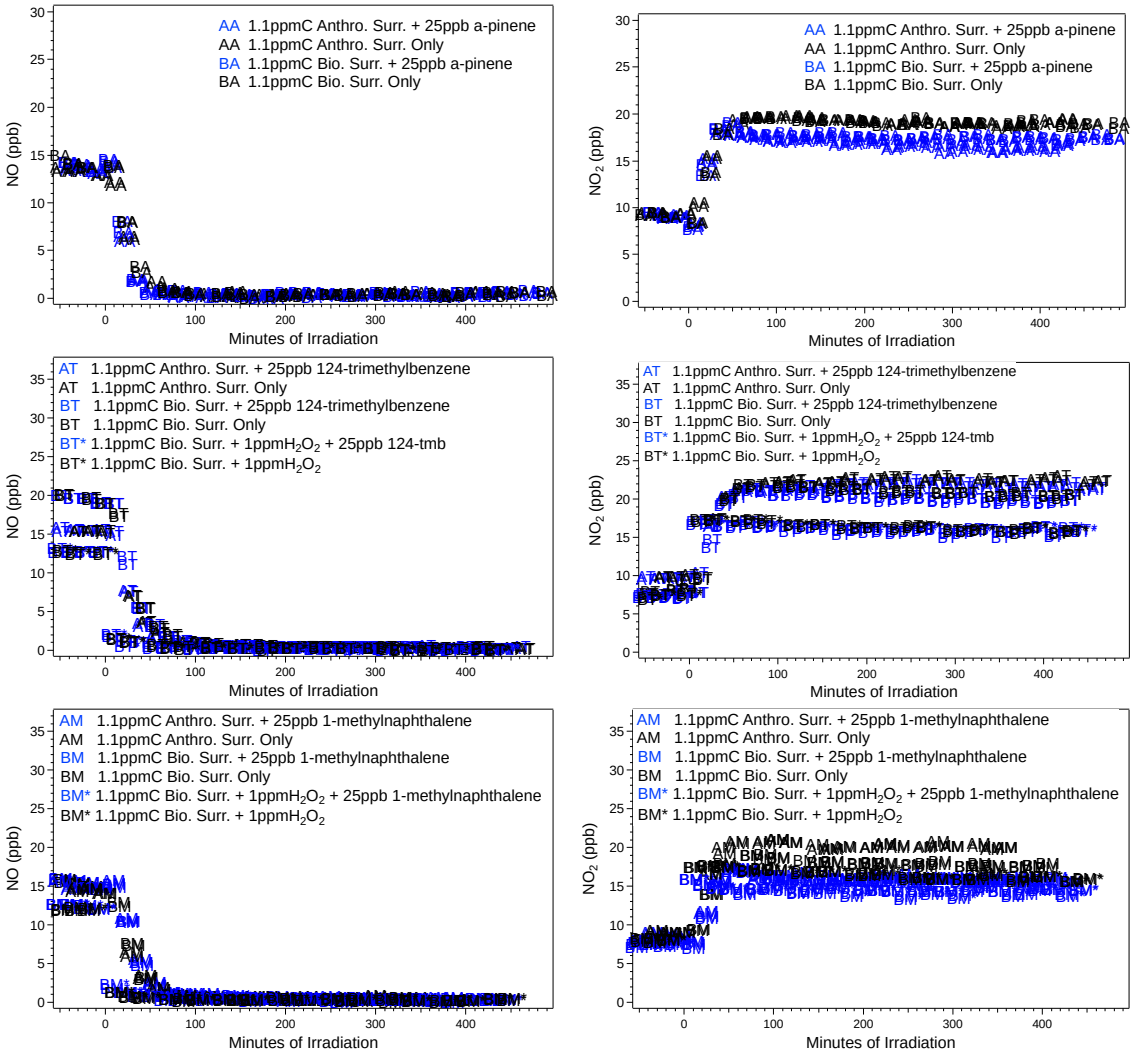

Figure 6.1: NO and NO_2 traces for all runs with α-pinene, 1,2,4-trimethylbenzene, and 1-methylnaphthalene added to the anthropogenic and biogenic surrogates

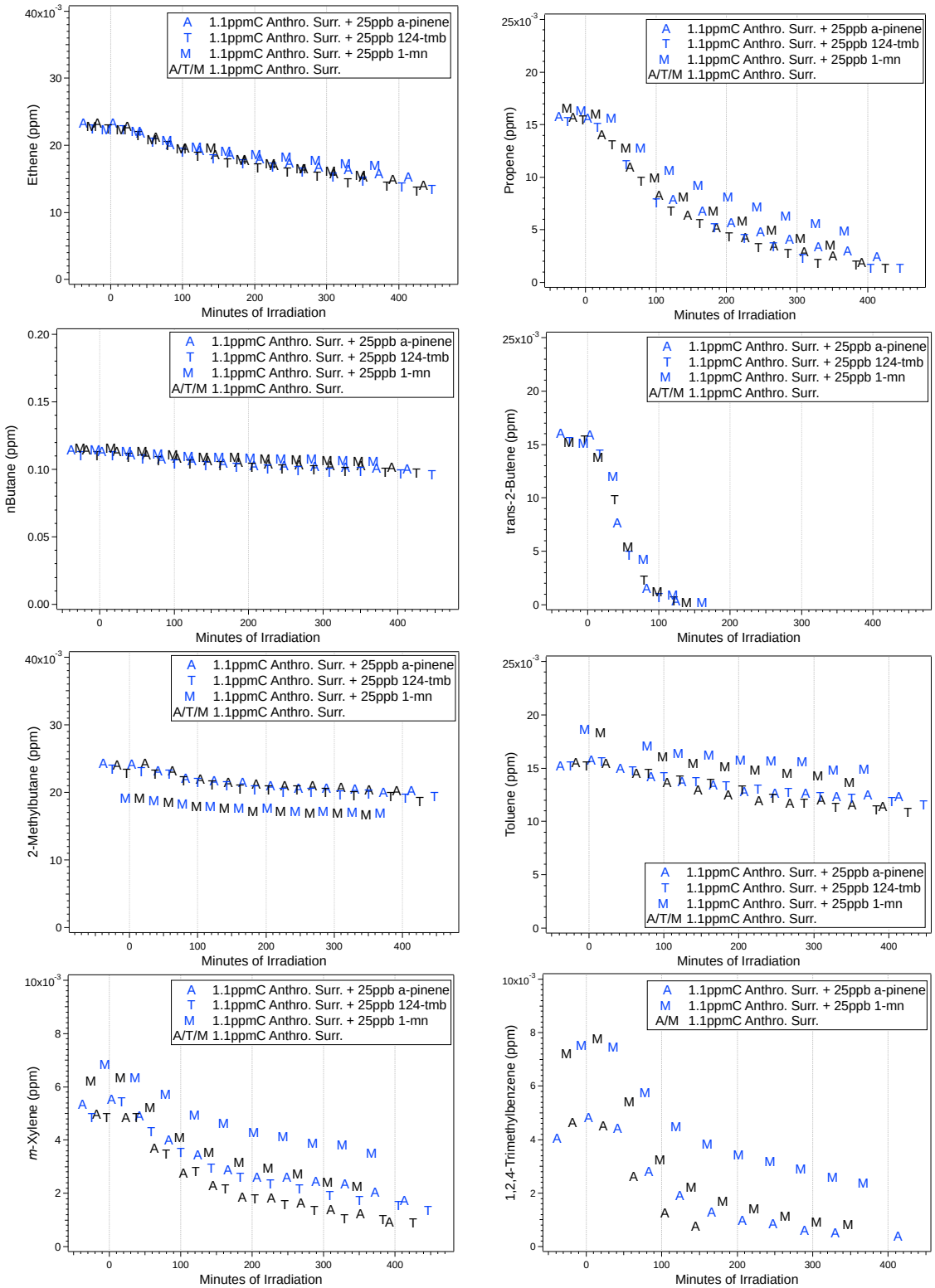

Figure 6.2: Gas phase traces for all anthropogenic surrogate runs

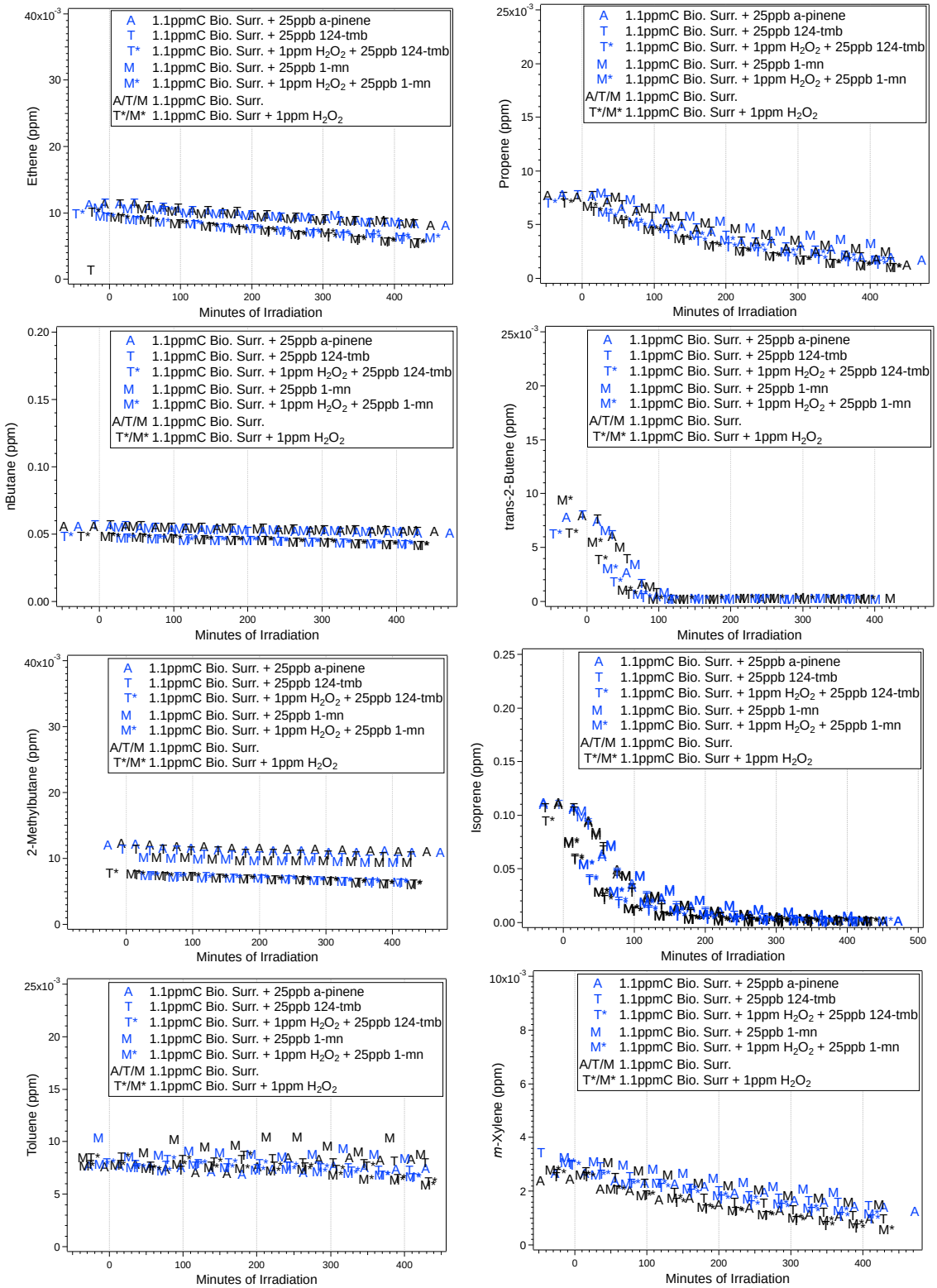

Figure 6.3: Gas phase traces for all biogenic surrogate runs

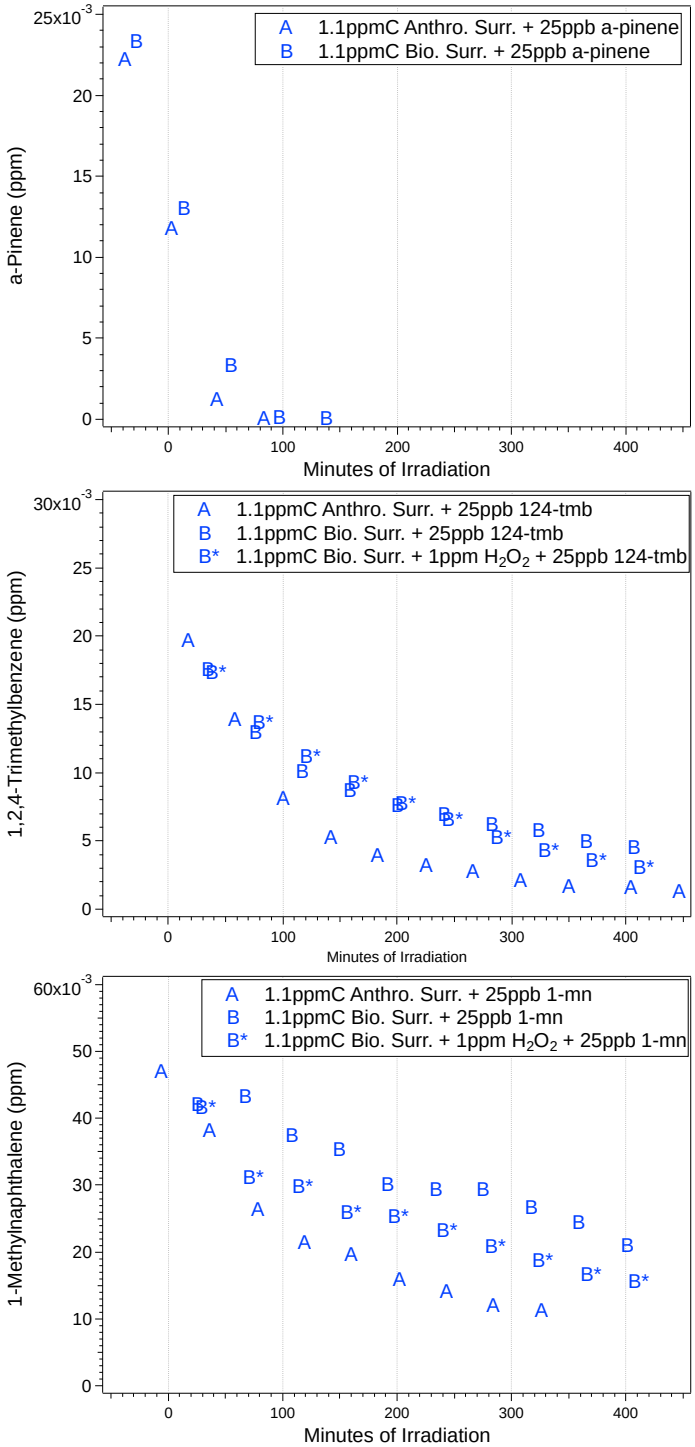

Figure 6.4: Gas phase decay of α-pinene, 1,2,4-trimethylbenzene, and 1-methylnaphthalene in the anthropogenic and biogenic surrogate mixtures

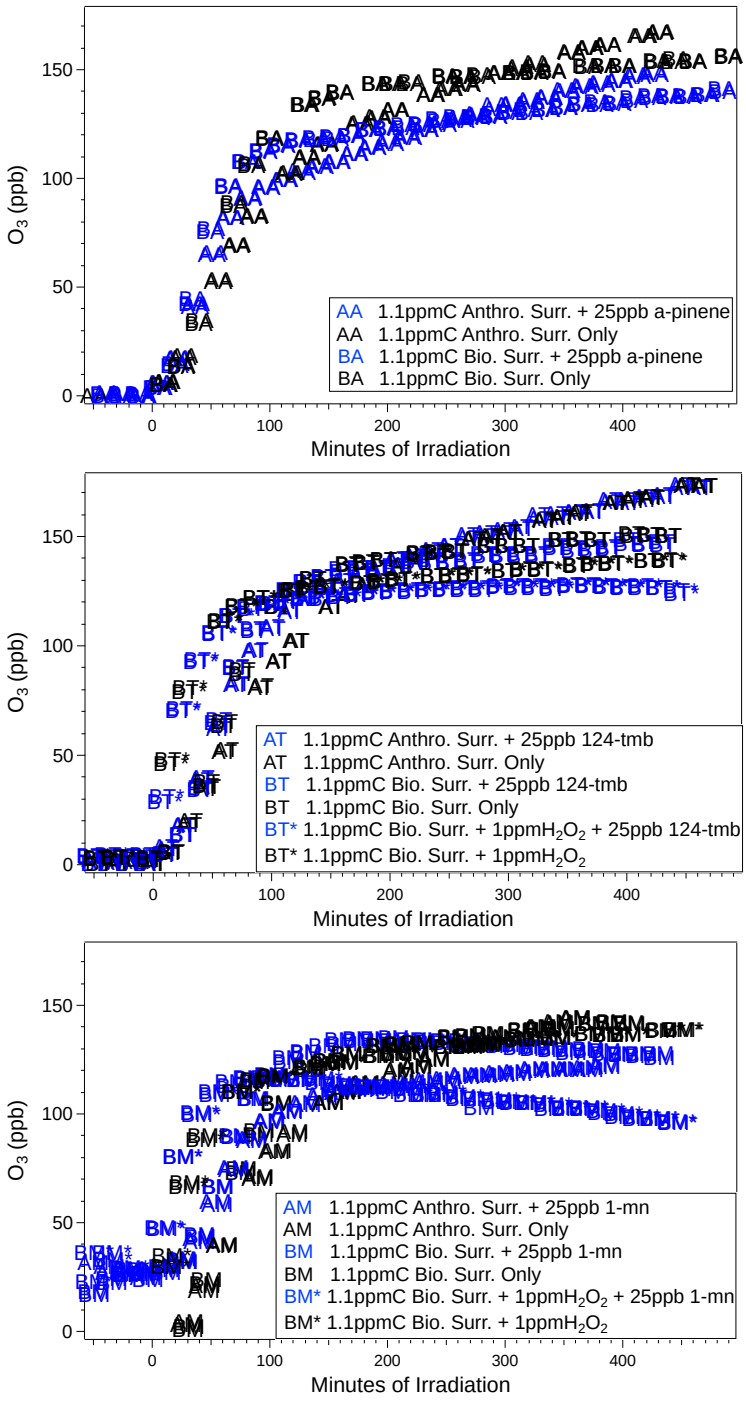

Figure 6.5: O_3 formation from α-pinene, 1,2,4-trimethylbenzene, and 1-methylnaphthalene in the anthropogenic and biogenic surrogates

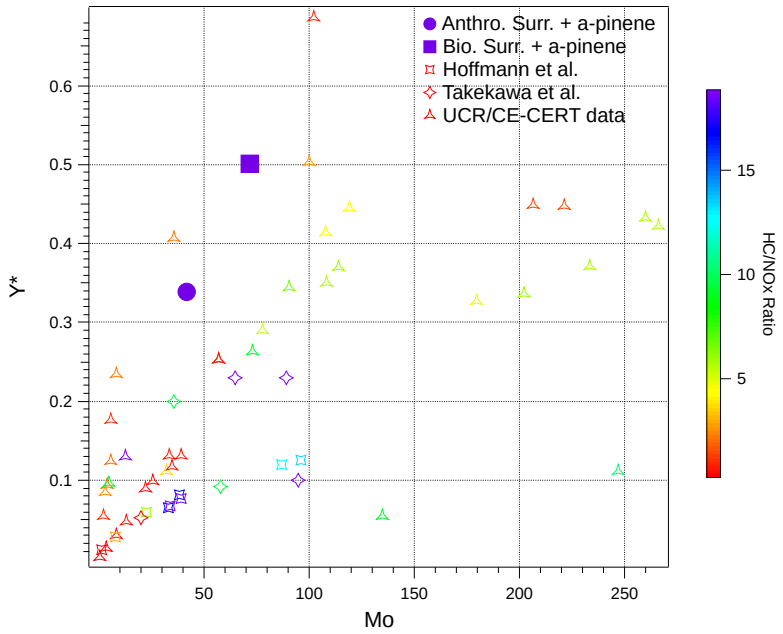

Figure 6.6: Incremental α-pinene yields in the anthropogenic and biogenic surrogate mixtures along with single precursor α-pinene/NO_X yields from literature and the UCR/CE-CERT chamber

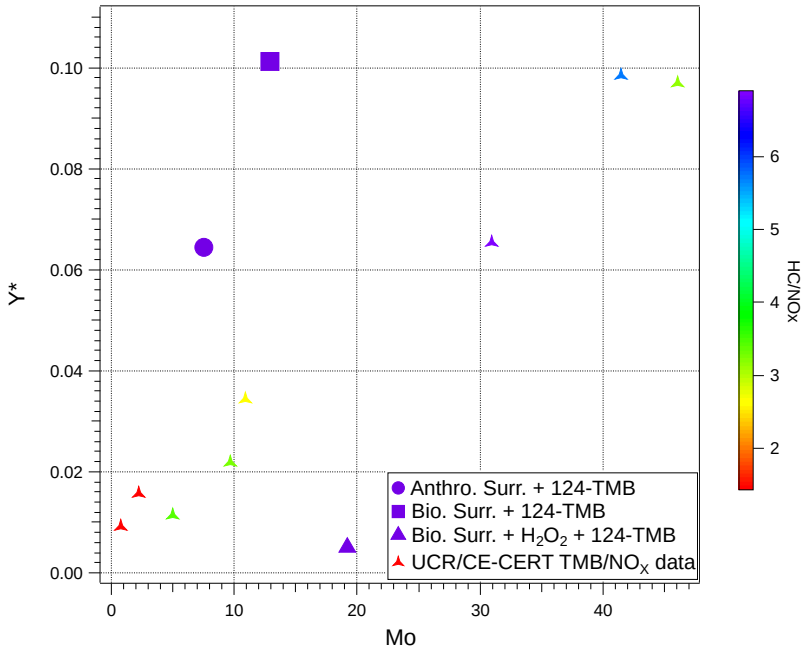

Figure 6.7: Incremental 1,2,4-trimethylbenzene yields in the anthropogenic and biogenic surrogate mixtures along with single precursor 1,2,4-trimethylbenzene/NO_X yields from the UCR/CE-CERT chamber

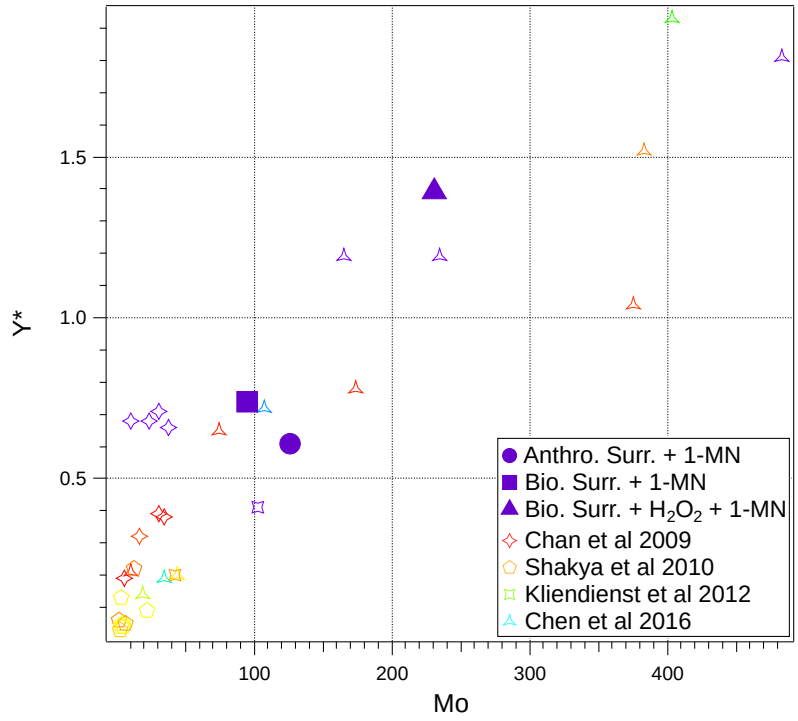

Figure 6.8: Incremental 1-methylnaphthalene yields in the anthropogenic and biogenic surrogate mixtures along with single precursor 1-methylnaphthalene/NO_X yields from literature

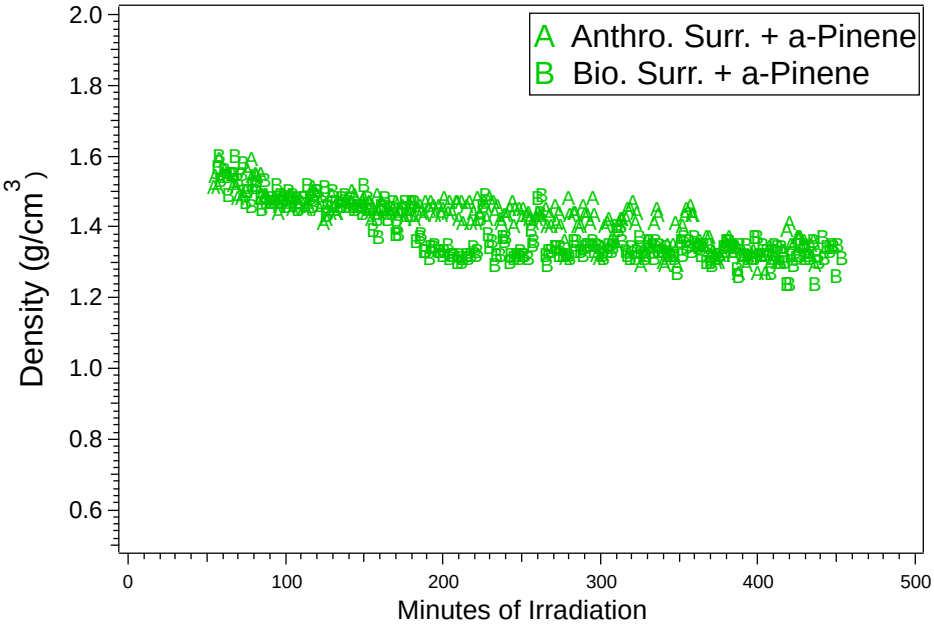

Figure 6.9: Density traces of α-pinene incremental SOA in the anthropogenic and biogenic surrogate mixtures

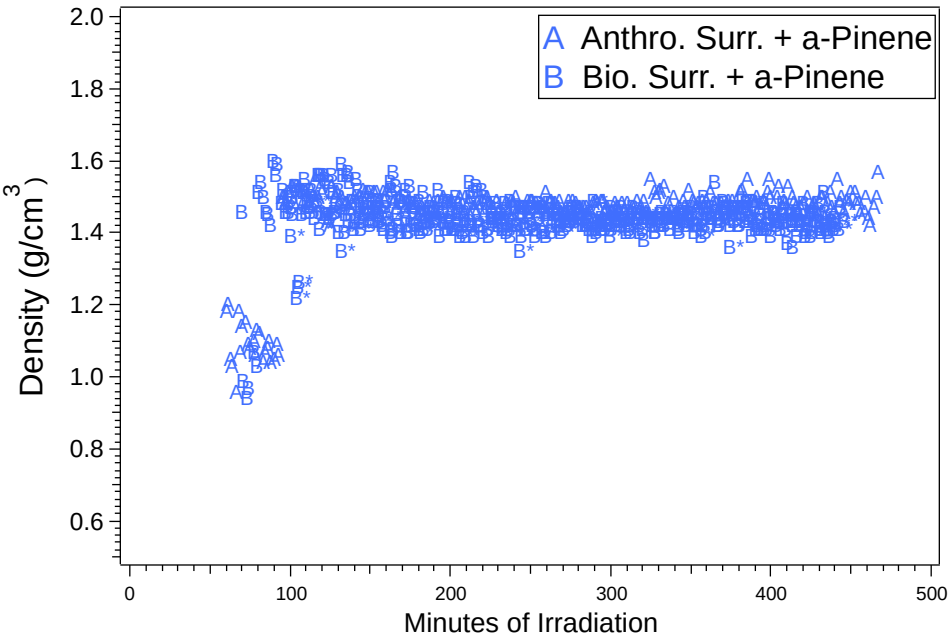

Figure 6.10: Density traces of 1,2,4-trimethylbenzene incremental SOA in the anthropogenic and biogenic surrogate mixtures

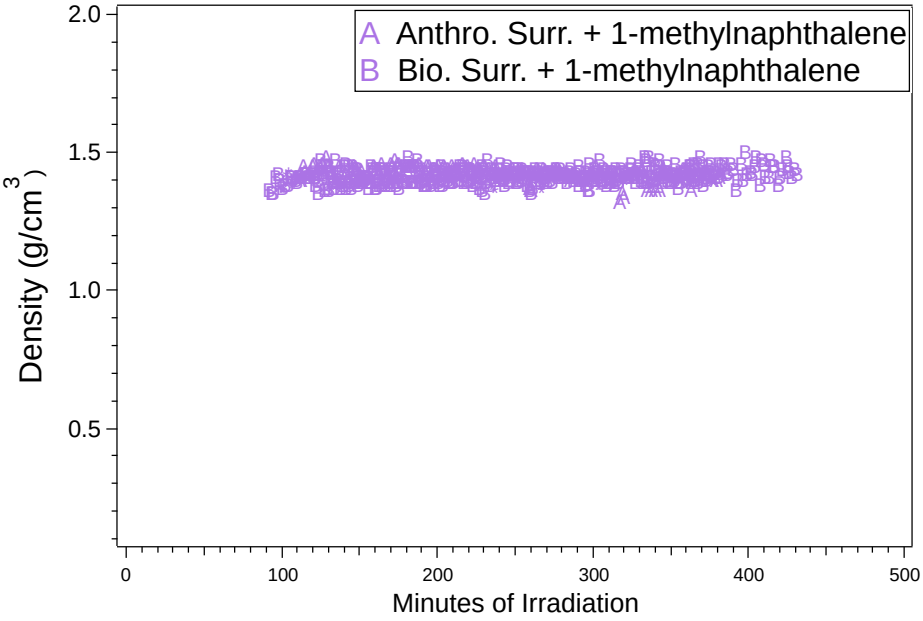

Figure 6.11: Density traces of 1-methylnaphthalene incremental SOA in the anthropogenic and biogenic surrogate mixtures

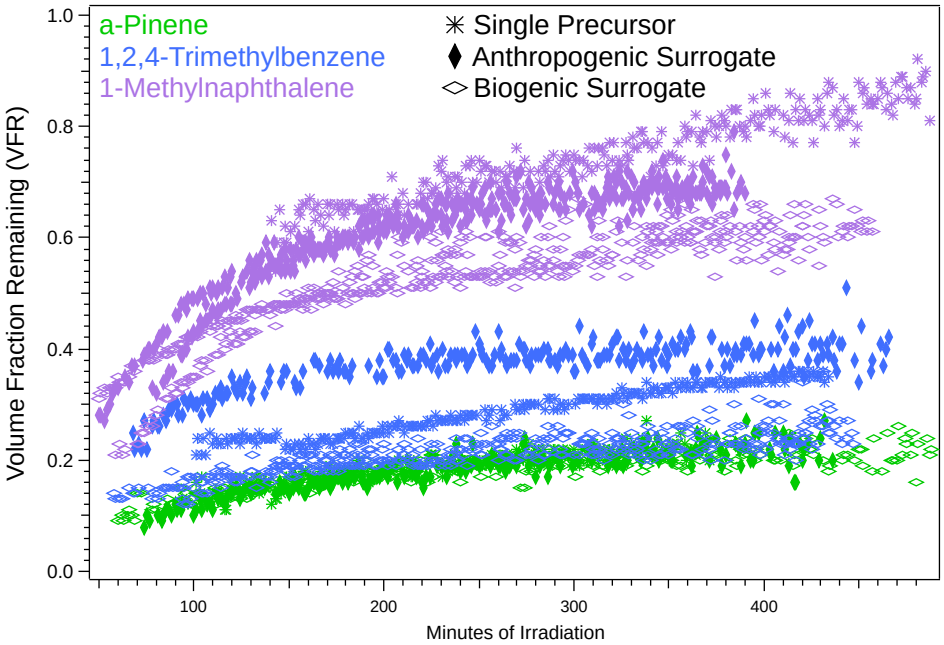

Figure 6.12: Volume fraction remaining at 100°C for α-pinene, 1,2,4-trimethylbenzene, and 1-methylnaphthalene in the anthropogenic and biogenic surrogates and in single precursor/NO_X environments (Li et al, Chen et al)

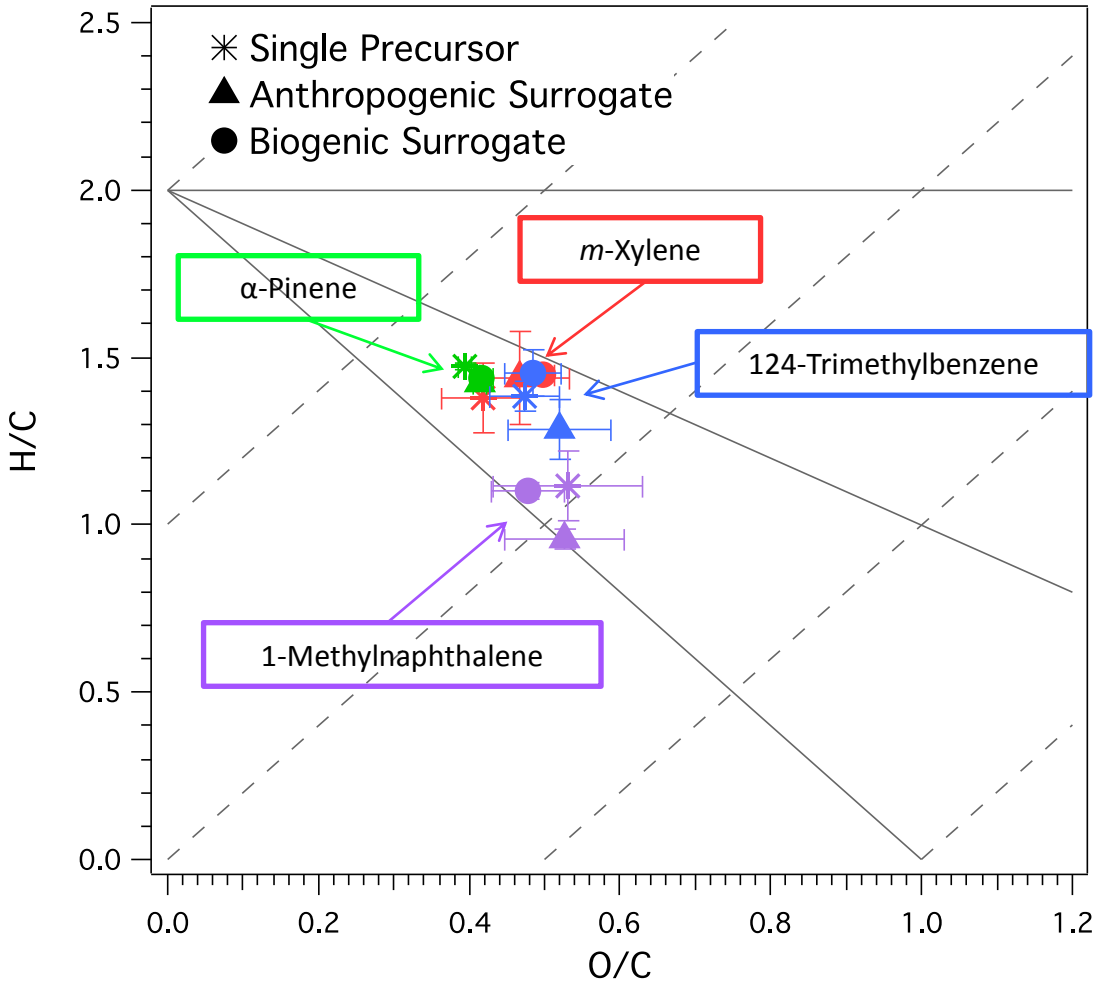

Figure 6.13: Van Krevelen diagram for incremental aerosol from all compounds

Chapter 7: Temperature Effects on α-Pinene Ozonolysis Aerosol Formation with and without Hydroxyl Radical Scavenger

Introduction

Another attempt made by this work to increase the complexity of the chamber experiment was to revisit and expand upon studying the effects of ambient temperature on aerosol formation from the α-pinene ozonolysis system. α-Pinene is the most abundant tropospheric monoterpene and is a classically studied aerosol forming system (Hoffmann, et al. 1997; Yu, et al. 1999; Griffin, et al. 1999; Iinuma, et al. 2005; Presto, et al. 2005; Lee, et al. 2006; Saathoff, et al. 2009; Shilling, et al. 2009; Warren, et al. 2009; Zhao, et al. 2015; Zhang, et al. 2015). Despite the abundance of work looking at aerosol formation in the α-pinene/O_3 system, interest in it still continues to mount as new pieces of the puzzle are gathered.

The α-pinene/O_3 system was chosen here due to its extreme temperature dependence. Previous work in the UCR/CE-CERT chambers has shown that its yields exhibit a hysteresis effect as the temperature of the chamber is cycled (Warren et al., 2009). Much higher yields were observed at a cold temperature of 278K than at a hot temperature of 313K. To the author's knowledge, this is the second study to-date to look at the aerosol formation from α-pinene ozonolysis through these temperature cycles and the first to evaluate effects on aerosol density, volatility, and bulk chemical composition. The additional information gained from these physical and chemical properties can help

give insight into what is causing the severe hysteresis in aerosol formation at different initial temperatures.

Experimental Methods

All experiments were run in the UCR/CE-CERT dual chambers, as described in Chapter 2. The temperature of the chamber enclosure was maintained within ±3K of the set point within a range of 278K-313K for all experiments shown here. Once initial wall-loss corrected aerosol volume stabilized, the temperature was ramped up or down and then held at its second set-point. After a short while the temperature was adjusted back to its initial set-point, as long as there was enough volume left in the reactor.

Results & Discussion

Initial concentrations and resulting aerosol mass and calculated yields for all experiments can be found in Table 7.1. These results verify the work done by Warren et al. and again highlight a drastic hysteresis in aerosol formation at different temperatures. A time series of aerosol formation through the two different temperature cycles can be seen in Figure 7.1. The aerosol formed at the cold temperature (278K) has about four times more mass than the aerosol formed at the hot temperature (313K). Once the temperature is switched from cold to hot, the aerosol mass in the cold initial temperature system drops by about 20%, still significantly higher than the aerosol formed in the hot initial temperature system. When the initial temperature is adjusted from hot to cold, only slight additional aerosol formation is observed. When the temperature is returned back to the original set-point, aerosol formation in both systems returns to near the initial mass

observed, though slightly lower. This slightly lower mass, especially in the cold initial temperature system, is thought to be mainly due to the difficulty in applying the particle wall-loss correction to the system that has already lost a significant amount of particles to the wall. Calculated aerosol yields for both temperature cycles can be found in Figure 7.2. It is found that the change in yields as temperature is cycled in the two systems are very consistent across different experiments. The size distribution of non-wall-loss-corrected aerosol throughout the course of the temperature cycle experiments can be seen in Figure 7.3. Initial particle size in both systems is fairly comparable. As would be expected, when the cold initial temperature aerosol is heated, the peak size distribution slightly shrinks as components partition back into the gas phase. Conversely, as the hot initial temperature aerosol is cooled, the peak size distribution slightly increases as gas phase species partition onto the existing aerosol to re-establish equilibrium. Surprisingly, a small amount of new particle formation is indicated in the hot initial temperature cycle data.

The average density and volatility of aerosol throughout each stage of the different temperature cycles can be found in Table 7.2. Aerosol density does not undergo any drastic changes with temperature, though a slight shift can be observed between the different temperatures (Figure 7.4). Initial aerosol density in the cold-start system is slightly higher than in the hot-start system and slowly decreases over time. No change in density is seen moving from the initial cold temperature to the hot temperature, however, when then moving back to the initial cold temperature, a small, sharp increase in density is observed, which then returns back to the original value. Throughout the hot initial

temperature cycle, barely any change is observed in density, aside from a very slight increase as the temperature decreases. The volatility of the aerosol exhibits drastic dissimilarities at the different initial temperatures (Figure 7.5). As would be expected, the cold initial temperature aerosol is extremely volatile at 100C (with a VFR of only ~0.1). This low VFR undergoes a sharp increase as temperature is increased, rising up to 0.3-0.4, which is comparable to the value seen in the hot initial temperature system. As the temperature is decreased in both systems, the VFR does not return back to its very low initial value, but rather lingers at the same value seen at the hot temperature. This could possibly indicate the presence of thermally labile compounds that are highly volatile in the particle phase and are only available for partitioning at the cold initial temperature step, but are either not formed or are too volatile to partition for reaction in the particle phase at the hot initial temperature. However, if this is the case, than it would be expected that aerosol mass would not only decrease much more when the cold initial temperature aerosol is heated, but that there would be no aerosol mass regained upon the cooling the system back down to its initial cold temperature, as those thermally labile compounds would be lost and not available to go back into the aerosol phase. It is also considered possible that the drastic hysteresis of the volatility in the cold initial temperature cycle indicates a possible change in the phase state of the aerosol.

The average bulk oxygen-to-carbon (O:C) and hydrogen-to-carbon (H:C) ratios for all experiments throughout the different temperature cycles can be found in Table 7.3. The fraction of the organic mass at *m/z44* plotted against the fraction of the organic mass at *m/z43* in a triangle plot can be seen in Figure 7.6. Neither temperature system sees a

drastic change in these two markers over the course of aging and temperature cycles. However, the hot initial temperature system consistently displays a slightly higher *f44* content than is observed in the cold initial temperature system. *f44* is typically used as a marker for how "aged" an aerosol is. Further, the bulk H:C and O:C ratios for both systems can be found on a subset of a traditional Van Krevelen diagram in Figure 7.7. Again, each system is lumped together over time in a slightly different location on the plot, indicating a small difference in bulk chemistry at the different temperatures but no real difference as the temperatures are cycled. This again indicates that thermally labile compounds may be playing a role in the strong temperature effects seen in the α-pinene ozonolysis system.

In light of recent work indicating vapor wall losses in chamber experiments (Zhang, et al. 2014, La, et al. 2016, Krechmer, et al. 2016), two seeded α-pinene ozonolysis experiments were run at the different temperature cycles. The dual chamber system allows for the injection of precursor hydrocarbons into both bags and subsequent mixing to ensure the same concentrations on both sides. Then the two reactors were isolated from each other and seed was added to one side only before O_3 was injected. The aerosol mass time series for these experiments can be found in Figure 7.8. No significant difference was seen between the two sides for either temperature cycle. Most significant is the identical aerosol formation in the hot initial temperature experiment, as it would be expected that vapor wall loss would be increased by the high temperature and lower gas-to-particle partitioning.

Conclusion

The aerosol formation from α-pinene ozonolysis throughout different temperature cycles ranging from 278K to 313K was revisited and confirmed the observation of drastic hysteresis effects exhibit by the cold initial temperature system. This observation was further explored by looking into the bulk aerosol properties throughout the temperature cycles. It was found that the cold temperature aerosol had a significantly different VFR at 100C than the hot temperature aerosol and that once the aerosol was heated the VFR would not decrease back to its initial low value. A slight difference in bulk aerosol chemistry was indicated by the HR-ToF-AMS data by both the *f44/f43* comparison and the oxygen to carbon and hydrogen to carbon bulk ratios. These results indicate the possibility of thermally labile aerosol precursors that are only available for partitioning at the cold initial temperature. Further, it is hypothesized that the phase state of the aerosol may be playing significant role in the gas-to-particle partitioning at the different temperatures. It is recommended that a method for evaluating the phase of the aerosol particles be developed and applied to the temperature cycled α-pinene ozonolysis aerosol system.

Tables & Figures

Table 7.1: Initial conditions and yields at different temperatures for α-pinene ozonolysis runs with and without added CO

Run	ΔαPinene (ppb)	$O_{3,o}$ (ppb)	CO_o (ppm)	$M_{O,T1}$ (μg/m^3)	Y_{T1} (%)	$M_{O,T2}$ (μg/m^3)	Y_{T2} (%)	$M_{O,T3}$ (μg/m^3)	Y_{T3} (%)
Cold-Hot-Cold (CHC) Cycle:				T_1:278K		T_2:313K		T_3:278K	
2020B	21	388	38	102.0	81.5	86.1	68.8	91.8	73.3
1995A	64	196	24	262.1	69.0	207.3	54.5	225.3	59.2
1995B	64	185	24	236.6	62.6	164.1	43.4	207.0	54.8
2086A	48	409	44	253.5	89.2	223.5	78.7	231.8	81.6
2086B	48	303	44	231.9	80.5	205.8	71.4	213.8	74.2
2116A[a]	44	401	49	165.1	63.7	124.9	48.2	129.8	50.1
2116B	45	328	49	173.6	65.5	138.7	52.3	144.5	54.5
1760A	62	205	-	237.2[b]	64.5[b]	210.7	57.3	246.3	66.9
1760B	61	220	-	224.0[b]	62.2[b]	186.5	51.7	232.1	64.4
Hot-Cold-Hot (HCH) Cycle:				T_1:313K		T_2:278K		T_3:313K	
2021B	28	343	72	29.0	17.4	34.0	20.4	24.2	14.5
1996A	58	175	17	82.6	24.0	101.2	29.4	67.6	19.6
1996B	58	169	17	67.9	19.7	107.8	31.2	51.0	14.8
2089A	49	261	44	71.5	24.8	80.2	27.8	47.1	16.3
2089B	49	256	44	68.7	23.7	73.2	25.2	47.0	16.2
2117A[a]	41	366	40	62.3	25.7	77.3	31.9	59.3	24.5
2117B	40	270	40	65.0	27.7	77.6	33.0	52.5	22.3
1764A	35	227	-	139.4	66.8	152.0	72.8	-	-
1764B	54	200	-	112.7	34.9	145.9	45.2	-	-

a. Seeded with ammonium sulfate b. initial particle formation had not stabilized before temperature was cycled

Table 7.2: Aerosol physical properties for all runs throughout the temperature cycles

Run	Density (g/cm^3)			Volume Fraction Remaining (*VFR*)		
CHC	T_1:278K	T_2:313K	T_3:278K	T_1:278K	T_2:313K	T_3:278K
1995A	1.31±0.06	1.35±0.02	1.38±0.05	-	-	-
2086A	1.35±0.03	1.33±0.03	1.33±0.05	-	-	-
2116A[a]	1.36±0.07	1.40±0.02	1.40±0.02	0.10±0.02	0.21±0.03	0.21±0.09
1760A	1.33±0.01	1.29±0.01	1.32±0.02	0.14±0.02	0.31±0.03	0.32±0.06
HCH	T_1:313K	T_2:278K	T_3:313K	T_1:313K	T_2:278K	T_3:313K
1996A	1.28±0.03	1.31±0.03	1.27±0.03	-	-	-
2089A	1.29±0.04	1.25±0.05	1.24±0.06	-	-	-
2117A[a]	1.39±0.03	1.38±0.04	1.37±0.07	-	0.22±0.08	0.30±0.10
1764A	1.33±0.02	1.31±0.02	-	0.37±0.05	0.36±0.03	-

a. Seeded with ammonium sulfate

Table 7.3: Aerosol bulk chemical ratios from HR-ToF-AMS throughout temperature cycles

Run	H:C			O:C		
CHC	T_1:278K	T_2:313K	T_3:278K	T_1:278K	T_2:313K	T_3:278K
1995A	1.49±0.006	1.47±0.006	1.49±0.003	0.25±0.011	0.27±0.004	0.26±0.002
2086A	1.47±0.016	1.47±0.010	1.47±0.009	0.29±0.020	0.31±0.010	0.30±0.004
2116A[a]	1.43±0.016	1.42±0.013	1.41±0.006	0.28±0.016	0.31±0.011	0.29±0.006
HCH	T_1:313K	T_2:278K	T_3:313K	T_1:313K	T_2:278K	T_3:313K
1996A	1.45±0.025	1.47±0.003	1.43±0.010	0.33±0.014	0.29±0.002	0.33±0.007
2089A	1.43±0.011	1.44±0.009	1.42±0.018	0.37±0.007	0.35±0.006	0.37±0.019
2117A[a]	1.38±0.011	1.39±0.007	1.36±0.019	0.38±0.014	0.33±0.003	0.39±0.012

a. seeded with ammonium sulfate

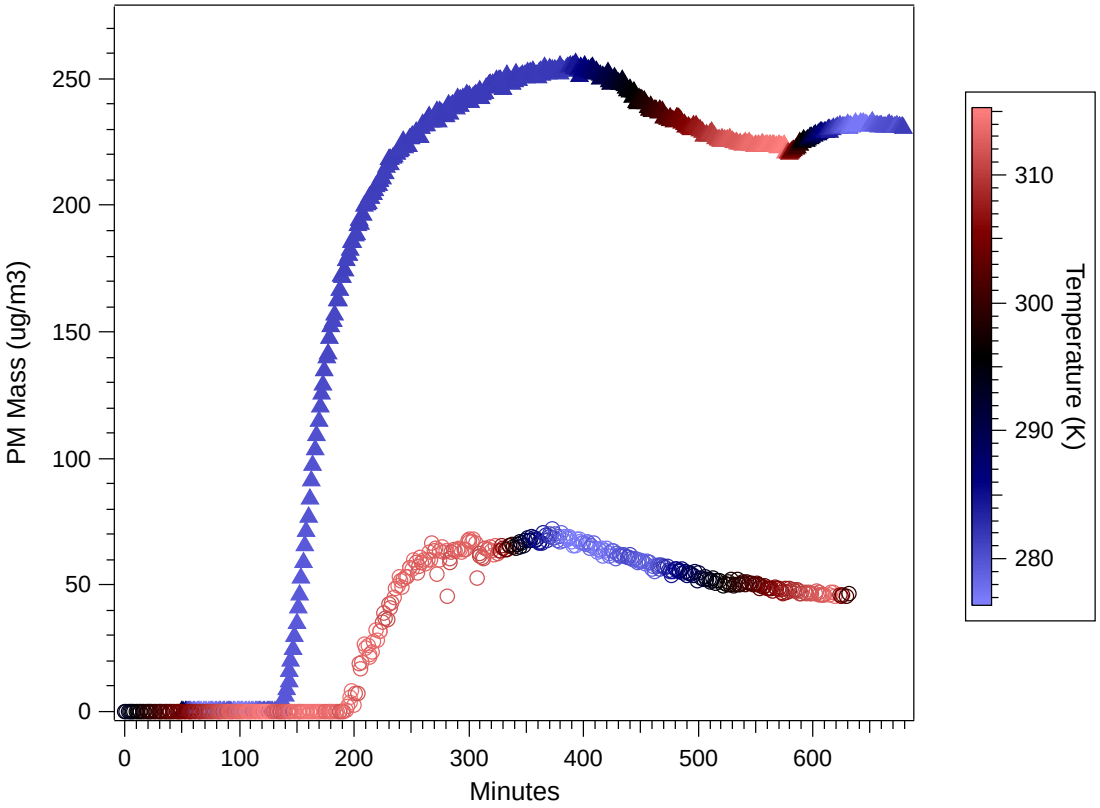

Figure 7.1: Aerosol formation trends through the two temperature cycles

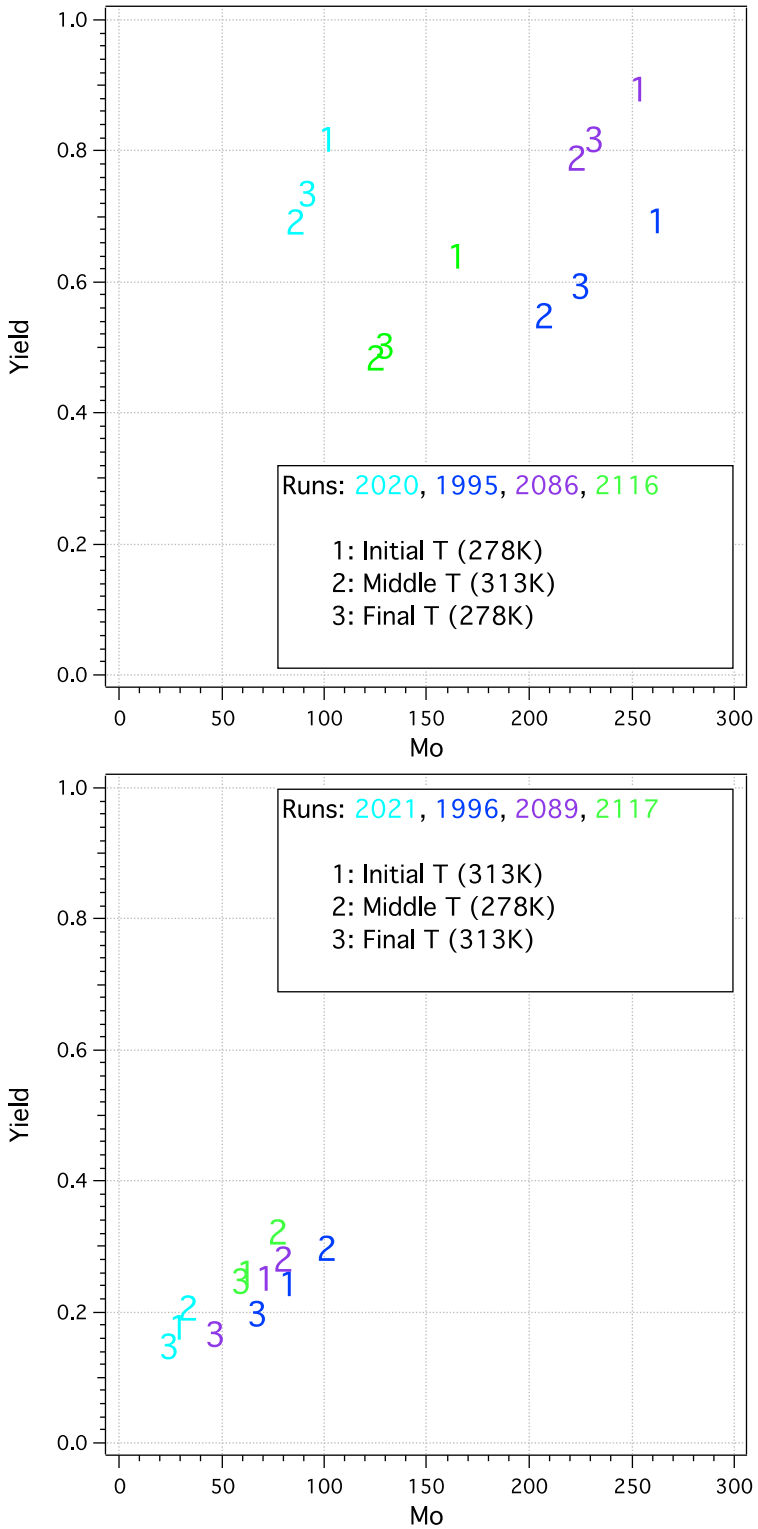

Figure 7.2: Aerosol yields throughout the two different temperature cycles

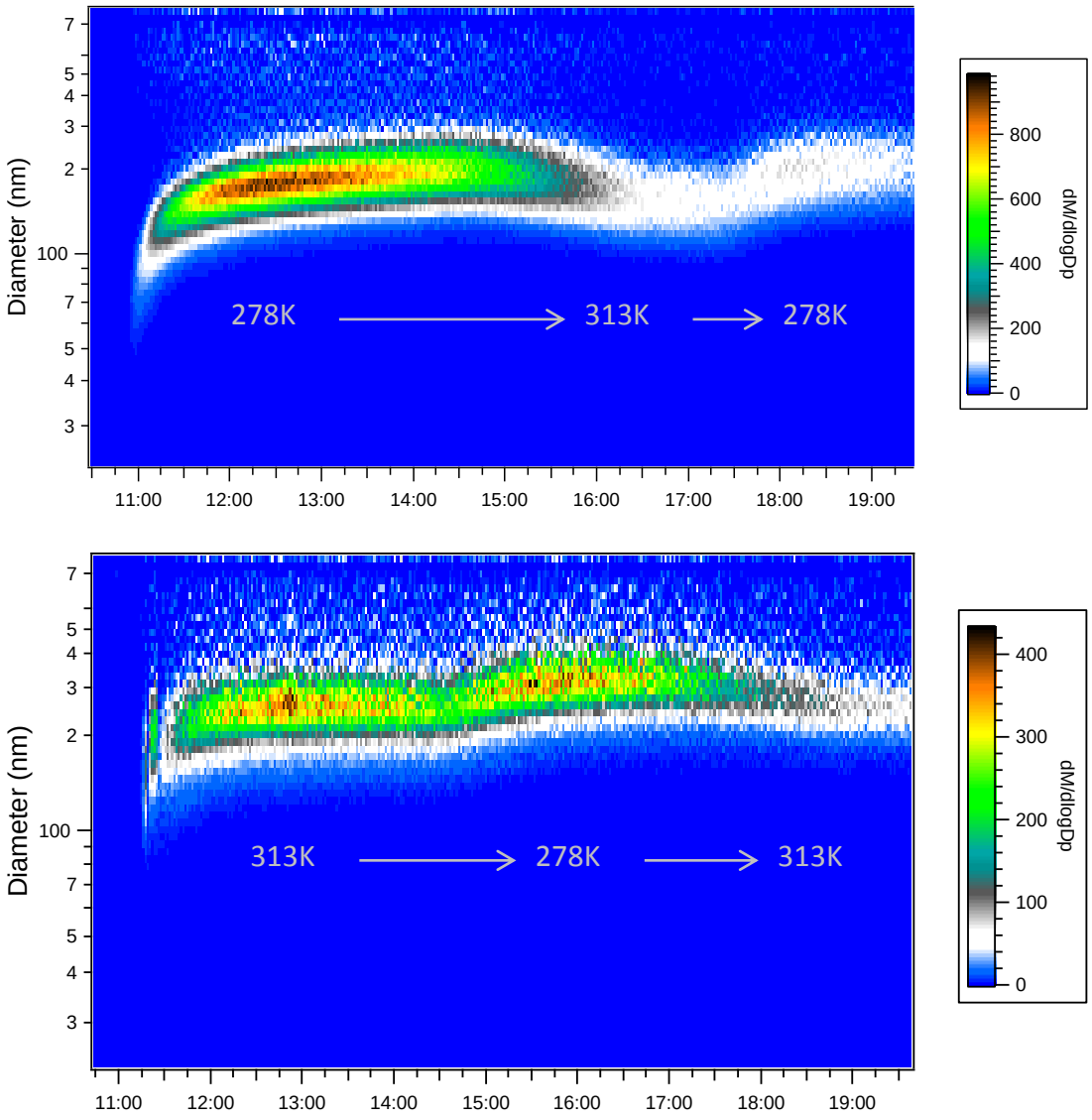

Figure 7.3: Non-wall-loss-corrected aerosol mass size distributions and evolution throughout different temperature cycles

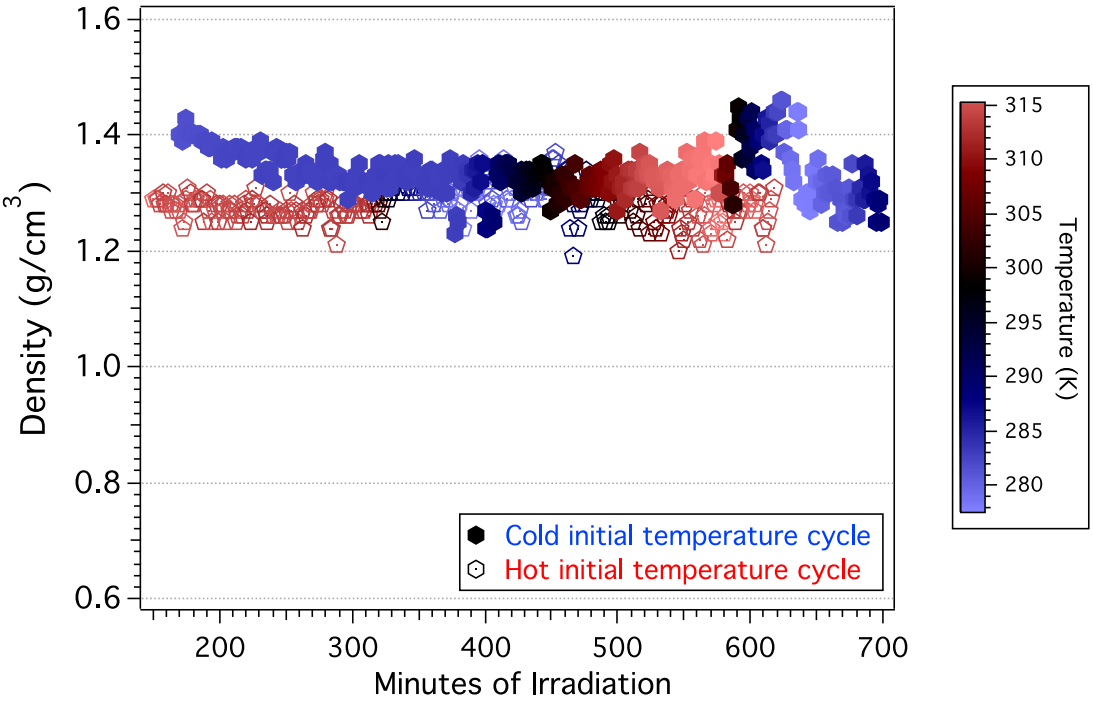

Figure 7.4: Density of α-pinene aerosol throughout different temperature cycles

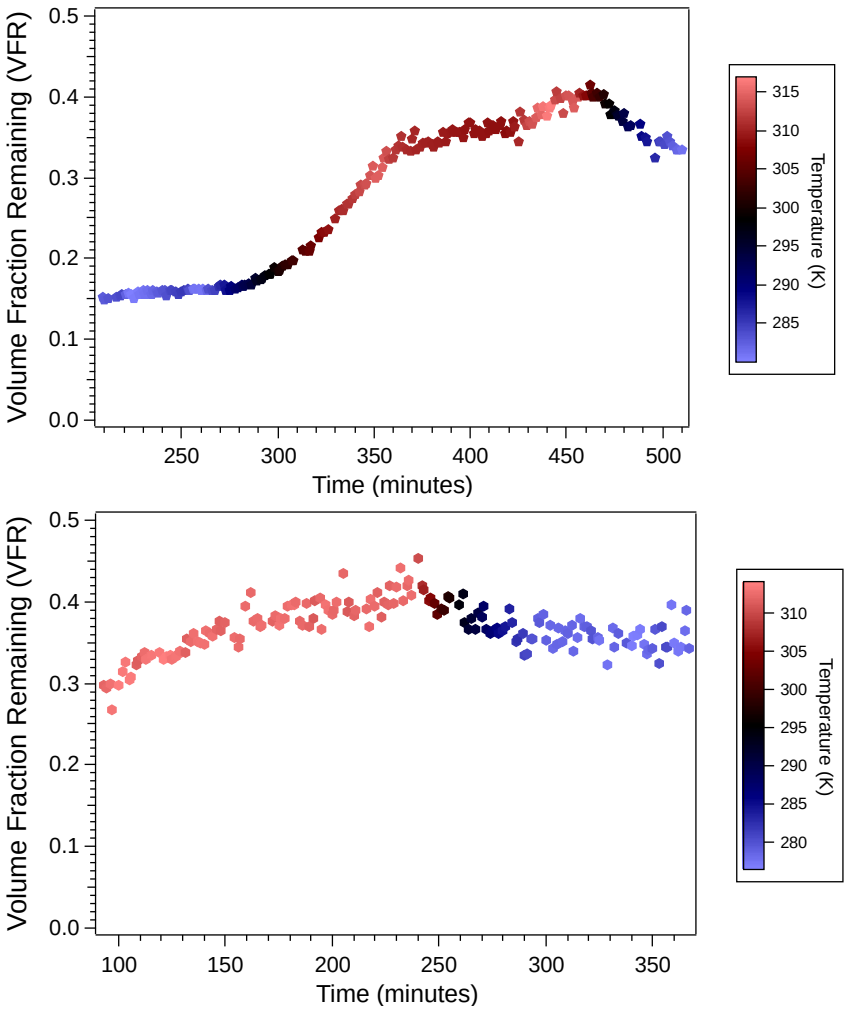

Figure 7.5: Volatility of α-pinene aerosol at 100C throughout temperature cycled experiments

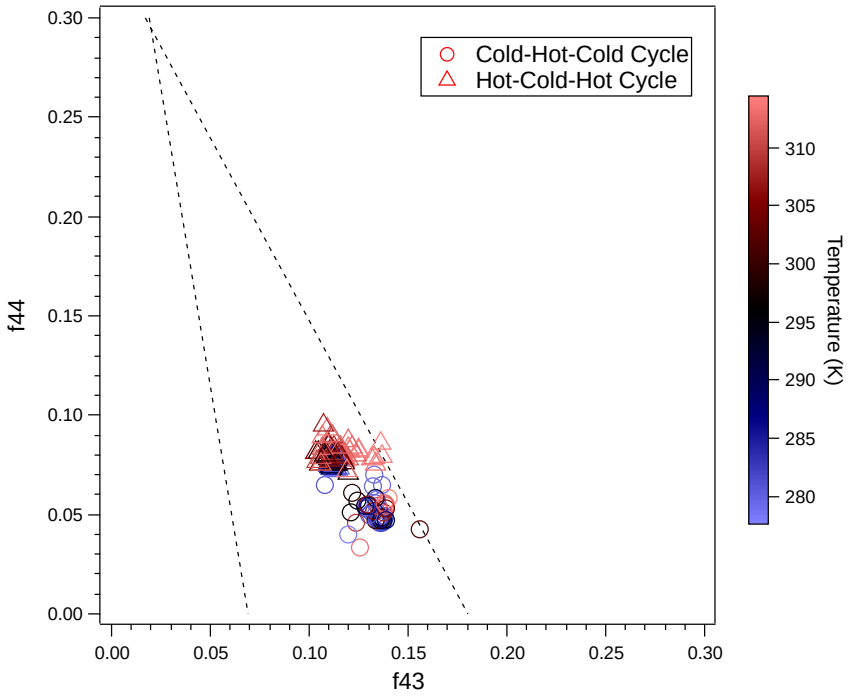

Figure 7.6: Triangle plot comparing *f43* and *f44* evolution of α-pinene aerosol throughout temperature cycles

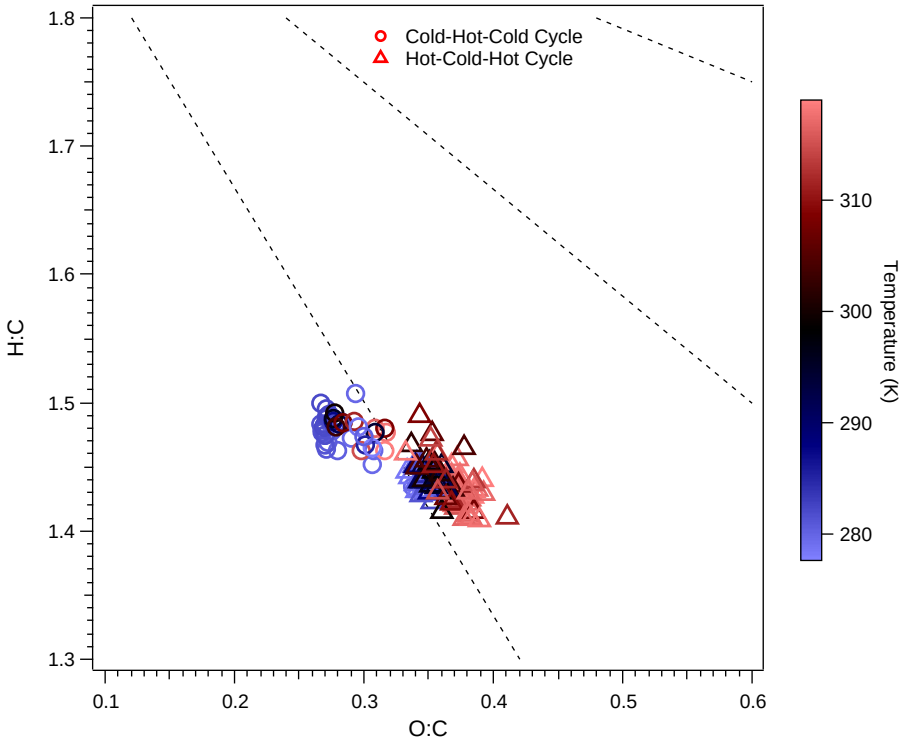

Figure 7.7: Van Krevelen diagram of α-pinene aerosol through different temperature cycles

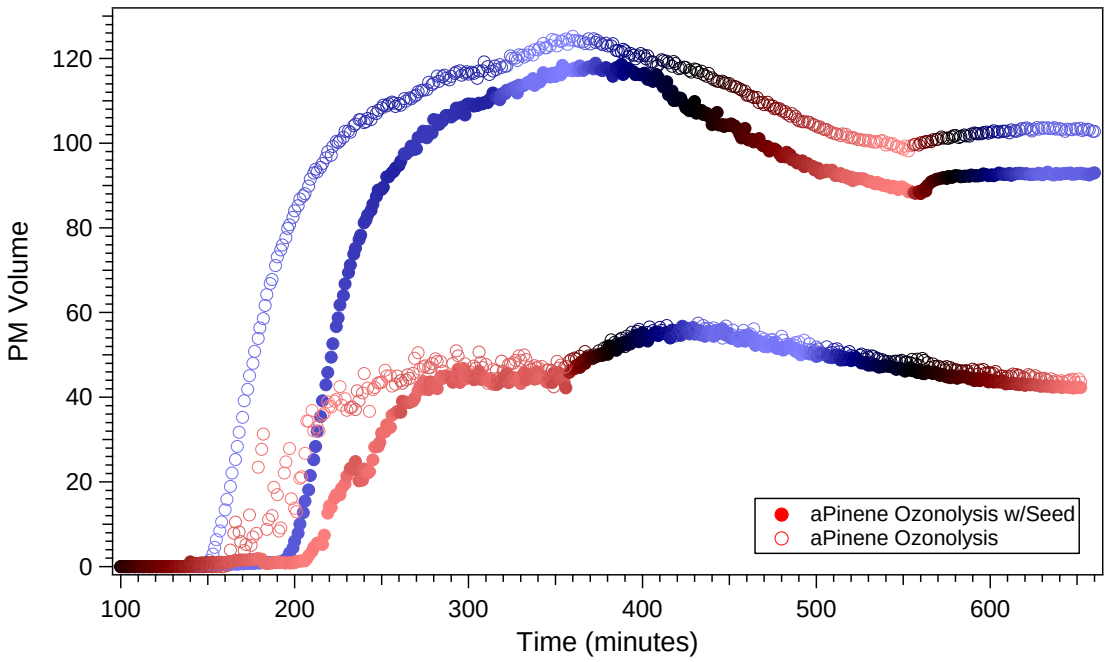

Figure 7.8: Aerosol mass in seeded and non-seeded side-by-side chamber runs throughout the two temperature cycles

Chapter 8: Secondary Organic Aerosol Formation from the Cyclohexene Ozonolysis System under Different Temperatures

Introduction

In an attempt to better understand the aerosol formation trends at different temperatures seen in the α-pinene ozonolysis system, the same types of experiments were done on the cyclohexene ozonolysis system. Cyclohexene ozonolysis was performed with CO as a hydroxyl radical scavenger, so as to limit the possible oxidation pathways. This system was chosen due to its theoretical simplicity compared with the α-pinene system. Experiments were again run throughout temperature cycles as described in Chapter 7.

Results & Discussion

Initial conditions and aerosol formation for all experiments can be found in Table 8.1. Bulk aerosol mass formed in the cyclohexene system was found to be surprisingly high due to extremely large particles formed compared to previous work (Kalberer, et al. 2000). Throughout all experiments the size distribution of the aerosol throughout the temperature cycles was found to be surprisingly large and often fairly wide compared to other nucleated chamber aerosol systems. Size distributions over time for the two temperature cycles can be found in Figure 8.1. The cold initial temperature aerosol grew to a size of approximately 300nm. Once the temperature was heated, the peak size shrank to about 200nm and then increased back to 300nm upon the second cooling cycle. The hot initial temperature aerosol formed a small number of even larger particles, with the

peak size distribution growing out of range of the SMPS (max 712nm), especially upon cooling. This finding was distressing, as cyclohexene is a relatively small and simple molecule and previous work has not found such drastically large size distributions. This finding is also unique to the cyclohexene ozonolysis system, as aerosol formation was within the typical range seen for all other experiments (including standard quality control checks) run in the UCR/CE-CERT chambers during the time period these experiments were run. It is thought that the *C** of cyclohexene might be at such values that at the hot temperature it cannot reach the nucleator needed to start a nice size distribution for aerosol formation, thus the portioning in the system is not well controlled.

Experiments with ammonium sulfate seed were run in an attempt to control the aerosol size distribution to a lower, more manageable size (thus keeping the hot temperature cycle experiments within the range of the instruments). Size distribution results for these experiments can be found in Figure 8.2. The cold temperature cycle system displays similar trends as were seen in the non-seeded experiments, but the peak diameter is about half the size seen in the non-seeded experiments at approximately 150nm. The hot temperature cycle experiments also exhibited a much lower peak diameter, however, the overall aerosol formation was still too low to make any significant observations about the characteristics of the aerosol formed at 313K.

Aerosol density for the cold temperature cycle can be found in Figure 8.3. Very little change is seen in the bulk density throughout the course of the temperature cycle. The volatility of the aerosol at 100C for the cold temperature cycle aerosol is seen in Figure 8.4. A similar trend to the α-pinene ozonolysis cold initial temperature is found,

where the initial aerosol exhibits a very low volume fraction remaining, which increases as temperature increases and then does not return back to its initial volatility once the temperature is cooled back down again. The volume fraction remaining at the second cold temperature does decrease a fair amount compared with that seen in hot temperature section, which is a slightly different trend than was observed in the α-pinene system.

Bulk chemical composition for the two temperature cycle systems can be found in Figures 8.5 and 8.6. It is seen that the aerosol evolution on the triangle plot displays fairly similar values, however, the trends over the course of temperature cycles do exhibit some differences. The hot initial temperature aerosol displays a higher *f44* value, which decreases as the system is cooled and then increases again upon reheating. Initially, the cold start system has a comparable *f44*, which quickly drops as aerosol evolves and then does not increase again, even with heating. The bulk O:C and H:C ratios for both systems are quite similar, with the O:C decreasing from 0.5 to 0.3 in both systems throughout aerosol evolution and H:C remaining fairly constant. It is thought there could be something interesting happening in the aerosol chemistry throughout different temperature cycles and especially at different formation temperatures, but the more concerning and curious result seen is that in the very large sizes seen for aerosol from such a small and relatively simple compound.

Conclusion

Aerosol formation and evolution was examined for the cyclohexene ozonolysis system at throughout different temperature cycles. Both temperature cycles exhibited

extremely large particle formation, with the hot initial temperature aerosol growing out of the range of the SMPS. Seeding the experiment allowed for better size control in the cold initial temperature system. However, seeding the hot initial temperature system controlled the overall size distribution, but much less aerosol mass was then formed. The volatility of the cold temperature cycle aerosol displayed comparable results to that seen in the α-pinene ozonolysis system, where the VFR does not return back to the original reading once the aerosol is cooled again. This indicates that some sort of change in either the chemistry or the phase of the aerosol is happening upon heating the cold initial temperature system. Bulk chemical composition indicating some differences in temperature between the two cycles, mainly when looking at the *f44* and *f43* ratio throughout aerosol evolution. It is recommended that further investigation be done into this system to explore what is causing the erratic and large nucleation bursts at the different temperatures. It is especially interesting that the aerosol nucleated at the hot formation temperature is so much larger than when nucleating at the cold temperature and that it does not seem to have any affinity for nucleating on the ammonium sulfate seed. This system should be evaluated with an organic seed to further investigate the cyclohexene aerosol formation. Additionally, it is thought that the aerosol phase could be playing a significant role in both the formation and properties of the cyclohexene ozonolysis system at different temperatures.

Tables & Figures

Table 8.1: Initial conditions and yields at different temperatures for the cyclohexene ozonolysis system with CO as a hydroxyl radical scavenger

Run	**Δ**cyclohex (ppb)	$O_{3,o}$ (ppb)	CO (ppm)	$M_{O,T1}$ (μg/m^3)	Y_{T1} (%)	$M_{O,T2}$ (μg/m^3)	Y_{T2} (%)	$M_{O,T3}$ (μg/m^3)	Y_{T3} (%)
Cold-Hot-Cold Cycle				T1: 278K		T2: 313K		T3: 278K	
1977A	265	342	62	466.5	52.8	282.7	32.0	292.2	33.4
1977B	265	263	62	425.9	48.2	241.0	27.3	329.8	37.3
2081A	104	349	39	137.5	41.3	107.2	32.1	118.1	35.4
2081B	105	292	39	336.8	34.9	99.2	29.5	112.2	33.3
2114A[a]	105	409	44	167.8	47.1	74.7	21.0	108.8	30.5
2114B	106	407	45	110.0	31.0	85.8	24.2	80.8	22.8
Hot-Cold-Hot Cycle				T1: 313K		T2: 278K		T3:313K	
1983A	293	382	63	b	b	b	b	b	b
1983B	294	301	63	b	b	b	b	b	b
2082A	102	478	45	b	b	b	b	b	b
2082B	101	423	45	b	b	b	b	b	b
2115A[a]	105	366	44	-	-	-	-	-	-
2115B	106	381	45	-	-	-	-	-	-

a. seeded with ammonium sulfate; b. particle size distribution grew out of range of SMPS

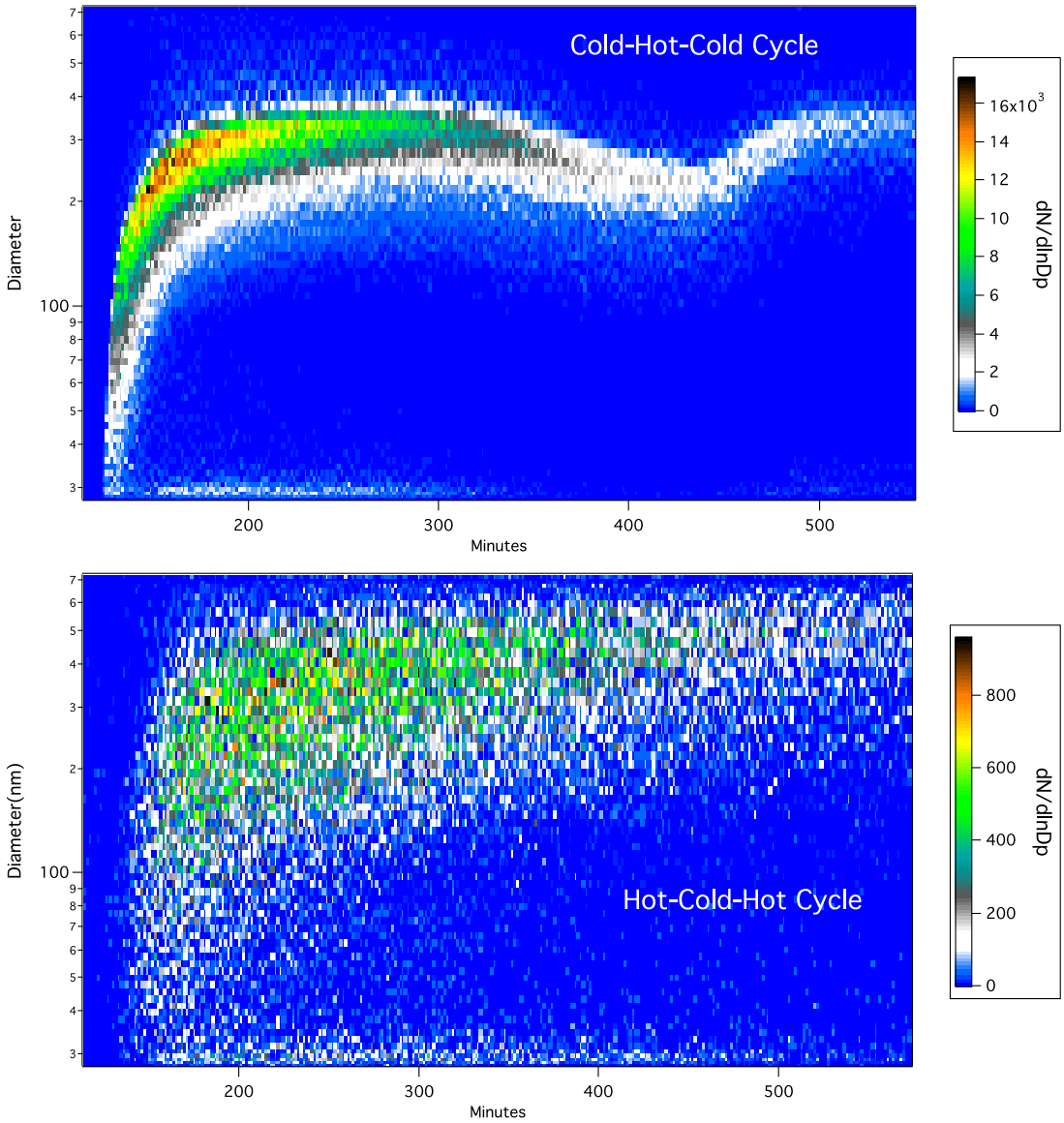

Figure 8.1: Image plots of aerosol growth throughout non-seeded temperature experiments

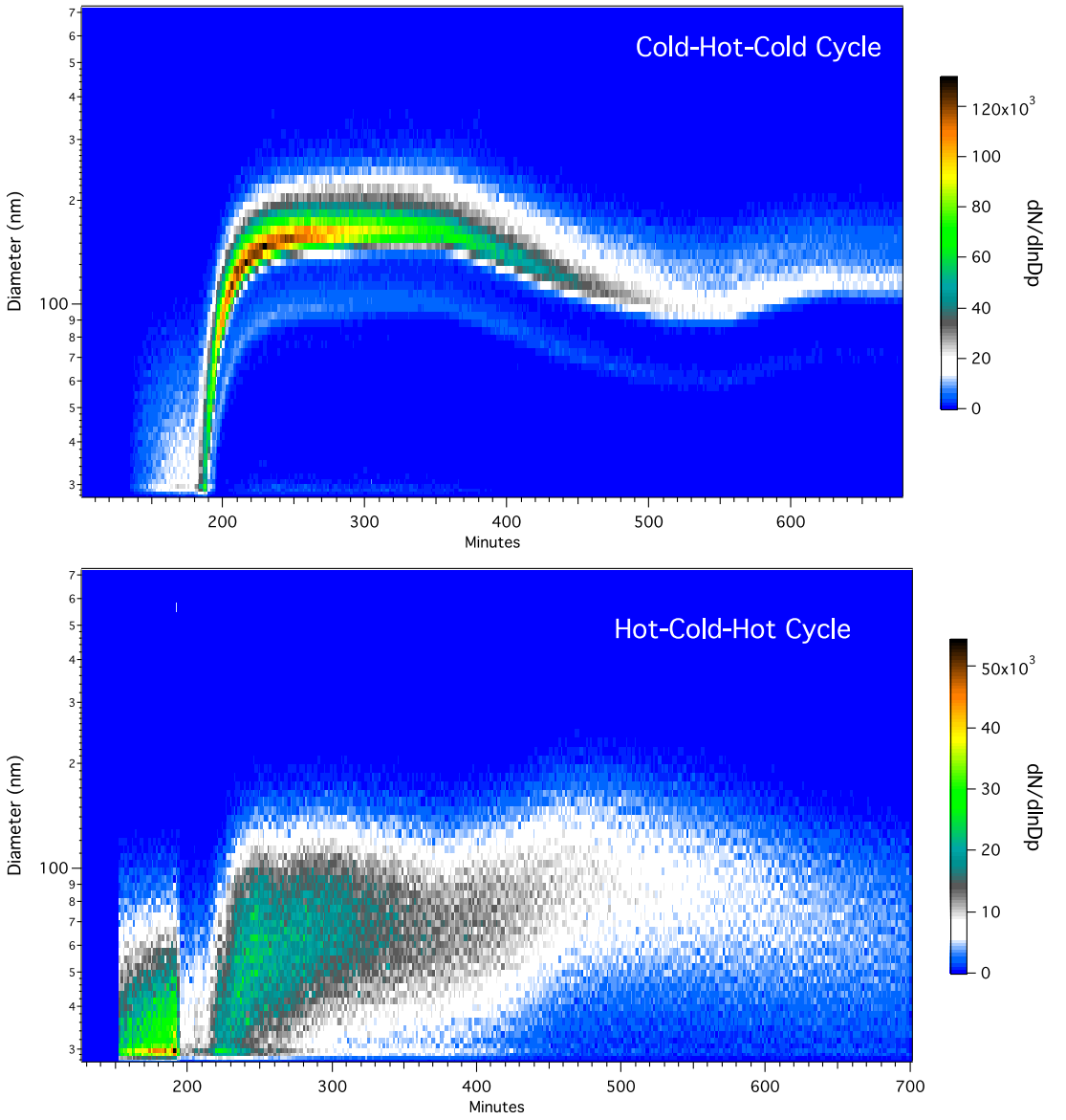

Figure 8.2: Image plots of aerosol growth throughout seeded temperature experiments

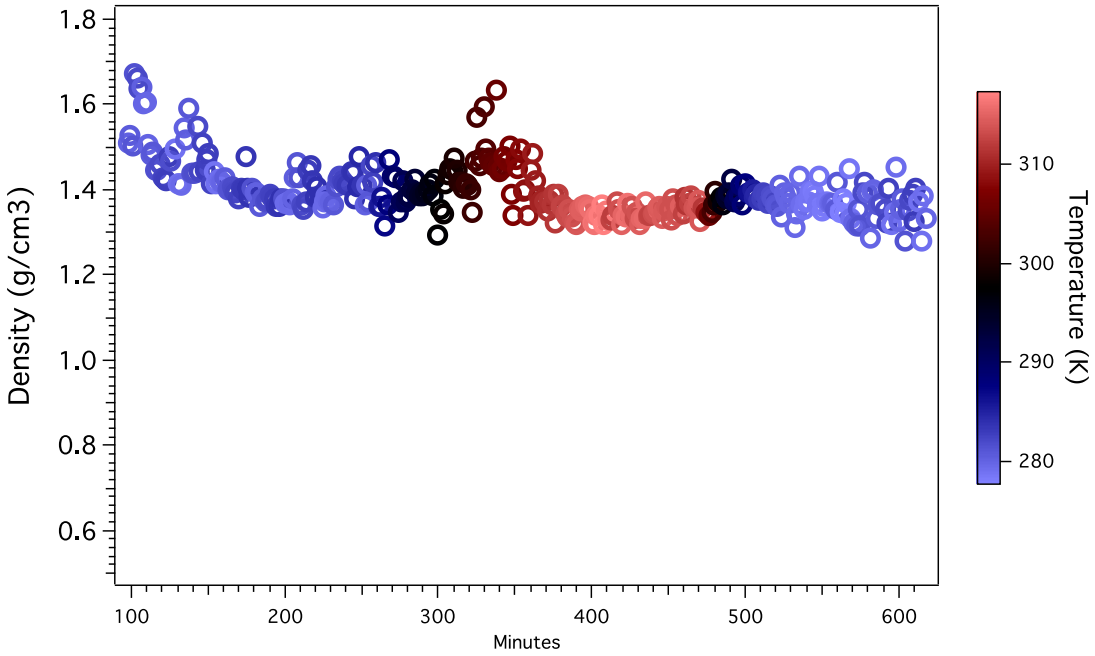

Figure 8.3: Density of cold initial temperature cycle cyclohexene aerosol

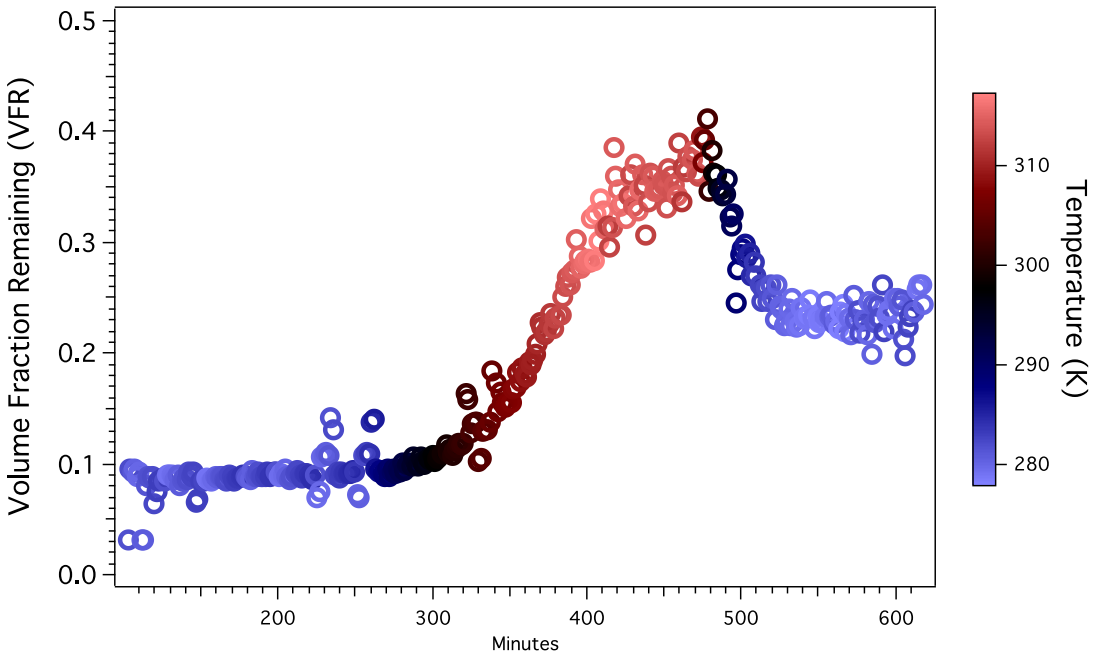

Figure 8.4: Volatility at 100C of cold initial temperature cycle cyclohexene aerosol

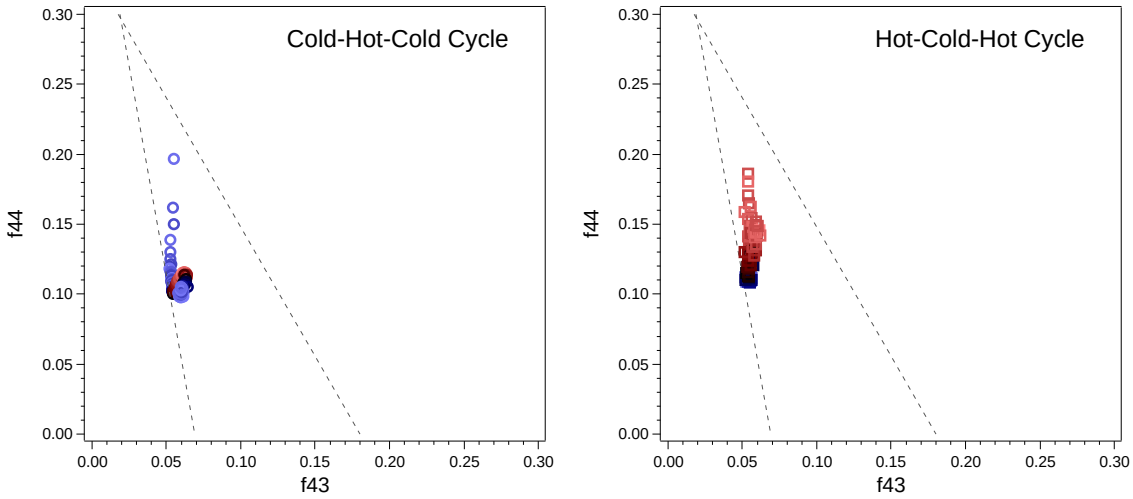

Figure 8.4: Triangle plots of *f44* vs *f43* over the course of the two temperature cycles

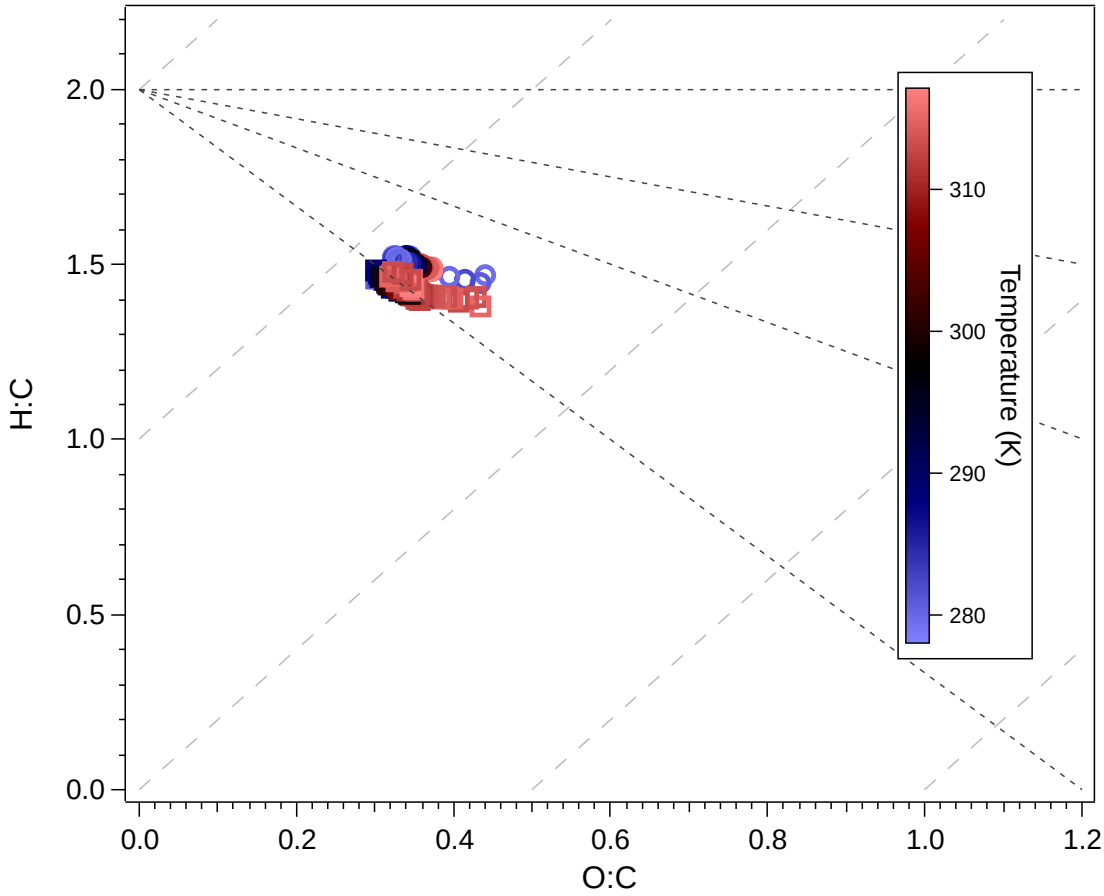

Figure 8.5: Van Krevelen Diagram showing the evolution in bulk chemical ratios through the two temperature cycles

Chapter 9: Temperature Effects on Aerosol Formation and Properties from *m*-Xylene and NO Photo-oxidation

Introduction

The effects of temperature hysteresis on secondary organic aerosol formation and properties were further explored for the *m*-xylene/NO_X irradiation system. *m*-Xylene is a classic aromatic hydrocarbon studied for SOA formation (Izumi et al., Odum et al., Cocker et al., Song et al., Ng et al., Li et al.). Aromatic hydrocarbons are well-known aerosol formers and, in urban areas, may be responsible for 50-70% of SOA formation in urban environments (Calvert et al., Na et al., Kanakidou et al.). Laboratory studies investigating the ambient temperature effects on the aerosol formation from *m*-xylene are quite limited and have only looked at aerosol formation at a constant temperature (Takekawa et al) or, at the UCR/CE-CERT chamber, with one temperature change in the experiment (Qi et al). This work seeks to revisit the temperature effects on the *m*-xylene/NO system to further explore any physical or bulk chemical composition changes in the aerosol throughout the temperature changes and to complete the full temperature cycle by returning the aerosol system back to its initial formation temperature. Throughout the irradiation experiments, different numbers of blacklights were used according to Qi et al to maintain a constant NO_2 photolysis rate at the different temperatures.

Results & Discussion

Initial conditions for all experiments along with aerosol mass formed and yields for all experiments can be found in Table 9.1. Two experiments were run for each temperature cycle at slightly different hydrocarbon-to-NO_X ratios. The hot initial temperature system took so long for aerosol formation to stabilize that only one temperature change could be accommodated within the lifetime of the reactor. The cold initial temperature cycle was able to be accomplished through all three temperature set points. Aerosol formation over time throughout the temperature changes can be seen in Figure 9.1. A large temperature hysteresis effect was again seen between the two temperature cycles, with the initial temperature dictating the overall amount of aerosol formation. Interestingly, in the hot initial temperature *m*-xylene/NO system, barely any additional particle growth was seen when the system was cooled down to 278K. This contrasts with the results seen in the α-pinene ozonolysis system, where additional particle growth occurred with the decrease in temperature. Further, this indicates very little effect of temperature according to traditional gas-to-particle partitioning in this hot *m*-xylene aerosol system. The cold initial temperature cycle formed over twice as much aerosol mass as was seen in the hot initial temperature system. Only a small amount is lost due to partitioning when the system is heated up, with almost twice as much aerosol still being present compared to the amount formed at the hot temperature. When the system is cooled down again, the entire amount of aerosol lost to heating is regained, which also contrasts with the α-pinene ozonolysis system, which does not regain all of

the aerosol species formed at the cold temperature upon returning to the final cold setpoint.

The *m*-xylene decay for all runs can be found in Figure 9.2. Slower *m*-xylene decays were seen in runs 2090 and 2091, which had lower NO concentrations than 2125 and 2126. Further, in run 2090 (cold initial temperature cycle), an increase in the *m*-xylene decay rate is seen as the system is heated. This is thought to be due to the potential presences of peroxyacetyl nitrate (PAN) or other reactive nitrogen species forming at the hot temperature as the NO_X in the system runs out. This trend is also present in the higher NO_X cold initial temperature system (run 2125), but only causes a very slight change in the *m*-xylene decay. The NO_2 formation and evolution throughout the temperature cycles for all runs can be found in Figure 9.3. Some NO_2 loss is consistently seen every time the system is hot and subsequently cooled down. In Figure 9.4 the ozone formation trends for all experiments can be observed. The initial cold temperature system forms significantly less ozone than the hot initial temperature system. Once the system is heated, however, the O_3 concentration increases and then levels off as the system is cooled again, resulting in overall comparable final O_3 levels for both temperature cycles.

Aerosol density does not seem to be affected by the temperature cycling, as seen in Figure 9.7 and , for the cold temperature system, displays a very similar trend to that seen in room temperature *m*-xylene/NO systems, where the initial density is slightly higher (close to 1.5g/cm^3) and decreases over the course of the experiment to be closer to 1.4g/cm^3. The hot initial temperature system does not have this slightly higher density in the initial aerosol formation. The volume fraction remaining at 100C for the temperature

cycles can be seen in Figure 9.8. As was observed in the other temperature systems studied, the aerosol formed at the initial cold temperature is extremely volatile at 100C, with VFR increasing along with temperature and then not returning to its original value upon being cooled down again. This could, again, be an indication of a phase state change in the aerosol formed at the cold temperature. The volatility of the aerosol in the hot initial temperature system is overall comparable to that seen in static room temperature *m*-xylene/NO systems.

Triangle plots (Ng et al., 2010) comparing the fraction of organic aerosol mass at *m/z43* and *m/z44* are found in Figure 9.9. The *f44* signal (indicating CO_2^+, a marker of a more oxidized aerosol) between the two temperature systems is quite comparable and does not change throughout either temperature cycle. The *f43* signal, however, decreases throughout the cold initial temperature cycle, indicating a loss of $C_2H_3O^+$, leading to overall a more oxidized aerosol. This loss in *f43* is not observed in the hot initial temperature cycle, which indicates that there is some difference in the bulk aerosol chemistry occurring at the cold initial temperature. Van Krevelen diagrams comparing the bulk H:C and O:C ratios of the aerosol through the different temperature cycles can be seen in Figure 9.10. Overall, the bulk aerosol ratios compare well with each other through the two cycles, only shifting slightly with temperature changes as the O:C marginally increases with heating and decreases with cooling, as was observed by Qi et al. These values are very comparable to that seen from constant room temperature *m*-xylene/NO systems (Li et al).

Conclusion

The effect of initial temperature of aerosol formation and temperature cycling throughout aerosol evolution was explored and evaluated for the *m*-xylene/NO photo-oxidation system. As was observed in other systems studied under temperature cycles, the aerosol formation at the cold initial temperature was drastically higher than that observed at the hot initial temperature and the two values were not found to be comparable to each other upon heating/cooling of each system. In contrast to other aerosol systems studied through temperature cycles, no substantial additional aerosol growth was seen upon cooling the hot initial temperature system. This indicates a potential loss of thermally labile compounds, which are then not available for reaction upon cooling. This system was not evaluated for vapor wall loss through the different temperature cycles, though the cold-hot-cold cycle results would indicate that vapor wall losses in the system are minimal, as the system regains the complete amount of aerosol back that had been formed at the cold temperature after heating then cooling again. Due to the potential of slightly different chemistry occurring at the different initial temperatures, it is recommended that seeded experiments be run in the hot initial temperature cycle to confirm that vapor wall losses are not playing a role in these results.

Further, a temperature effect was observed on the NO_X/O_3 chemistry in the cold initial temperature system, with less O_3 being formed at the cold temperature and increasing once the system is heated. When going from the hot temperature to the cold temperature, all systems indicated some loss of NO_2. The bulk aerosol density was comparable at all temperatures to the density of previous *m*-xylene/NO aerosol at room

temperature. Furthermore, volatility of aerosol at 100C exhibited the same trends in the cold initial temperature cycle as was seen in other systems studied for temperature hysteresis effects. Again, it is recommended that the phase of the aerosol be explored at these different temperatures of aerosol formation. Bulk aerosol chemistry remained fairly similar throughout the temperature cycles, with some shifts in O:C seen. The *m/z*43 signal indicates some difference in chemical composition occurring at the initial cold temperature.

Tables & Figures

Table 9.1: Initial conditions and yields at different temperatures for *m*-Xylene/NO_X system

Run	Δ*m*-Xylene (ppb)	NO_{init} (ppb)	$M_{O,T1}$ (μg/m^3)	Y_{T1} (%)	$M_{O,T2}$ (μg/m^3)	Y_{T2} (%)	$M_{O,T3}$ (μg/m^3)	Y_{T3} (%)
2090A	55	19	26.7	11.3	23.6	9.9	30.2	12.7
2090B	55	19	27.3	11.5	23.9	10.1	29.5	12.4
2125A	66	44	34.0	11.9	30.9	10.8	36.7	12.8
2125B	66	45	30.2	10.5	28.2	9.9	33.5	11.7
2091A	57	21	9.9	4.1	12.6	5.2	-	-
2091B	57	21	12.0	4.9	12.7	5.3	-	-
2126A	64	29	11.9	4.3	13.5	4.9	-	-
2126B	64	29	15.2	5.6	16.2	5.9	-	-

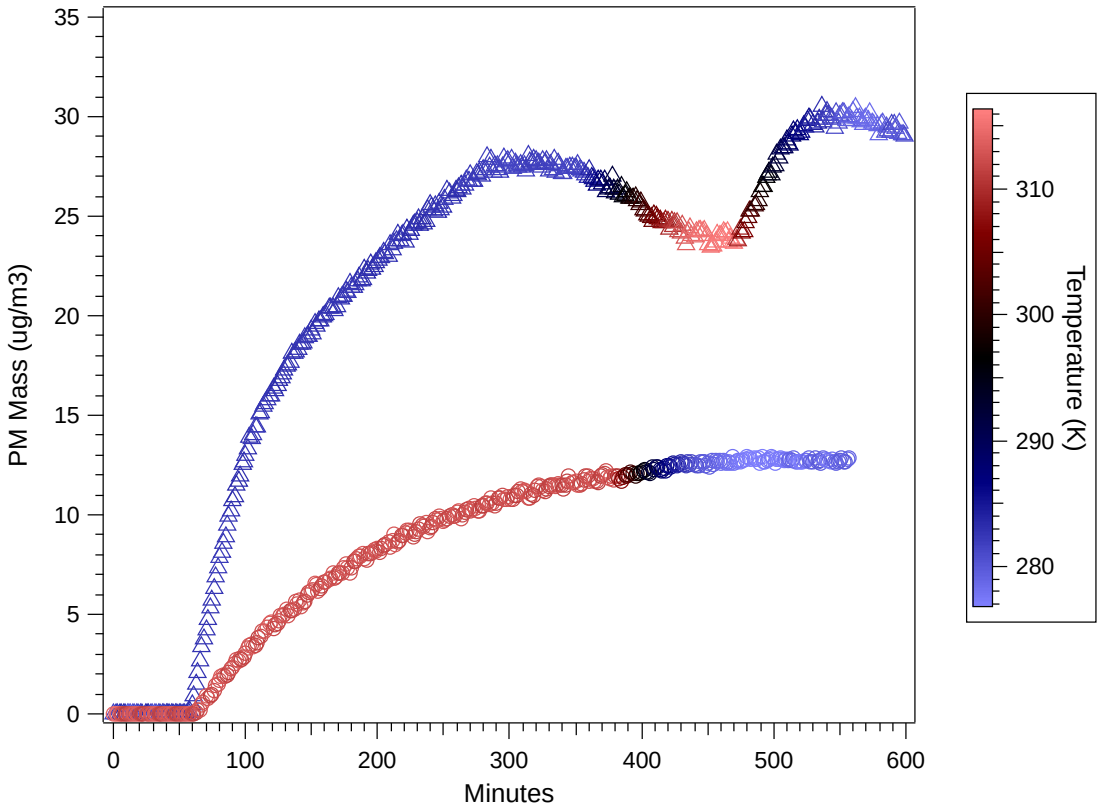

Figure 9.1: Aerosol formation over time throughout temperature cycles

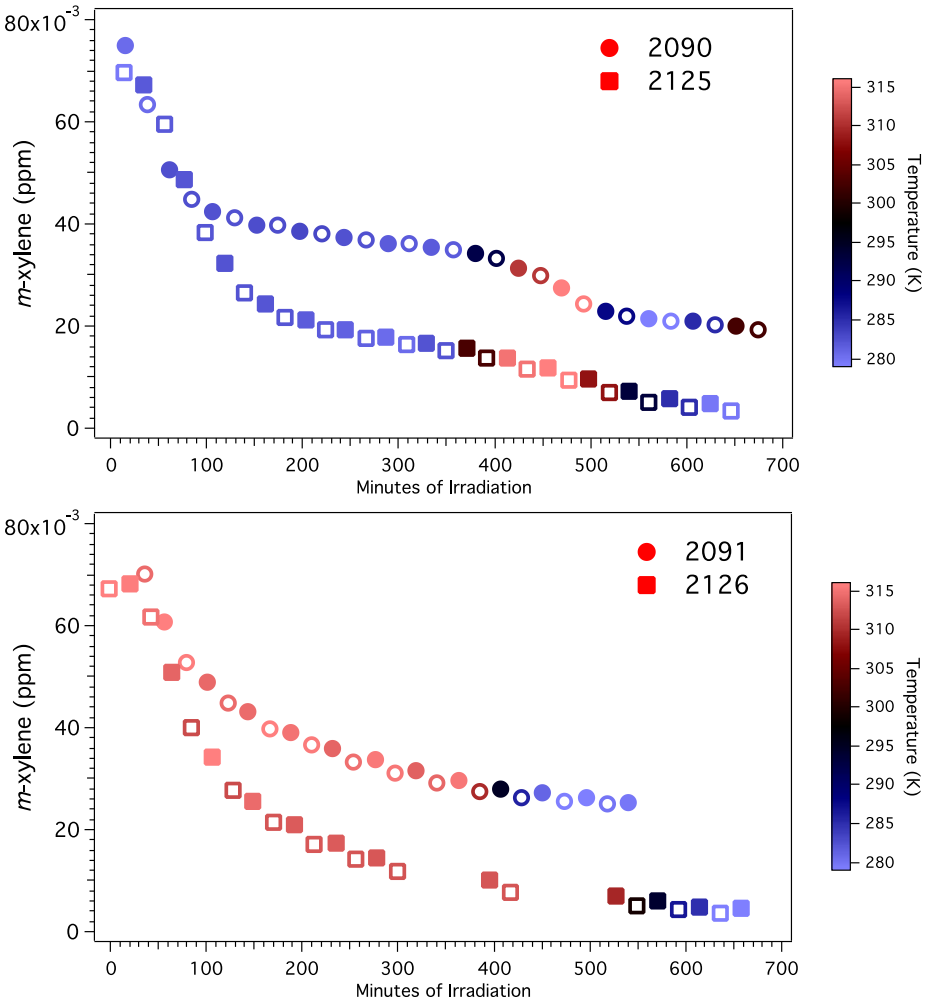

Figure 9.2: *m*-Xylene decay in temperature cycled experiments

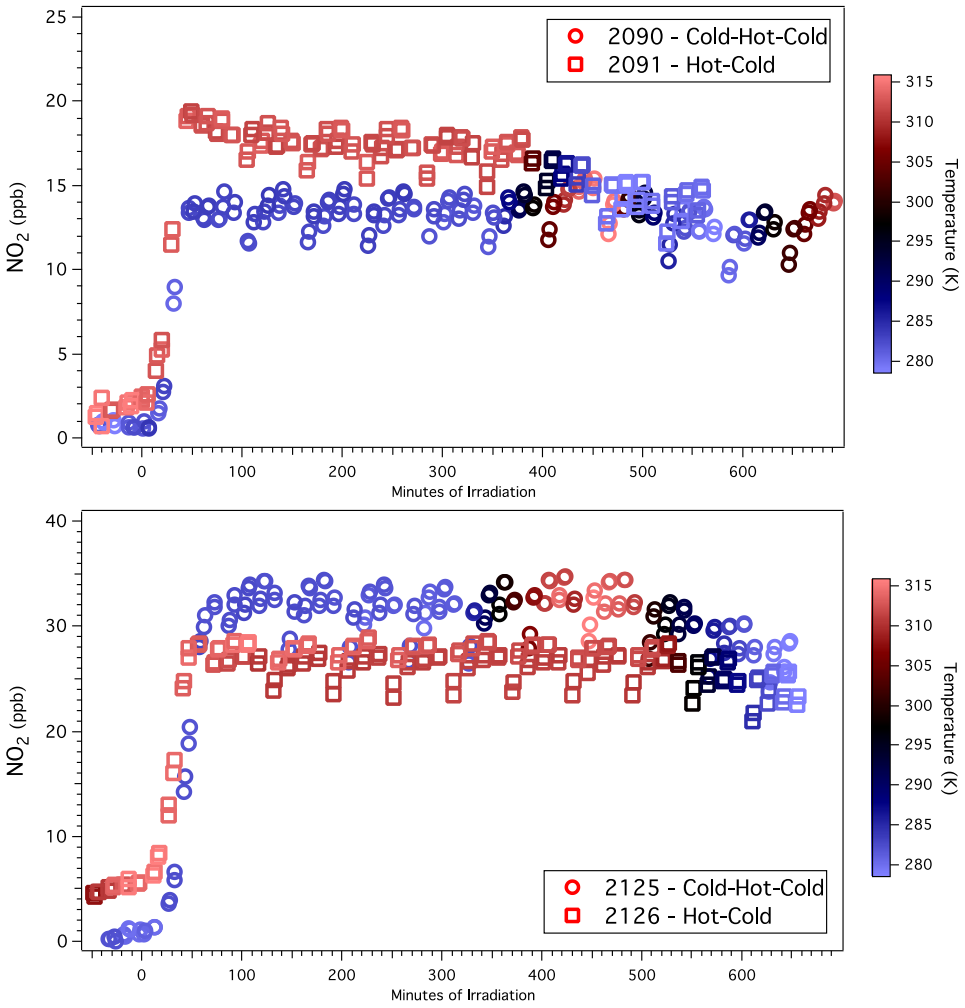

Figure 9.3: NO_2 traces throughout temperature runs

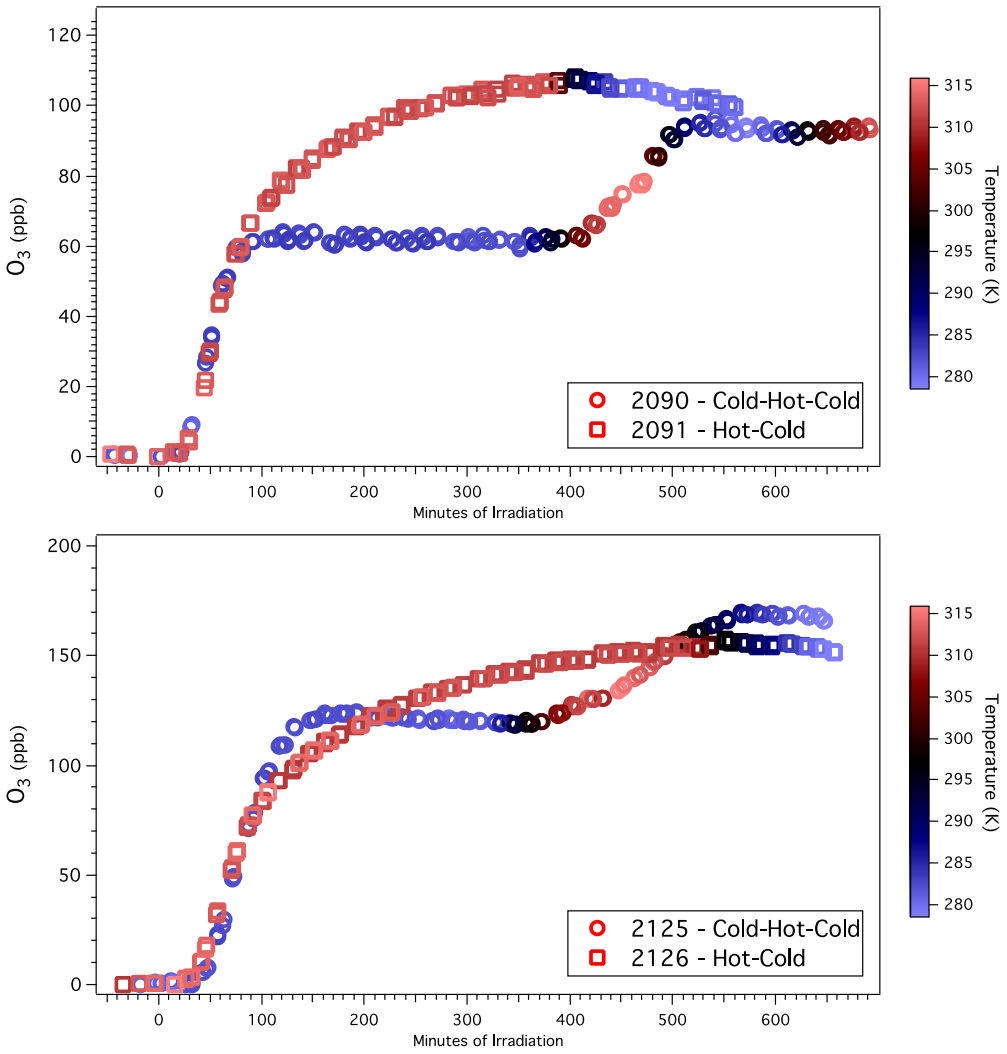

Figure 9.4: O_3 formation throughout temperature runs

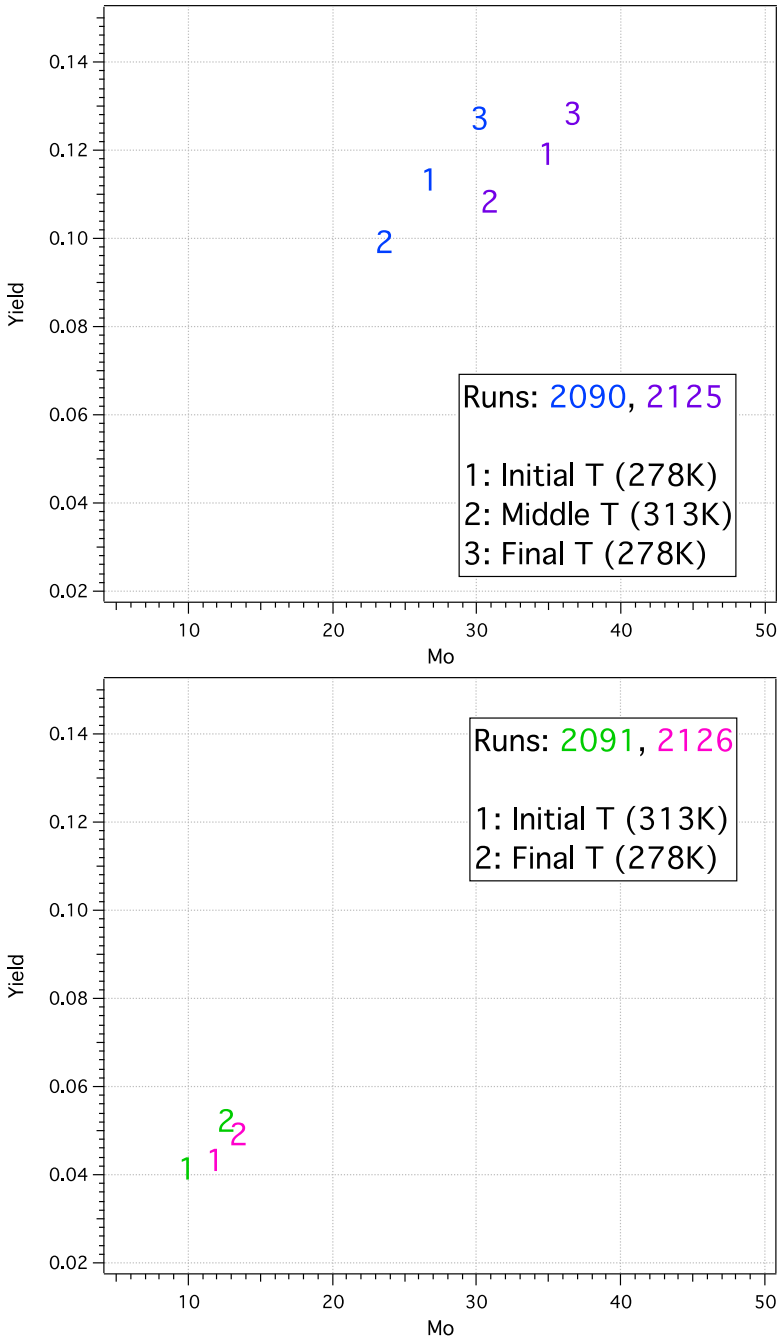

Figure 9.5: Aerosol yields throughout different temperature cycles

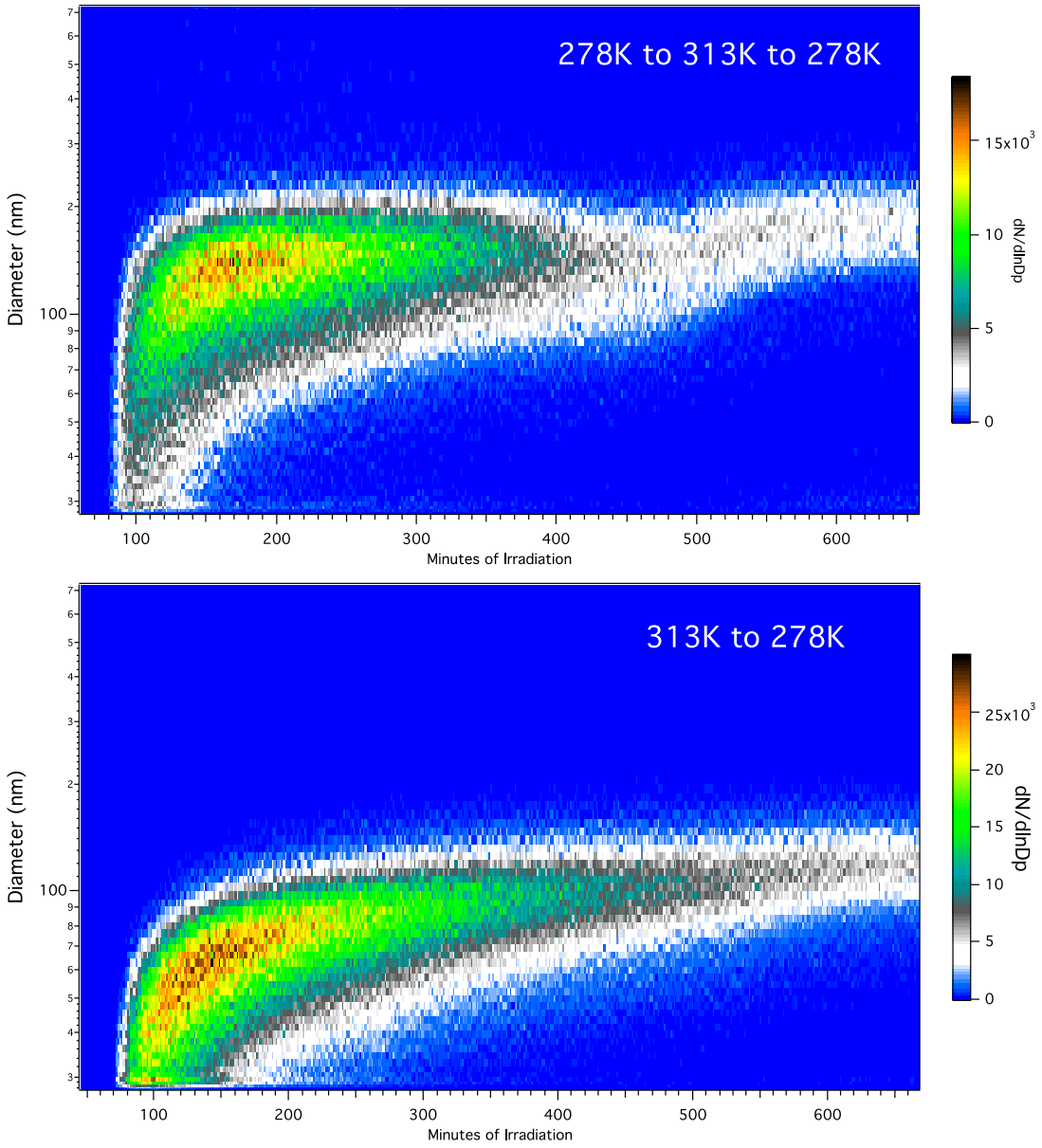

Figure 9.6: Aerosol size distributions throughout different temperature cycles

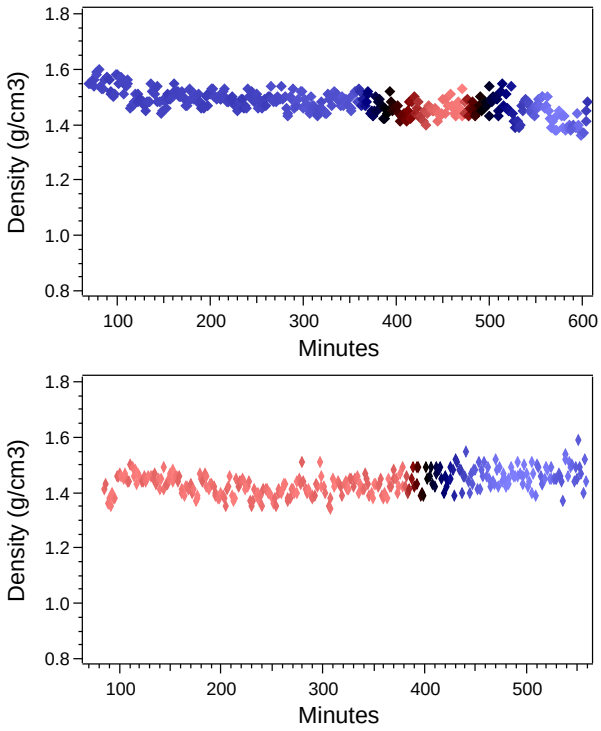

Figure 9.7: Aerosol density throughout different temperature cycles

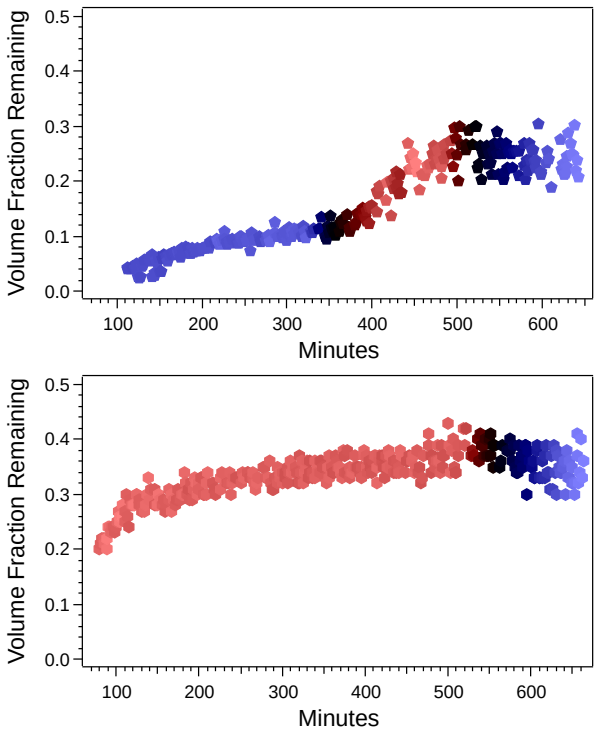

Figure 9.8: Aerosol volatility at 100C throughout temperature cycles

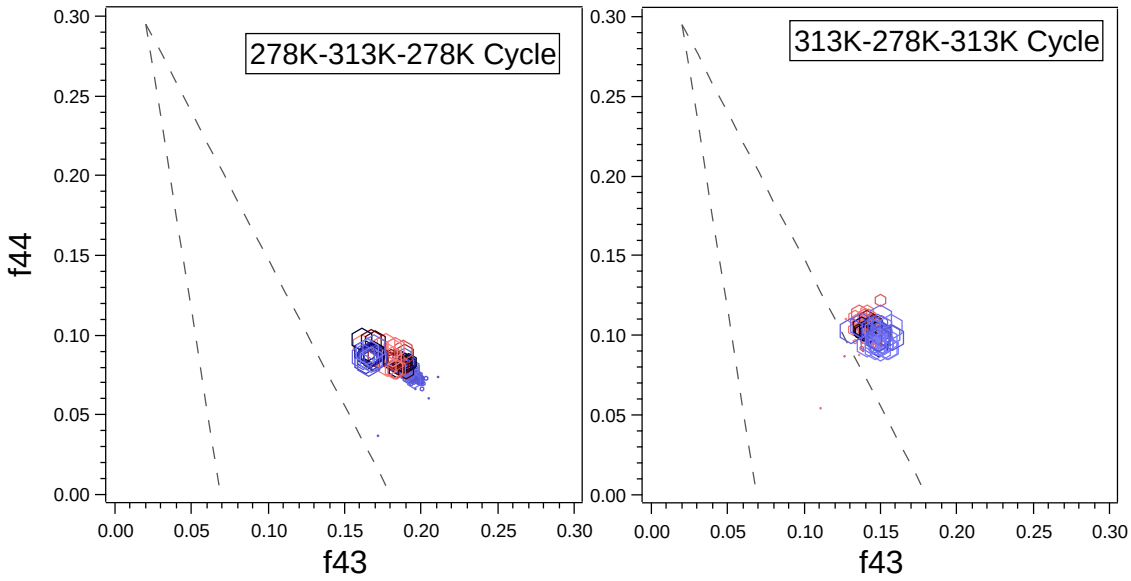

Figure 9.9: Triangle plots showing *f44* vs *f43* for *m*-xylene/NO photooxidation aerosol throughout temperature cycles, with markers sized by irradiation time

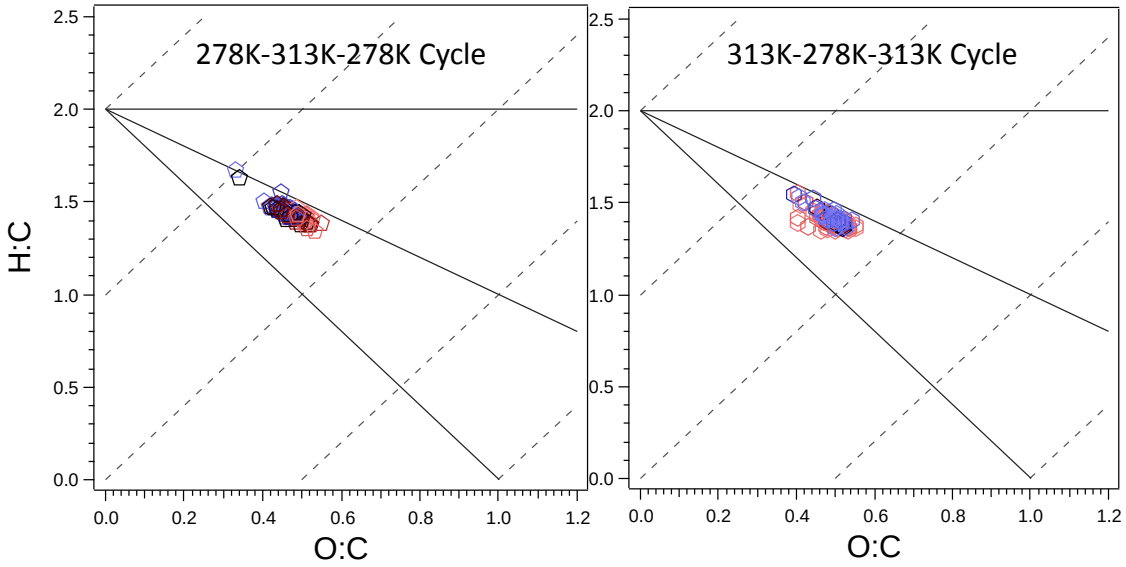

Figure 9.10: Van Krevelen diagram exhibiting bulk aerosol composition throughout temperature cycles

Chapter 10: Temperature Effects on Secondary Organic Aerosol Formation from Vehicle Exhaust

Introduction

Exhaust from gasoline passenger vehicles has recently been targeted as a significant source of secondary organic aerosol formation, with more aerosol formation being attributed to gasoline vehicles than diesel vehicles (Bahreini, et al. 2012). Chamber studies have been done looking at aging diesel exhaust and have found significant secondary aerosol formation (Robinson, et al. 2007; Nakao et al). Currently, much work is being done to evaluate the secondary organic aerosol formation from gasoline passenger vehicles (Platt, et al. 2013, Gordon, et al. 2014). This study seeks to evaluate the temperature effects on aerosol formation from aged dilute emissions from a light-duty gasoline passenger vehicle.

Experimental Methods

Exhaust was collected in the UCR/CE-CERT 90m^3 chamber from a 2007 light-duty gasoline passenger vehicle (in-line 4 cylinder, 1.799L displacement, LEV2 Tier 2, 87 octane fuel). The vehicle was warmed up and then idled (outside the building at ~20C) for 2 hours during exhaust collection. A ~2500:1 dilution was achieved in the chamber. A diagram of the injection process into the UCR/CE-CERT chamber can be found in Figure 10.1. 1ppm of H_2O_2 was added to the chamber as an OH radical source. Comparable amounts of vehicle exhaust were determined to be injected between the experiments

based off of the observed CO_2 levels (by which all aerosol results are normalized) and mass spectral signals for aromatic compounds expected to be present in the exhaust (Figure 10.2). The temperature was then cycled throughout the aging of the aerosol, as had been done in previous chapters, with different number of blacklights used at the different temperatures to maintain a constant NO_2 photolysis rate throughout the experiment (Qi et al).

Results & Discussion

Aerosol formation from the aged, dilute gasoline vehicle exhaust can be found in Figure 10.3. In significant contrast to all the other secondary organic aerosol systems studied for temperature effects, no drastic difference is seen in aerosol formation at the different temperatures for this system. In some respects, the trend in aerosol formation through the cold-hot-cold cycle is comparable to that seen in the *m*-xylene/NO cold-hot-cold system, with aerosol formation returning upon the being cooled again after heating. The hot initial temperature system also mimics the *m*-xylene/NO system in that it forms almost no additional aerosol mass when it is cooled. However, the system is not comparable at all in the respect that the two temperature cycles result in almost the same mass overall, regardless of temperature cycling.

The volatility at 100C of the aerosol throughout the different temperature cycles can be found in Figure 10.4. It is again observed in this system that the aerosol formed at the cold temperature is extremely volatile. The volatility increases as the system is heated and then upon cooling does not drop back down to the initial extremely low VFR that is

initially measured. A strongly increasing slope is seen over time in the VFR at the hot temperature in both experiments. It is interesting to observe in the hot initial temperature experiment that as soon as the system is cooled, the VFR trend becomes almost completely flat.

The bulk chemical composition was also studied for this system over the course of the different temperature cycles. The *f44* and *f43* triangle plots can be seen in Figure 10.5 and the data is colored by temperature and sized by irradiation time. In contrast with the observations of the *m*-xylene/NO *f43* signal, which slightly changed over the temperature shift, it is found the *f43* is not only comparable between the two different initial temperature systems, but remains relatively unchanged throughout the course of aging and temperature cycles. The signal at *f44*, however, changes significantly with the temperature cycles. The cold initial temperature has a high *f44* value of about 0.2, which consistently decreases as the system ages and is heated then cooled again, finally reaching a lower value of ~0.1. In contrast, the hot initial temperature system initially has an *f44* value of about 0.1, which increases as it ages and is cooled then heated again, finally reaching a higher value of ~0.2, thus exhibiting opposite trends in the *m/z44* marker between the two temperature systems. The bulk H:C and O:C ratios (Figure 10.6) do not change much over time throughout the two temperature cycles, however, it is observed that the hot initial temperature system has a slightly higher H:C than the cold initial temperature system. This is also contrasting with previous temperature studies of the bulk chemical composition, as typically any change with temperature is observed mainly in the O:C ratio.

Conclusion

This work evaluated the aerosol formation from aged, dilute exhaust from a light-duty gasoline passenger vehicle through different temperature cycles. In sharp contrast to previous temperature-cycled chamber data, no significant difference was found from the aerosol at the different temperatures. It is thought that the hysteresis effect often observed in SOA chamber studies is variable between compounds (e.g. a much larger difference is seen between aerosol formed at different temperatures from α-pinene ozonolysis than in *m*-xylene/NO photooxidation), however so far this is the first study on temperature cycled experiments that has exhibited no significant difference between aerosol at the different formation temperatures. It is thought that, due to the complexity of the gasoline exhaust mixture, there is a possible presence of compounds that are highly unaffected by temperature changes and could be buffering the effects expected from known aerosol forming compounds like *m*-xylene and other aromatic hydrocarbons.

The trends in aerosol volatility at 100C were markedly similar to that observed for all other temperature cycled aerosol systems, with a very low initial VFR observed at the cold temperature which then increases upon heating and does not return to its initial value on cooling. Again, this is thought to be indicative of either thermally labile compounds affecting the physical properties of the aerosol or a transition in the aerosol phase from solid to liquid as the system moves from cold to hot. Trends in aerosol bulk composition in the aged vehicle exhaust system through the temperature changes were markedly different than those observed in other systems studied. The main differences observed here were in the *f44* component as compared to typically being seen (if at all) in the *f43*

component in other systems. This work highlights the need for better understanding of the formation, properties, and composition of aerosol from complex mixtures such as vehicle exhaust. Further, it continues to challenge the traditional perspective of how temperature is affecting aerosol partitioning with no difference being seen at the different temperatures.

Tables & Figures

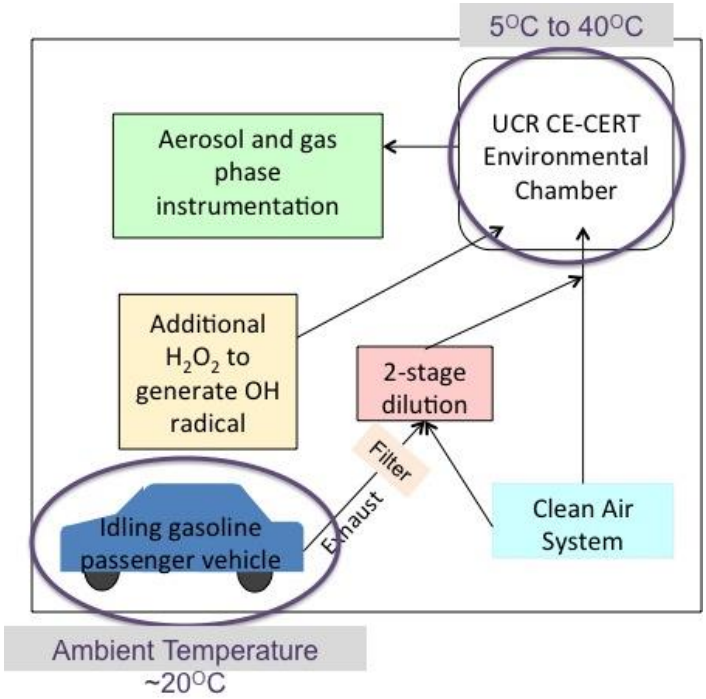

Figure 10.1: Experimental set-up for gasoline exhaust chamber experiments

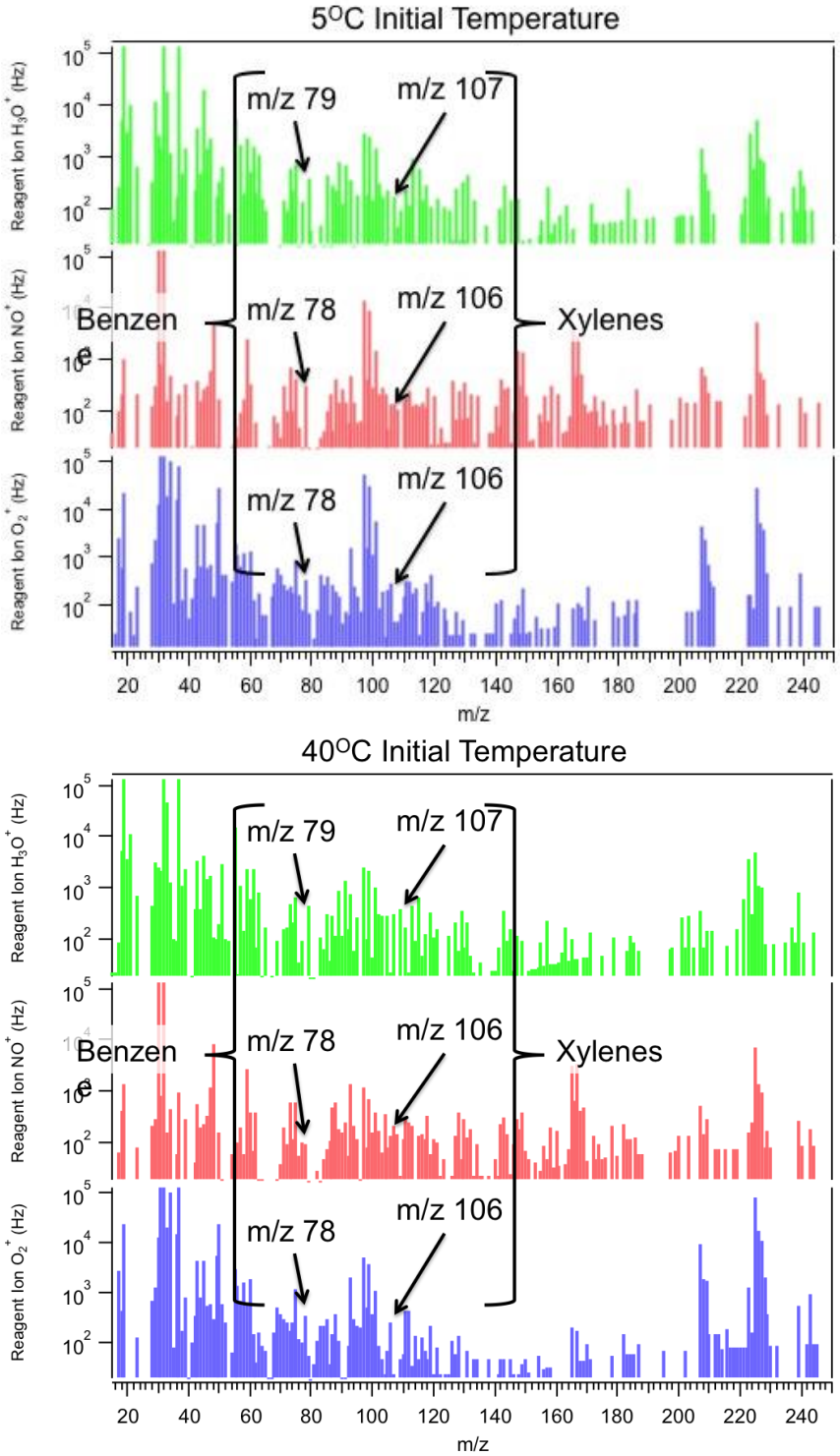

Figure 10.2: Initial gas-phase mass spectra showing comparable presence of aromatic compounds at the different initial temperatures

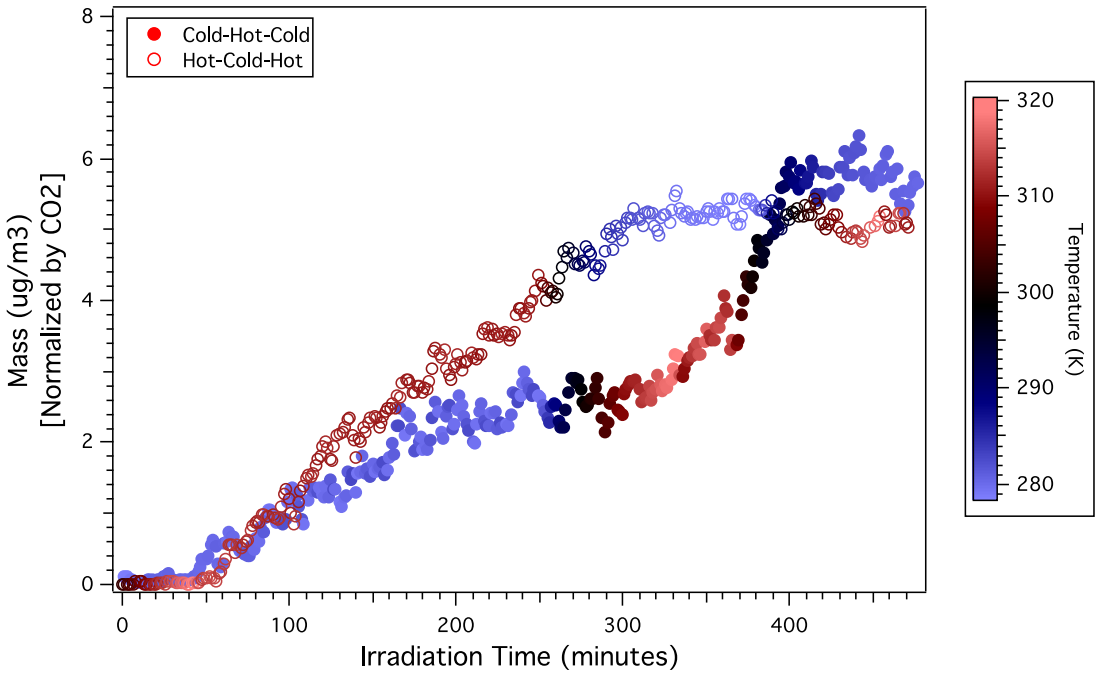

Figure 10.3: Aerosol formation from dilute gasoline vehicle exhaust with added H_2O_2 through different temperature cycles

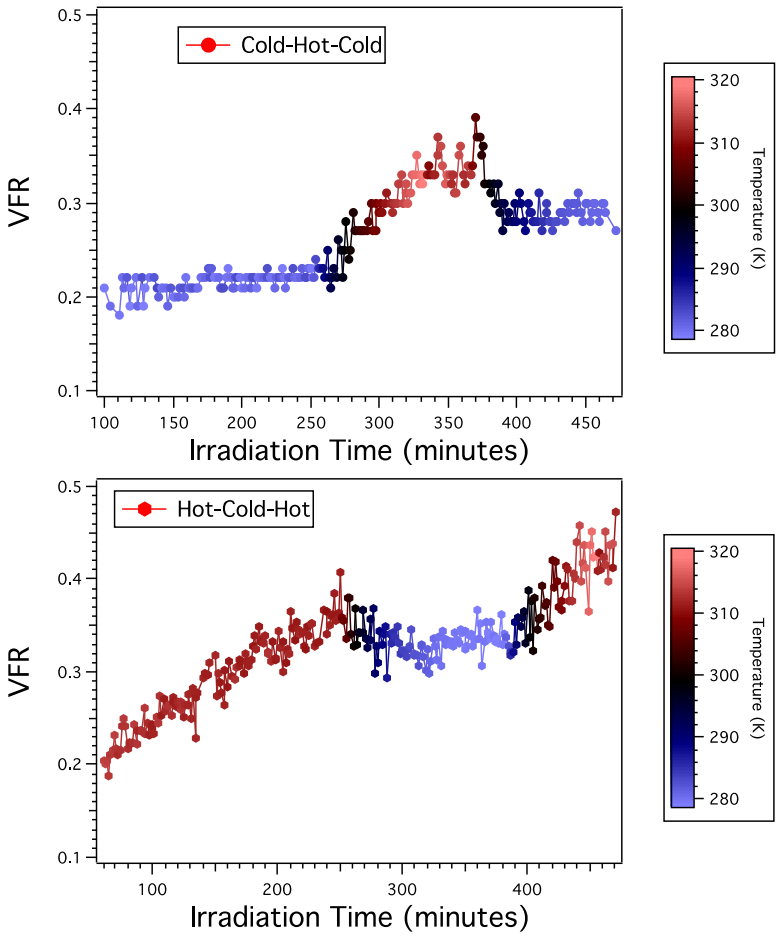

Figure 10.4: Aerosol volatility at 100C through both temperature cycles

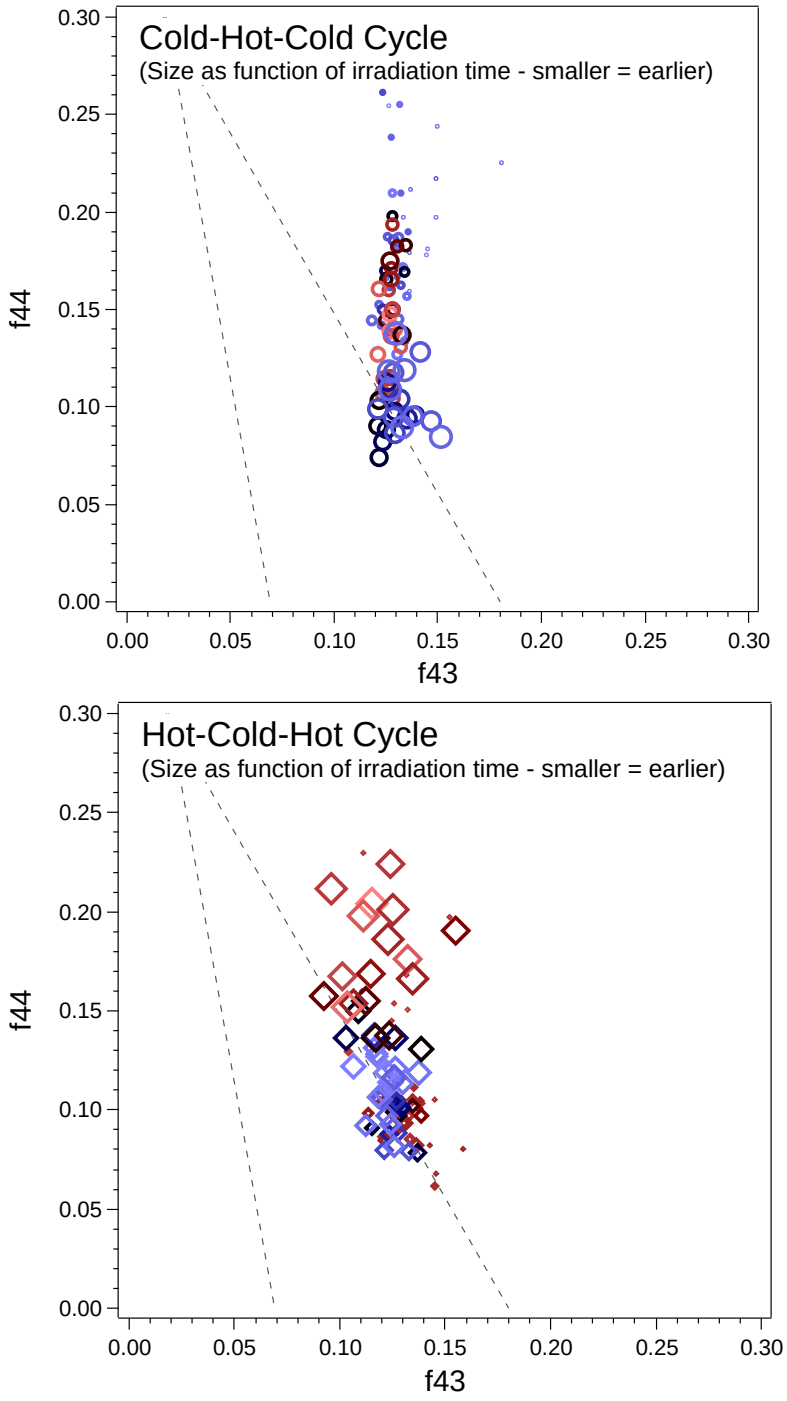

Figure 10.5: Triangle plots showing *f44* vs *f43* of organic aerosol formed from vehicle exhaust through the different temperature cycles

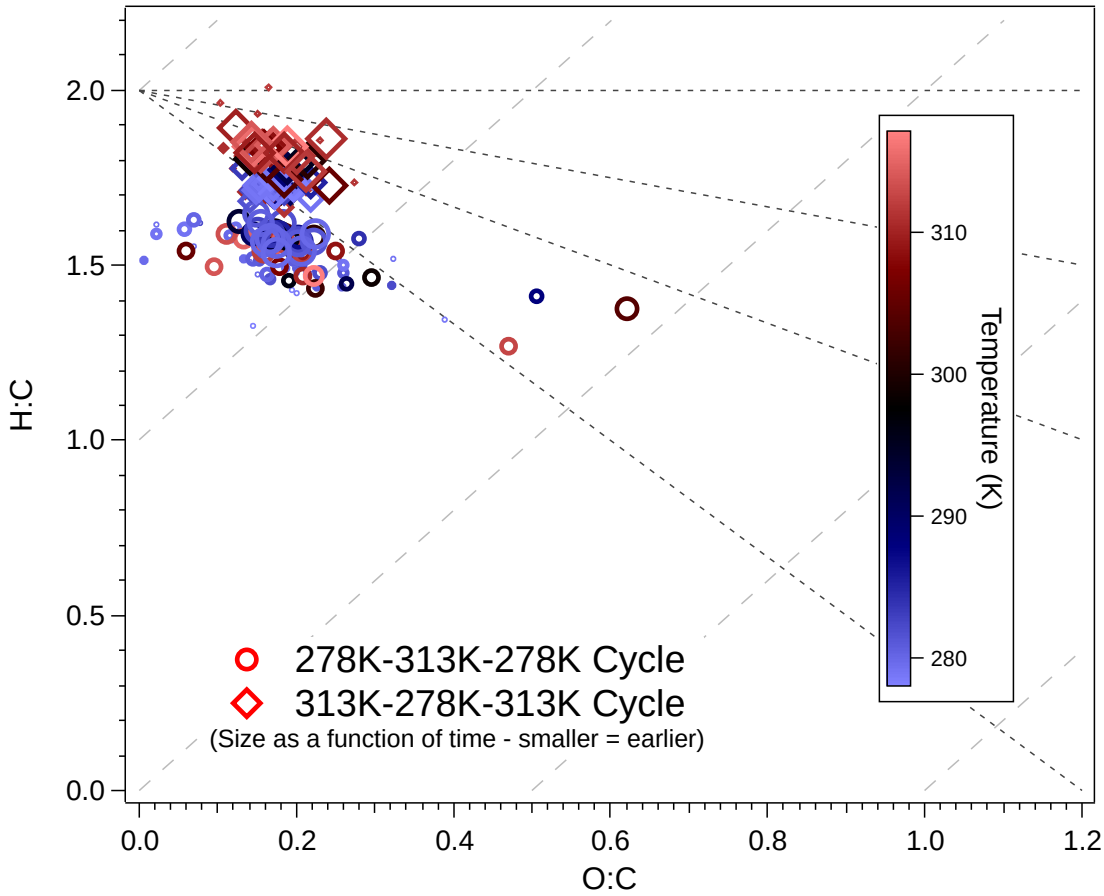

Figure 10.6: Van Krevelen diagram comparing bulk aerosol H:C and O:C ratios for vehicle exhaust SOA through the different temperature cycles

Chapter 11: Future Work & Conclusions

Overall, this thesis has sought to increase the complexity of chamber studies on secondary organic aerosol so as to better understand different drivers of aerosol yields and properties. The effects of controlling the overall reactivity of the chamber system on aerosol formation were explored through the development and use of two different surrogate reactive organic gas mixtures representing different urban atmospheric environments with and without a strong biogenic influence represented by isoprene. The surrogate mixture gas phase components were verified to not be heavily affected by the addition of a small amount of an aerosol-forming hydrocarbon, thus verifying the robustness of the surrogate in controlling the overall chamber reactivity. The biogenic surrogate mixture, of which half of the total ppmC is isoprene, allowed for further study of the aerosol formation from isoprene, an important and unique aerosol-forming hydrocarbon. The yields from isoprene in the biogenic surrogate mixture were found to be comparatively high compared to previous isoprene/NO_X chamber studies. This is especially interesting considering single precursor isoprene chamber experiments tend to have larger yields in lower isoprene/NO_X environments, however, the overall HC/NO_X ratio in the surrogate system is very high in the surrogate experiments.

Incremental aerosol formation was defined as the difference in the amount of aerosol formed between the surrogate mixture alone and the surrogate mixture with an added aerosol-forming hydrocarbon. It was found that the incremental aerosol formation of added compounds (*m*-xylene, α-pinene, 1,2,4-trimethylbenzene, or 1-methylnaphthalene) was consistently higher in the biogenic surrogate than in the

anthropogenic surrogate. Furthermore, it was found that regardless of which surrogate the aerosol-forming hydrocarbon was added to, the bulk physical and chemical properties were seemingly dictated by the added aerosol former as opposed to the surrogate system. Furthermore, the properties for each added precursor also compared well with physical and chemical properties observed from single precursor/NO_X chamber systems. These results are both interesting and encouraging, as they indicate that the reactivity of the system can provide some control over the overall yield of aerosol formed from a specific precursor, however, the incremental aerosol precursor still seems to have a lot of control on the chemistry and properties of the aerosol phase.

The effects of cycling temperature were also explored on four different aerosol-forming systems: α-pinene ozonolysis, cyclohexene ozonolysis, *m*-xylene/NO irradiation, and vehicle exhaust/H_2O_2 irradiation. Drastic hysteresis effects on aerosol formation were observed for the α-pinene and *m*-xylene systems, with far greater aerosol being formed at the cold initial temperature of 278K than at the hot initial temperature of 313K. When the hot initial temperature system was cooled down, the aerosol formation did not increase as would be expected to match the aerosol observed at the cold initial temperature. There are small differences in bulk aerosol chemistry observed at the different formation temperatures and sometimes through the temperature cycles, however, the differences in bulk chemistry do not appear to be significant enough to be the main driver of the drastic disparities observed in the aerosol yields at different temperatures. It is suspected that the aerosol phase may be different between the aerosol formed at the different temperatures in these systems (some indication for this in aerosol properties, especially by volatility).

The potential for vapor wall loss in the α-pinene ozonolysis system was explored with seeded experiments through the two temperature cycles and no indication of vapor wall loss was observed. The cyclohexene ozonolysis aerosol was found to form extremely large particles, with no nucleation mode observed at the hot temperature of formation. Attempts to resolve and control the size of the hot temperature formed cyclohexene aerosol with ammonium sulfate seed resulted in extremely low aerosol formation. It is thought that cyclohexene may be so resistant to nucleation at the hot temperature that the aerosol formation is almost random and thus occurs at a large size, rather than being able to reach the point of having a "nucleator" at the small size, which is typically thought to start off aerosol formation. In sharp contrast to the other systems, the aged vehicle exhaust secondary organic aerosol formation exhibited no temperature effects on overall mass formed through the different cycles, though the volatility and bulk chemistry of the aerosol still indicated some change with temperature.

This work raises some important questions about how the reactivity of the chamber system is affected by the presence of a surrogate mixture, in particular with the biogenic surrogate mixture. The isoprene yields seen in the biogenic mixture proved to be fairly comparable with each other. However, the *m*-xylene incremental yields were often inconsistent when added to the biogenic mixture – an effect that was not observed in the anthropogenic surrogate mixture. Further study is recommended on a range of isoprene-to-surrogate ratios in order to better understand some of the reactivity drivers of the isoprene aerosol system. Furthermore, the idea of incremental aerosol formation

established here should be further explored with more compounds at a range of concentrations and k_{OH} values.

Further work on the effect of temperature on different aerosol systems is recommended, especially in terms of looking at the phase state of the aerosol, which is suspected to be a major role player in the cold initial temperature system in this work. The one system studied here that didn't exhibit strong temperature hysteresis in aerosol yields was the aged gasoline passenger vehicle exhaust, highlighting the need for the study of aerosol formation from more complex mixtures such as this and also for study of many different systems at these different temperatures.

Works Cited

Atkinson, R.: Kinetics and mechanisms of the gas-phase reactions of the hydroxyl radical with organic compounds under atmospheric conditions. Chem. Rev., 1986, 86 (1), 69-201.

Atkinson, R., Aschmann, S.M.: Kinetics of the gas-phase reactions of alkylnaphthalenes with O_3, N_2O_5, and OH radicals at 298 ± 2 K, Atmos. Env., 1987, 21 (11), 2323-2326.

Bahreini, R., Middlebrook, A.M., de Gouw, J.A., Warneke, C., Trainer, M., Brock, C.A., Stark, H., Brown, S.S., Dube, W.P., Gilman, J.B., Hail, K., Holloway, J.S., Kuster, W.C., Perring, A.E., Prevot, A.S.H., Schwarz, J.P., Spackman, J.R., Szidat, S., Wagner, N.L., Weber, R.J., Zotter, P., Parrish, D.D.; Gasoline emissions dominate over diesel in formation of secondary organic aerosol mass, Geophys. Res. Lett., 2012, 39, L06805.

Carlton, A.G., Wiedenmyer, C., Kroll, J.H.: A review of secondary organic aerosol (SOA) from isoprene, Atmos. Chem. Phys., 2009, 9, 4987–5005.

Carter, W.P.L. and Atkinson, R.: An experimental study of incremental hydrocarbon reactivity, Env. Sci. Tech., 1987, 21, 670-679.

Carter, W.P.L.: Development of Ozone Reactivity Scales for Volatile Organic Compounds, Journal of the Air and Waste Management Association, 1994,44, 881-899.

Carter, W.P.L., Pierce, J.A., Luo, D., and Malkina, I.L.: Environmental chamber study of maximum incremental reactivities of volatile organic compounds, Atmos. Env., 1995, 29, No. 18, 2499-2511.

Carter, W.P.L., Cocker III, D.R., Fitz, D.R., Malkina, I.L., Bumiller, K., Sauer, C.G., Pisano, J.T., Bufalino, C., and Song, C.: A new environmental chamber for evaluation of gas-phase chemical mechanisms and secondary aerosol formation, Atmos. Env., 2005, 39, 7768-7788.

Carter, W.P.L.: Development of the SAPRC-07 chemical mechanism, 2010, Atmos. Env., 44 (40), 5324-5335.

Carter, W.P.L., Heo, G.: Development of Revised SAPRC Aromatics Mechanisms, Atmos. Env., 2013, 77, 404-414.

Clark, C.H., Kacarab, M., Nakao, S., Asa-Awuku, A., Sato, K., Cocker III, D.R.: Temperature Effects on Secondary Organic Aerosol (SOA) from the Dark Ozonolysis and Photo-Oxidation of Isoprene, Env. Sci. Tech, 2016, in-press.

Cocker III, D.R., Flagan, R.C., and Seinfeld, J.H.: State-of-the-art chamber facility for studying atmospheric aerosol chemistry, Environ. Sci. Technol., 2001, 35, 2594-2601.

DeCarlo, P.F., Kimmel., J.R., Trimborn, A.M., Northway, M., Jayne, J.T., Aiken, A.C., Gonin, M., Fuhrer, K., Horvath, T., Docherty, K., Worsnop, D.R., Jimenez, J.L.: Field-deployable, high-resolution, time-of-flight aerosol mass spectrometer, Anal. Chem., 2006, 78, 8281-8289.

de Gouw, J. A., C.A. Brock, E.L. Atlas, T.S. Bates, F.C. Fehsenfeld, P.D. Goldan, J.S. Holloway, W.C. Kuster, B.M. Lerner, B.M. Matthew, A.M. Middlebrook, T.B. Onasch, R.E. Peltier, P.K. Quinn, C.J. Senff, A. Stohl, A.P. Sullivan, M. Trainer, C. Warneke, R.J. Weber, and E.J. Williams: Sources of particulate matter in the northeastern United States in summer: 1. Direct emissions and secondary formation of organic matter in urban plumes, J. Geophys. Res., 2008, 113, D08301.

Dommen, J., A. Metzger, J. Duplissy, M. Kalberer, M. R. Alfarra, A. Gascho, E. Weingartner, A. S. H. Prevot, B. Verheggen, and U. Baltensperger (2006), Laboratory observation of oligomers in the aerosol from isoprene/NOx photooxidation, Geophys. Res. Lett., 33, L13805.

Eldering, A. and Cass, G.R.: Source-oriented model for air pollutant effects on visibility, J. Geophys. Res., 1996, 101, 19343–19369.

Ensberg, J.J., Hayes, P.L., Jimenez, J.L., Gilman, J.B., Kuster, W.C., de Gouw, J.A., Holloway, J.S., Gordon, T.D., Jathar, S., Robinson, A.L., and Seinfeld, J.H.: Emission factor ratios, SOA mass yields, and the impact of vehicular emissions on SOA formation, Atmos. Chem. Phys., 2014, 14, 2383-2397.

Gordon, T.D., Presto, A.A., May, A.A., Nguyen, N.T., Lipsky, E.M., Donahue, N.M., Gutierrez, A., Zhang, M., Maddox, C., Rieger, P. and Chattopadhyay, S.: Secondary organic aerosol formation exceeds primary particulate matter emissions for light-duty gasoline vehicles, Atmos. Chem. Phys., 2014, 14(9), 4661-4678.

Griffin, R. J., Cocker, D. R., Flagan, R. C., and Seinfeld, J.H.: Organic aerosol formation from the oxidation of biogenic hydrocarbons, J. Geophys. Res.-Atmos., 1999, 104, 3555–3567.

Griffin, R., Cocker III, D.R., Seinfeld, J.: Incremental aerosol reactivity: application to aromatic and biogenic hydrocarbons, Env. Sci. Tech., 1999, 33, 2403-2408.

Guenther, A., Karl, T., Harley, P., Wiedinmyer, C., Palmer, P. I., and Geron, C.: Estimates of global terrestrial isoprene emissions using MEGAN (Model of Emissions of Gases and Aerosols from Nature), Atmos. Chem. Phys., 2006, 6, 3181-3210.

Hallquist, M., Wenger, J.C., Baltensperger, U., Rudich, Y., Simpson, D., Claeys, M., Dommen, J., Donahue, N.M., George, C., Goldstein, A.H., Hamilton, J.F., Herrmann, H., Hoffmann, T., Iinuma, Y., Jang, M., Jenkin, M.E., Jimenez, J.L., Kiendler-Scharr, A., Maenhaut, W., McFiggans, G., Mentel, Th. F., Monod, A., Prévôt, A.S.H., Seinfeld, J.H., Surratt, J.D., Szmigielski, R., and Wildt, J.: The formation, properties and impact of secondary organic aerosol: current and emerging issues, Atmos. Chem. Phys., 2009, 9, 5155-5236.

Hoffmann, T., Odum, J. R., Bowman, F., Collins, D., Klockow, D., Flagan, R. C., and Seinfeld, J. H.: Formation of organic aerosols from the oxidation of biogenic hydrocarbons, J. Atoms. Chem., 1997, 26, 189–222.

Iinuma, Y., Boge, O., Miao, Y., Sierau, B., Gnauk, T., and Herrmann, H.: Laboratory studies on secondary organic aerosol formation from terpenes, Faraday Discuss., 2005, 130, 279–294.

IPCC, 2014: Climate Change 2014: Synthesis Report. Contribution of Working Groups I, II and III to the Fifth Assessment Report of the Intergovernmental Panel on Climate Change [Core Writing Team, R.K. Pachauri and L.A. Meyer (eds.)]. IPCC, Geneva, Switzerland, 151 pp.

Jimenez, J.L., Canagaratna, M.R., Donahue, N.M., Prevot, A.S.H., Zhang, Q., Kroll, J.H., DeCarlo, P.F., Allan, J.D., Coe, H., Ng, N.L., Aiken, A.C., Docherty, K.S., Ulbrich, I.M., Grieshop, A.P., Robinson, A.L., Duplissy, J., Smith, J.D., Wilson, K.R., Lanz, V.A., Hueglin, C., Sun, Y.L., Tian, J., Laaksonen, A., Raatikainen, T., Rautiainen, J., Vaattovaara, P., Ehn, M., Kulmala, M., Tomlinson, J.M., Collins, D.R., Cubison, M.J., E, Dunlea, J., Huffman, J.A., Onasch, T.B., Alfarra, M.R., Williams, P.I., Bower, K., Kondo, Y., Schneider, J., Drewnick, F., Borrmann, S., Weimer, S., Demerjian, K., Salcedo, D., Cottrell, L., Griffin, R., Takami, A., Miyoshi, T., Hatakeyama, S., Shimono, A., Sun, J.Y., Zhang, Y.M., Dzepina, K., Kimmel, J.R., Sueper, D., Jayne, J.T., Herndon, S.C., Trimborn, A.M., Williams, L.R., Wood, E.C., Middlebrook, A.M., Kolb, C.E., Baltensperger, U., and Worsnop, D.R.: Evolution of organic aerosols in the atmosphere, Science, 2009, 326, 1525–1529.

Kalberer, M., Yu, J., Cocker III, D.R., Flagan, R.C., Seinfeld, J.H.: Aerosol formation in the cyclohexene ozone system, Env. Sci. Tech, 2000, 34, 4894-4901.

Kanakidou, M., Seinfeld, J. H., Pandis, S. N., Barnes, I., Dentener, F. J., Facchini, M. C., Van Dingenen, R., Ervens, B., Nenes, A., Nielsen, C. J., Swietlicki, E., Putaud, J. P., Balkanski, Y., Fuzzi, S., Horth, J., Moortgat, G. K., Winterhalter, R., Myhre, C. E. L., Tsigaridis, K., Vignati, E., Stephanou, E. G., and Wilson, J.: Organic aerosol and global climate modelling: a review, Atmos. Chem. Phys., 2005, 5, 1053-1123.

Keywood, M.D., Kroll, J.H., Varutbangkul, V., Bahreini, R., Flagan, R.C., Seinfeld, J.H.: Secondary organic aerosol formation from cyclohexene ozonolysis: effect of OH scavenger and the role of radical chemistry, Env. Sci. Tech., 2004, 38, 3343-3350.

Krechmer, J.E., Pagonis, D., Ziemann, P.J., Jimenez, J.L.: Quantification of gas-wall partitioning in Teflon environmental chambers using rapid bursts of low-volatility oxidized species generated in situ, Env. Sci. Tech., 2016, in press.

Kroll, J.H., Ng, N.L., Murphy, S.M., Flagan, R.C., Seinfeld, J.H.: Secondary organic aerosol formation from isoprene photooxidation, Env. Sci. Tech. 2006, 40, 1869-1877.

Kroll, J.H. and Seinfeld, J.H.: Chemistry of secondary organic aerosol: Formation and evolution of low volatility organics in the atmosphere, Atmos. Env., 2008, 42, 3593-3624.

La, Y.S., Camredon, M., Ziemann, P.J., Valorso, R., Matsunaga, A., Lannuque, V., Lee-Taylor, J., Hodzic, A., Madronich, S., and Aumont, B.: Impact of chamber wall loss of gaseous organic compounds on secondary organic aerosol formation: explicit modeling of SOA formation from alkane and alkene oxidation, Atmos. Chem. Phys., 2016, 16, 1417-1431

Lee, A., Goldstein, A. H., Keywood, M. D., Gao, S., Varutbangkul, V., Bahreini, R., Ng, N. L., Flagan, R. C., and Seinfeld, J.H.: Gas-phase products and secondary aerosol yields from the ozonolysis of ten different terpenes, J. Geophys. Res.-Atmos., 2006, 111, D07302

Li, L., Tang, P., and Cocker III, D.R.: Instantaneous nitric oxide effect on secondary organic aerosol formation from *m*-xylene photooxidation, Atmos. Env., 2015, 119, 144-155.

Malloy, Q.G.J., Nakao, S., Qi, L., Austin, R., Stothers, C., Hagino, H., and Cocker III, D.R.: Real-time aerosol density determination utilizing a modified scanning mobility particle sizer-aerosol particle mass analzyer system, Aerosol Sci. Technol., 2009, 43, 673-678.

Matsui, H., M. Koike, N. Takegawa, Y. Kondo, R. J. Griffin, Y. Miyazaki, Y. Yokouchi, and T. Ohara (2009), Secondary organic aerosol formation in urban air: Temporal variations and possible contributions from unidentified hydrocarbons, J. Geophys. Res., 114, D04201.

Odum, J.R., Hoffmann, T., Bowman, F., Collins, D., Flagan, R.C., and Seinfeld, J.H.: Gas/particle partitioning and secondary organic aerosol yields, Environ. Sci. Technol., 1996, 30, 2580-2585.

Nakao, S., Shrivastava, M., Nguyen, A., Jung, H., Cocker III, D. R.: Interpretation of secondary organic aerosol formation from diesel exhaust photooxidation in an environmental chamber, Aerosol Sci. Tech., 2011, 45, 954-962.

Odum, J. R., Hoffmann, T., Bowman, F., Collins, D., Flagan, R.C., and Seinfeld, J. H.: Gas/particle partitioning and secondary aerosol yields, Environ. Sci. Technol., 1996, 30, 2580–2585.

Odum, J. R., Jungkamp, T. P. W., Griffin, R. J., Forstner, H. J. L., Flagan, R. C., and Seinfeld, J. H.: Aromatics, reformulated gasoline, and atmospheric organic aerosol formation, Environ. Sci. Technol., 1997, 31, 1890–1897.

Pankow, J. F.: An absorption model of gas/particle partitioning of organic compounds in the atmosphere, Atmos. Environ., 28, 185–188, 1994a.

Pankow, J. F.: An absorption model of the gas/aerosol portioning involved in the formation of secondary organic aerosol, Atmos. Environ., 28, 189–193, 1994b.

Platt, S. M., Haddad, I.E., Zardini, A.A., Clairotte, M., Astorga, C., Wolf, R., Slowik, J.G., Temime-Roussel, B., Marchand, N., Ježek, I. and Drinovec, L.: Secondary organic aerosol formation from gasoline vehicle emissions in a new mobile environmental reaction chamber, Atmos. Chem. Phys., 2013, 13.18, 9141-9158.

Pope III, C.A. and Dockery, D.W.: Health effects of fine particulate air pollution: lines that connect, J. AirWaste Manage., 2006, 56, 709-742.

Pope III, C.A., Ezzati, M. and Dockery, D.W.: Fine-particulate air pollution and life expectancy in the United States, N. Engl. J. Med., 360, 376-86, 2009.

Presto, A. A., Hartz, K. E. H., and Donahue, N. M.: Secondary organic aerosol production from terpene ozonolysis. 2. Effect of NOx concentration, Environ. Sci. Technol., 2005, 39, 7046–7054.

Prince, B.J., Milligan, D.B., and McEwan, M.J.: Application of selected ion flow tube mass spectrometry to real-time atmospheric monitoring, Rapid Commun. Mass Spectrom., 2010, 24, 1763-1769.

Robinson, A.L., Donahue, N.M., Shrivastava, M.K., Weitkamp, E.A., Sage, A.M., Grieshop, A.P., Lane, T.E., Pierce, J.R., Pandis, S.N.: Rethinking Organic Aerosols: Semivolatile Emissions and Photochemical Aging, Science, 2007, 315 (5816), 1259-1262.

Saathoff, H., Naumann, K.-H., Möhler, O., Jonsson, Å. M., Hallquist, M., Kiendler-Scharr, A., Mentel, Th. F., Tillmann, R., and Schurath, U.: Temperature dependence of yields of secondary organic aerosols from the ozonolysis of α-pinene and limonene, Atmos. Chem. Phys., 2009, 9, 1551–1577.

Sato, K., Nakao, S., Clark, C.H., Qi, L., Cocker III, D.R.: Secondary organic aerosol formation from the photooxidation of isoprene, 1,3-butadiene, and 2,3-dimethyl-1,3-butadiene under high NOx conditions, 2011, Atmos. Chem. Phys., 11, 7301–7317.

Shilling, J. E., Chen, Q., King, S. M., Rosenoern, T., Kroll, J.H., Worsnop, D. R., DeCarlo, P. F., Aiken, A. C., Sueper, D., Jimenez, J. L., and Martin, S. T.: Loading-dependent elemental composition of α-pinene SOA particles, Atmos. Chem. Phys., 2009, 9, 771–782.

Song, C., Na, K., and Cocker III, D.R.: Impact of the hydrocarbon to NO_X ratio on secondary organic aerosol formation, Environ. Sci. Technol., 2005, 39, 3143-3149.

Sullivan, D.W., Kimura, Y., Allen, D.T.: Development of an updated base case ambient VOC mixture for assessing atmospheric reactivity, Report to the California Air Resources Board and California Environmental Protection Agency, Contract No. 08-327, 2011.

Volkamer, R.; Jimenez, J.L.; San Martini, F.; Dzepina, K.; Zhang, Q.; Salcedo, D.; Molina, L.T.; Worsnop, D.R.; Molina, M.J. Secondary organic aerosol formation from anthropogenic air pollution: rapid and higher than expected. Geophys. Res. Lett. 2006, 33, No. L17811.

Yu, J. Z., Cocker, D. R., Griffin, R. J., Flagan, R. C., and Seinfeld, J. H.: Gas-phase ozone oxidation of monoterpenes: Gaseous and particulate products, J. Atoms. Chem., 1999, 34, 207–258.

Zhang, X., Cappa, C.D., Jathar, S.H., McVay, R.C., Ensberg, J.J., Kleeman, M.J., Seinfeld, J.H.: Influence of vapor wall loss in laboratory chambers on yields of secondary organic aerosol, Proc. Nat. Acad. Sci., 2014, 111 (16), 5802-5807.

Zhang, X., McVay, R.C., Huang, D.D., Dalleska, N.F., Aumont, B., Flagan, R.C., Seinfeld, J.H.: Formation and evolution of molecular products in α-pinene secondary organic aerosol, Proc. Nat. Acad. Sci., 2015, 112 (46), 14168-14173.

Zhao, D. F., Kaminski, M., Schlag, P., Fuchs, H., Acir, I.-H., Bohn, B., Häseler, R., Kiendler-Scharr, A., Rohrer, F., Tillmann, R., Wang, M. J., Wegener, R., Wildt, J., Wahner, A., and Mentel, Th. F.: Secondary organic aerosol formation from hydroxyl radical oxidation and ozonolysis of monoterpenes, Atmos. Chem. Phys., 2015, 15, 991-1012.